UNIVERSITY OF CALIFORNIA

SANTA CRUZ

HYDROLOGIC SYSTEM RESPONSE TO ENVIRONMENTAL CHANGE: THREE CASE STUDIES IN CALIFORNIA

A dissertation submitted in partial satisfaction
of the requirements for the degree of

DOCTOR OF PHILOSOPHY

in

EARTH SCIENCES

by

Tess A. Russo

September 2012

The Dissertation of Tess A. Russo
is approved:

_____
Professor Andrew T. Fisher, Chair

_____
Professor Slawek Tulaczyk

_____
Assistant Professor Noah Finnegan

_____
Peter Swarzenski, Oceanographer, USGS

_____
Tyrus Miller
Vice Provost and Dean of Graduate Studies

TABLE OF CONTENTS

FIGURES and TABLES

ABSTRACT

Hydrologic system responses to environmental changes: three case studies in California

Tess A. Russo

Hydrologic systems are vulnerable to anthropogenic and natural environmental changes. When these changes impair a system's ability to function and serve as a resource, then restoration or mitigation may be needed. Successful management of freshwater resources requires a quantitative understanding of hydrologic processes and dynamics, and an assessment as to how hydrologic systems may respond to future changes. Some systems are sufficiently large or complex so as to defy direct control or restoration, but people can still benefit from understanding that will allow more reliable and thoughtful resource use, as part of a comprehensive management approach. The three chapters presented in this thesis examine hydrologic system response to a variety of environmental changes, including: (1) a recovering riparian wetland located downstream of a dam, (2) an overdrafted and seawater intruded coastal groundwater basin, and (3) a region experiencing an increase in the intensity of extreme precipitation events. In Chapter 1, our studies show that riparian wetland conditions can be improved while water is conserved in upstream reservoirs by utilizing surface infiltration to establish wetland saturation conditions, rather than

lateral and upward groundwater transport. Results from the second study indicate that ~13% of the study area (29 of 220 km^2 in the basin) may be suitable for managed aquifer recharge (MAR). Modeling suggests that MAR projects placed along the coast provide the greatest initial decrease in seawater intrusion, but MAR projects placed in suitable locations throughout the basin provides the greatest reduction in seawater intrusion over subsequent decades. In Chapter 3, we show that there has been a statistically significant increase in extreme precipitation, beyond proportional changes in mean annual precipitation, in the San Francisco Bay Area in the last 120 years. The extent of changes varies on a spatial scale of ~50 km, the scale at which city planning and risk management decisions should be based. The results of each chapter contribute to the fundamental understanding of hydrologic system dynamics, and demonstrate new field and computational methods. Results presented in Chapters 1 and 2 also compare the efficacy of hypothetical restoration and operational scenarios for improving resource conditions.

ACKNOWLEDGEMENTS and DEDICATION

I would like to acknowledge my advisor, Andy Fisher, for his unwavering support on all of my projects, for his thorough, thoughtful and tactful manuscript edits, and for always setting the highest bar. I also owe great thanks to the graduate students and faculty in the Department of Earth and Planetary Sciences, especially Emily Brodsky, Francis Nimmo, and my committee: Andy Fisher, Slawek Tulaczyk, Peter Swarzenski (USGS), and Noah Finnegan; I have never worked with and been taught by a more intelligent, motivated and collaborative group of people.

For Gaetano P. Russo

The Architect

INTRODUCTION

1. Motivation and summary

I use three case studies to examine hydrologic responses to a variety of environmental changes. These three studies elucidate: (1) infiltration and drainage dynamics in a riparian wetland; (2) groundwater recharge and aquifer response in an overdrafted, coastal basin; and (3) changes in the nature of extreme precipitation events in the San Francisco Bay Area. The environmental changes imposed on each hydrologic system discussed in this thesis are unique, but they share characteristics with other hydrologic systems in many settings. Anthropogenic actions have impaired the hydrologic systems discussed in the first two case studies, whereas the mechanisms for changes observed in extreme precipitation in the third case study are likely a combination of natural atmospheric dynamics and human-induced climate warming.

Riparian wetlands provide valuable ecosystem services, aquifers provide resources for agricultural, industrial and consumptive needs, and precipitation extremes are important for runoff planning and hazard assessment. Each of these systems is important to humans, albeit in different ways, and each is vulnerable to anthropogenic and natural forcing. Within the last three decades, reports have stated that over half the world's wetlands had been damaged or destroyed (Barbier, 1993), seawater is contaminating coastal aquifers due to excessive groundwater extraction (Bond and Bredehoeft, 1987), and extreme precipitation events are increasing across the United States (Karl and Knight, 1998).

Opportunities for hydrologic restoration are feasible for the systems discussed in the first two case studies, but it is unclear whether the impacts observed in the third study can be reversed. Mitigation strategies are needed for past, ongoing and future changes that may occur within all three systems. Developing appropriate strategies (for example, managing flooding and groundwater recharge) requires an understanding of how hydrologic processes, properties and system responses are linked across a range of temporal and spatial scales. The studies presented in this thesis address these scientific, technical, and management needs through a combination of: (a) quantitative field observations, (b) laboratory measurements, (c) analytical and numerical modeling, and (d) statistical analyses.

Each chapter provides information that could help to restore aquatic habitats, protect water resources, and aid management decisions. Although this dissertation comprises a series of distinct projects, they are linked by common physics, similar analytical methods, and the recognition that groundwater, soil water, and surface water comprise a single linked resource (Winter 1995; 1998), particularly when considered in the context of the hydrologic cycle, increasing demand, and rapidly changing climate.

2. Overview of case studies

(1) Poopenaut Valley is located downstream of the Hetch Hetchy reservoir on the Tuolumne River, near the western edge of Yosemite National Park. Riparian wetlands in the valley have been impacted by a lack of natural flooding over the last 90 years

due to flow regulation by the O'Shaughnessy Dam. Recently, the San Francisco Public Utilities Commission and Yosemite National Park have implemented controlled flood releases which they hope will help restore the riparian wetland restoration in the valley. Our research project was designed to monitor the soil moisture and shallow groundwater response to flooding during one of these controlled events, to assess the relatively roles of groundwater rise and inundation in developing and sustaining wetland conditions adjacent to the river, and evaluate what kinds of "design floods" might be most useful in meeting wetland restoration requirements while reducing the total water release from the Hetch Hetchy Reservoir. We collected soil samples in several locations, and installed moisture content sensors, groundwater piezometers, and thermal probes for measuring streambed infiltration rates, prior to the Spring 2009 controlled flood release. We returned after the flood to recover instruments and data and assess the impacts of the flood. Our research suggests that inundation plays a more important role than rising groundwater levels in developing wetland conditions adjacent to the river, although groundwater does play a quantifiable role in this process. We also found that wetland restoration objectives might be met with a smaller release through pulsing of flood flows, by timing discharge peaks to take advantage of the drainage properties of shallow soils.

(2) Aquifer overdraft-induced seawater intrusion (SWI) is a pernicious problem for the Pajaro Valley Groundwater Basin (PVGB), central coastal California, where groundwater comprises the primary supply satisfying agricultural and municipal demand. The Pajaro Valley Water Management Agency, local land

owners, and other stakeholders are interested in protecting and enhancing the extent of groundwater recharge in the basin. We have evaluated the potential benefits of establishing a distributed system of managed aquifer recharge (MAR) projects that will help to get the PVGB back into hydrologic balance. We completed a two part project to help determine the potential for MAR in the basin. We used geographic information systems (GIS) to integrate surface and subsurface datasets to determine the relative suitability of MAR projects throughout the basin. The MAR suitability map produced in GIS helped determine locations for simulating MAR projects, by modifying a regional groundwater model of the Pajaro Valley. Various MAR project scenarios were run to test the impact of MAR locations and sizes throughout the valley on long-term groundwater resource conditions. MAR projects provide greater benefit by increasing groundwater head levels and reducing (or reversing) SWI over time. We found that placing MAR projects in locations classified as highly suitable in the GIS analysis reduced SWI by 25% compared to less suitable MAR locations.

(3) Climate change is expected to increase the frequency and intensity of extreme weather events, but few studies have explored the nature of hydrologic change occurring on local- to regional-scales – the scale at which city planning, engineering, and management decisions must be made. We use 120 years of precipitation data from the San Francisco Bay Area (SFBA), CA, collected from over 1000 stations, to determine how extreme rainfall events have changed during this time. Using an exceedance probability analysis, we show that storm events have increased in intensity across the SFBA by greater magnitudes than predicted by large,

continental-scale studies. In addition, storm intensity is generally increasing at a greater rate than mean annual precipitation (MAP). The scale of heterogeneity with respect to changing storm intensities in the SFBA is approximately ~50 km. Our research also suggests that there have been disproportionate increases in storm intensity in urban areas compared to MAP, relative to the SFBA overall. These results suggest that municipal planning, infrastructure design, and risk assessment should be updated in response to observed historical (and likely ongoing) trends, and in many cases should emphasize local historical observations.

3. References

Barbier, E. B. (1993) Sustainable use of wetlands - valuing tropical wetland benefits: Economic methodologies and applications. *Geogr. J.*, 159:22–32.

Bond, L. D. and J. D. Brehehoeft (1987) Origins of seawater intrusion in a coastal aquifer – a case study of the Pajaro Valley, California. *J. Hydrol.*, 92:363-388.

Karl, T. R. and R.W. Knight (1998) Secular trends of precipitation amount, frequency, and intensity in the United States. *B. Am. Meterol. Soc.*, 79:231-241.

Winter, T. C., J. W. Harvey, O. L. Franke, and W. M. Alley (1998) Groundwater and surface water, a single resource, Circular 1139, 79 pp, U. S. Geological Survey, Reston, VA.

Winter, T. C. (1995) Recent advances in understanding the interaction of groundwater and surface water, *Rev. Geophys.*, *33 Suppl.*, 985-994.

Chapter One

IMPROVING RIPARIAN WETLAND CONDITIONS BASED ON INFILTRATION AND DRAINAGE BEHAVIOR DURING AND AFTER CONTROLLED FLOODING

Published: Russo, T. A., A. T. Fisher, and J. Roche (2012) Improving riparian wetland conditions based on infiltration and drainage behavior during and after controlled flooding. *Journal of Hydrology* 432-43: 98-111.

Abstract

We present results of an observational and modeling study of the hydrologic response of a riparian wetland to controlled flooding. The study site is located in Poopenaut Valley, Yosemite National Park (USA), adjacent to the Tuolumne River. This area is flooded periodically by releases from the Hetch Hetchy Reservoir, and was monitored during one flood sequence to assess the relative importance of inundation versus groundwater rise in establishing and maintaining riparian wetland conditions, defined on the basis of a minimum depth and duration of soil saturation, and to determine how restoration benefits might be achieved while reducing total flood discharge. Soil moisture data show how shallow soils were wetted by both inundation and a rising water table as the river hydrograph rose repeatedly during the controlled flood. The shallow groundwater aquifer under wetland areas responded quickly to conditions in the adjacent river, demonstrating a good connection between surface and subsurface regimes. The observed soil drainage response helped to calibrate a numerical model that was used to test scenarios for controlled flood releases. Modeling of this groundwater–wetland system suggests that inundation of surface soils is the most effective mechanism for developing wetland conditions, although an elevated water table helps to extend the duration of soil saturation. Achievement of wetland conditions can be achieved with a smaller total flood release, provided that repeated cycling of higher and lower river elevations is timed to benefit from the characteristic drainage behavior of wetland soils. These results are robust to modest variations in the initial water table elevation, as might result from wetter or dryer conditions prior

to a flood. However, larger changes to initial water table elevation, as could be associated with long term climate change or drought conditions, would have a significant influence on wetland development. An ongoing controlled flooding program in Poopenaut Valley should help to distribute fine grained overbank deposits in wetland areas, extending the period of soil water retention in riparian soils.

1.1 Introduction

Wetlands provide essential environmental functions such as water quality improvement, carbon sequestration, nutrient cycling and biodiversity support (Brinson et al., 1981; Turner, 1991; Whiting and Chanton, 2001). More than 50% of the world's wetlands have been damaged or destroyed as a result of urbanization, agricultural development, reconfiguration of water ways, and other manipulation of the natural landscape (Barbier, 1993). California has lost 90% of its wetlands in the last 200 years, more than any of the other United States (Dahl, 1990), comprising a massive reduction in aquatic habitat area, a driving force for soil transformation (Ballantine and Schneider, 2009), and a significant release of nutrients into the environment (Orr et al., 2007). Because wetlands have high ecosystem, economic and hazard mitigation value (Costanza et al., 1997), restoration projects are increasingly common.

Riparian wetlands (located adjacent to rivers and streams) are particularly vulnerable to modification by human activities because these wetlands are readily influenced by subtle changes in event and seasonal hydrographs related to channel

modification, changes in land use and climate, and the construction of dams and other structures that regulate flow.

Different approaches have been applied to achieve wetland restoration goals, depending on the physical, biological and hydrologic setting, characteristics of available water, extent of landscape manipulation needed, and other factors. Some wetland restoration projects have focused on benefiting a small number of endangered or other species (Mahoney and Rood, 1998; Bovee and Scott, 2002), whereas other projects have assessed wetland conditions on the basis of broader ecological metrics such as species diversity or total species cover (Bendix, 1997; Brock and Rogers, 1998; Johansson and Nilsson, 2002; Capon, 2003; Siebentritt et al., 2004). Another approach is to attempt restoration of natural hydrologic dynamics, with the idea that native biomes that are adapted to pre-development conditions will be able to make rapid progress towards recovery once hydrologic restoration is achieved (Bayley, 1995; Schiemer et al., 1999; Ward et al., 2001).

This approach can be challenging because it requires that restoration projects be designed around a process-based understanding of wetland function, including complex links between hydrologic, biological, and soil conditions and function. In cases where the loss of wetlands has taken place over many years, there may be a lack of baseline information regarding fundamental system properties such as fluid flow pathways, residence times, and typical duration of inundation.

We present results of a study conducted as part of a long-term riparian wetland restoration project associated with controlled flooding downstream from a

water supply dam and reservoir. This project, a riparian wetland on a dammed river, is particularly challenging because of the need to simultaneously satisfy environmental and municipal needs. The site is in an area that is highly sensitive to ongoing and projected future climate change, and is difficult to access to set up instrumentation and collect data and samples prior to controlled flood events. All wetland restoration efforts are unique, but many of the characteristics present in the work site described in this study are also found in other wetlands undergoing restoration, as discussed below.

Dams influence discharge on 77% of the rivers in the northern third of the world (Dynesius and Nilsson, 1994), and there is similarly extensive river regulation in Latin America, Africa and South-East Asia (Revenga et al., 2000). In general, dams are designed specifically to regulate downstream flow, often resulting in reductions in the number, timing, and magnitude of high flow events, and reducing the variability of channel discharge in general (Graf, 1999). Dams also change the sediment capacity and load of downstream rivers; modify patterns of sediment supply, erosion, and channel morphology; and impact river temperature and nutrient and carbon contents (Kondolf, 1997; Brandt, 2000; Nilsson and Berggren, 2000). All of these modifications have ecosystem impacts, but riparian wetlands are especially vulnerable because their presence may depend on all of the factors listed above. Thus the restoration of riparian wetlands downstream from dams is a particularly important and vexing challenge.

Riparian wetlands and floodplain habitats are sensitive to the timing and extent of inundation. In some cases, groundwater can provide a significant fraction of the water that maintains shallow soil saturation in these systems (Brunke, 2002), but the relative influence of surface inundation versus groundwater inflow has rarely been quantified. The connectivity between shallow groundwater and wetland soils depends on sediment characteristics and understory growth, and may be correlated to physical river features such as backflow channels and oxbow lakes (Cabezas et al., 2008). Given uncertainties in the relative importance of surface water and groundwater in natural riparian wetland systems, it is not surprising that setting hydrologic goals for restoration can be difficult.

As an added complication in this study, the field site is located on the western side of the central Sierra Nevada mountains, western United States, in an area undergoing significant hydrologic transformation as a result of regional and global climate change. Recent climate modeling predictions suggest that much of the snow pack that accumulates annually in the Sierra Nevada mountains will fall as rain rather than snow by the year 2100 (Snyder and Sloan, 2005; IPCC, 2007). This will change the timing and magnitude of wet-season runoff events, in both unregulated basins and basins where discharge is controlled by dams. Changes in the distribution of the annual runoff hydrograph in many basins will impact the availability of environmental flows and water supplies for municipal, agricultural and industrial purposes, and it is essential to learn how controlled flood releases can be used

efficiently for the benefit of ecosystems and stakeholder communities so as to achieve the most benefit from limited resources.

Two primary questions are addressed through this study: (1) What are the relative roles of groundwater and surface water in developing and maintaining riparian wetland conditions during and after a controlled flood, and how might these roles change under varying antecedent groundwater conditions? (2) How can riparian wetland conditions be improved while simultaneously limiting the total amount of water released during controlled floods? These questions are addressed through a study comprising three main components: (a) quantitative observations of riparian wetland response to a controlled flood, (b) use of these data to calibrate a variably-saturated model of wetland soil and groundwater dynamics, and (c) application of the calibrated model to scenarios of controlled flooding that could achieve a similar wetland benefit as part of a smaller total reservoir release. For the purposes of this study, we follow an established riparian wetland definition that includes riverine wetlands and palustrine wetlands (emergent, scrub-shrub and forested) (Cowardin, 1978). We use the US Army Corps of Engineers (USACEs) wetland delineation definition, requiring saturation within 30 cm of the surface for 14 consecutive days, five out of every ten years (US Army Corps of Engineers, 2008). This metric is somewhat arbitrary, but it is widely applied, provides a clear test of observed and modeled wetland response, and is useful for comparative purposes. The emphasis of this study is on the physical hydrology of controlled flooding and wetland soil response, but results of this work have implications for related topics such as valley

geomorphology, biome development and support, and riparian nutrient cycling. The present study is based on field observations from a particular location, but a similar combination of field techniques and modeling can be used in other locations.

1.2 Site and hydrologic description

The study site is located in Poopenaut Valley, adjacent to the Tuolumne River on the western side of Yosemite National Park (YNP), USA (Figure 1-1). Poopenaut Valley covers an area of 25 hectares, trending northeast to southwest. The valley was carved from granitic rocks of the Sierra Nevada batholith primarily by glacial processes, the most recent of which, the Tioga glaciations, ended approximately 18 kya (Huber, 1990). Subsequent alluvial and fluvial processes have formed a broad valley with a gentle slope towards the southwest. Alluvial sedimentary fill extends across the valley floor, ending at the steep northwestern and southeastern valley walls, and abutting granitic massifs at upstream and downstream ends of the valley.

The O'Shaughnessy Dam is located at the northeastern end of Poopenaut Valley, forming the lower limit of the Hetch Hechy Reservoir. The dam was constructed to an initial height of 69 m in 1923, and subsequently raised to 95 m in 1938; the current storage capacity of the reservoir is 0.444 km3. The drainage basin that supplies water to Hetch Hechy Reservoir has an area of 1180 km2, and extends from an elevation of 1170 m to >3700 m on the northern slopes of Mt. Lyell. About 1/3 of the water collected behind the O'Shaughnessy Dam is conveyed to the San Francisco Bay Area using a pipeline and aquaduct, providing >85% of the water used

by 2.5 million people across five counties in northern California (San Francisco Public Utilities Commission: Water Enterprise, 2009). Additional benefit is provided through power generation and environmental flows, including those used for controlled flooding in the Poopenaut Valley, which is the focus of this paper. Precipitation averages 89 cm annually at the Hetch Hetchy weather station, with 75% of precipitation occurring between November and March. The US Geological Survey (USGS) has collected stage and discharge data on the Tuolumne River 3 km upstream of Poopenaut Valley since 1910 (Tuolumne River near Hetch Hetchy CA, Gage number 11276500). More than half of the runoff from the Tuolumne River results from snow melt, with pre-dam peaks in discharge occurring mainly between May and July when melting is most intense (Figure 2-2). Dam construction and operations subsequently reduced annual peak discharges by 35%, the duration of high flow periods by 40%, and average monthly discharge by 65%. In additon, much of Poopenaut Valley and the adjacent Hetch Hetchy Valley to the northeast were grazed by sheep and cattle in the 1800s and early 1900s, leading to biological and geomorphologic modification of stream and riparian systems (Greene, 1987).

Ten hectares of Poopenaut Valley adjacent to the Tuolumne River have been delineated as 12 distinct wetlands based mainly on vegetation and soil surveys (Fig. 3) (Stock et al., 2009). Cross sections perpendicular to the river that cross these wetland areas illustrate characteristic valley geometry: an asymmetric channel bounded by a levy to the southeast, an irregular flood plain on either side of the channel, and an abrupt break in slope where the valley floor meets the valley walls.

Riparian wetlands are strongly influenced by patterns of runoff, so it is not surprising that Poopenaut Valley wetlands have been impacted by a reduction in the number and duration of regular inundation periods following construction of the O'Shaughnessy Dam, in addition to historical grazing and other human activity. Staff of the US National Park Service and the San Francisco Public Utility Commission are evaluating the potential for adapting a program of controlled flooding, using increased releases from the Hetch Hechy Reservoir, as a means to provide recreational (rafting, kayaking) flows and increasing variability in an effort to restore hydrologic function along the Tuolumne River. Controlled floods have been completed along other river systems having a range of sizes and flow durations, in an effort to improve environmental conditions (Junk et al., 1989; Middleton, 1999; Tockner et al., 2000; Patten et al., 2001; Middleton, 2002; Robinson et al., 2004; Henson et al., 2007), but as in the present study, there are often challenges in balancing water supply, power generation, flood control, and a variety of environmental, social, and economic needs (Stanford et al., 1996; Poff et al., 1997; Michener and Haeuber, 1998; Sparks et al., 1998).

1.3 Materials and methods

There are three main components to the observational part of this study: characterization of shallow soils, quantifying infiltration and drainage response to controlled flooding, and measuring groundwater dynamics in response to vertical and horizontal flows from the Tuolumne River. Most of the sampling and monitoring

reported herein was completed in conjunction with a Spring 2009 controlled flood. Access to the Poopenaut Valley field site is limited, and all tools, supplies, and equipment had to be carried in and out on foot using steep trails. There is no power or telecommunication capability at the site, so all instrumentation was designed to work autonomously before, during, and after flooding. In addition, the 2009 project was initiated with only a few weeks notice and on a limited budget, so the field and associated modeling program was designed to take maximum advantage of existing information, focusing on one wetland area where there was the best opportunity to link surface water and groundwater processes and address key questions.

A series of shallow wells had been installed in Poopenaut Valley in 2007 along three transects, running perpendicular and parallel to the Tuolumne River, and additional wells with pressure gauges were added in 2009 (Figure 1-3). We focused instrumentation and modeling on a single cross-valley profile located at the southwestern end of the valley (referred to as the "primary transect"), for several reasons. Capturing the full three-dimensional variability of soil inundation, saturation, and drainage would be impractical, given limitations of time and instrumentation, so we selected a transect of sampling and measurements that (a) had a significant fraction of delineated wetland, (b) was already instrumented with piezometers, (c) had a topographic profile consistent with other parts of the valley (Fig. 3B), (d) included a pre-installed stream gauge at the river, and (e) was located where the dominant flow direction would be to and from the river (rather than down-valley parallel to the river). The latter was assured by the nearby pinch out of alluvial fill

against granitic bedrock (Fig. 3). A study of one wetland area such as this cannot be extrapolated across the entire valley with confidence, but provides critical information about one area and is useful for assessing the practicality, cost, effort, and potential benefit of a more extensive sampling and monitoring program prior to future flood events.

Soil properties were evaluated to gain insight into infiltration and drainage characteristics. Soil samples were collected at 10 cm intervals from the ground to a depth of 180 cm at locations L1, L2 and L3 along the primary transect (Fig. 3). A subset of soil samples was analyzed for grain size distribution and organic carbon content. Grain size distribution was measured using a laser diffraction particle size analyzer, after digestion in hydrogen peroxide to remove organics, freeze drying, and deflocculation in a liquid suspension with sodium metaphosphate. Grain size fraction was determined within 162 bins between 0.1 lm and 2 mm, then bins were combined along standard divisions of clay, silt and sand (4 lm and 63 lm). Soil organic carbon was measured on separate (undigested) sample splits using an elemental analyzer coupled to an isotope ratio mass spectrometer.

Volumetric soil moisture content sensors were installed in nests at locations L2 and L3, 55 m and 130 m from the Tuolumne River, respectively (Fig. 3). Sensors were placed at depths of 40 and 70 cm below ground surface (cm-bgs) at L3, and at 40, 70, and 100 cmbgs at L2. The soil moisture sensors use digital time domain transmissivity (TDT) to measure volumetric water content. The TDT sensors determine the soil moisture content within a spherical region having a diameter of 15

cm. Data collected with these TDT sensors has been compared to results based on time domain reflectometry, impedance probes, capacitance probes and other methods, and the TDT probes have proven accurate across a variety of soil types, environments, and temperatures (Blonquist et al., 2005). Soil moisture sensors were wired to a nearby control system and data logger, and were powered by a sealed lead-acid battery that was trickle-charged using a solar panel.

Autonomous pressure gauges were deployed in 19 shallow (water table) wells, arranged along three transects, and screened to depths of 1.6–4.9 m below ground surface (m-bgs) (Fig. 3). Half of the wells were installed in April 2007, and the remainder in April 2009, prior to the controlled flood discussed in this paper. Wells installed in 2007 were constructed with 5.1 cm (2 in.) diameter machine-slotted PVC, whereas the wells installed in 2009 used 3.2 cm (1.25 in.) diameter galvanized steel pipe with a 45.7 cm (18 in.) long screened drive-tip. Pressure gauges in the wells were programmed to record water levels at 15-min intervals. Absolute pressure readings were corrected for barometric response, based on a separate pressure logger deployed in air at the site. Corrected pressures were converted to water levels based on field measurements of absolute sensor depths below ground, and water levels were referenced to a common elevation datum (also used for measuring stream stage).

Instantaneous discharge values for the Tuolumne River used in this study were determined at US Geological Survey at Gage number 11276500 located at the outlet from the O'Shaughnessy Dam, with data recorded every 15 min. Local measurements of river stage were also made at 15-min intervals at temporary stations

located upstream and downstream from the ends of the primary wetland area discussed in this paper (locations TU and TD, respectively, Fig. 3), using pressure gauges deployed in stilling wells and referenced to staff plates. Precipitation data were collected by the California Department of Water Resources from the Hetch Hetchy Dam (Figure 1-1) station (HTH), operated by Hetch Hetchy Water and Power.

Subsurface temperature data were collected to quantify vertical seepage directions and rates in shallow soils in the wetland and adjacent streambed, using analytical methods described in the next section. Autonomous temperature loggers were installed in the shallow streambed of the Tuolumne River in sealed PVC tubes at locations TU and TD (Figure 1-3). Each thermal tube contained two loggers suspended 20 cm apart below the base of the stream, and the tubes were backfilled with water to ensure a good thermal contact with the surrounding soil. Thermal data were also collected at multiple depths by the soil moisture content sensors deployed at L2 and L3.

1.4 Analytical methods

1.4.1 Interpretation of seepage from thermal data

The magnitude and direction of vertical seepage were determined using heat as a tracer (e.g. Constantz and Thomas, 1996) based on time-series analysis of subsurface temperature data, summarized briefly herein (Hatch et al., 2006). Calculations were made only when conditions adjacent to subsurface temperature loggers (both in shallow wetland soils and below the Tuolumne River) were fully saturated. The

method is based on the observation that daily variations in subsurface temperatures propagate as a thermal wave, being reduced in amplitude and shifted in phase with time and depth. Data are interpreted based on the analytical solution to a one-dimensional (vertical) conduction–advection–dispersion equation, and changes in the amplitude and phase of thermal oscillations between a pair of subsurface sensors separated by a known distance. Temperature data from each sensor are filtered to isolate diurnal signals, and pairs of records are analyzed to determine the amplitude ratio (Ar) and phase shift ($\Delta\phi$) of propagating thermal waves. Thermal front velocities are calculated as:

$$v_{Ar} = \frac{2\kappa_e}{\Delta z} lnA_r + \sqrt{\frac{\alpha+v^2}{2}} \quad (1\text{-}1)$$

$$v_{\Delta\phi} = \sqrt{\alpha - 2\left(\frac{\Delta\phi 4\pi\kappa_e}{P\Delta z}\right)^2} \quad (1\text{-}2)$$

where v_{Ar} and $v_{\Delta\phi}$ are the thermal front velocities (m d^{-1}) calculated using the amplitude ratio and phase shift, respectively. κ_e is the effective thermal diffusivity of saturated soil between thermal sensors (m^2 d^{-1}), Δz is the vertical distance between sensors (m), P is period of temperature variations (d), and α is a function of fluid velocity, thermal diffusivity, and signal period. The apparent fluid velocity is calculated once per day as: $vf = v\gamma$, where vf is the velocity of the fluid front and γ is the ratio of heat capacity of the saturated soil to fluid. Because this analytical method

depends on temperature sensor spacing, rather than absolute depth, it is relatively insensitive to sedimentation and scour (common processes associated with flood events). The method is described in greater detail elsewhere (Hatch et al., 2006), and has been applied in streambeds and shallow soils undergoing managed aquifer recharge (Hatch et al., 2010; Racz et al., 2011).

1.4.2 Infiltration, drainage, and groundwater modeling

Modeling is a useful approach for understanding wetland hydrologic processes (Bradley and Gilvear, 2000; Bradley, 2002; Joris and Feyen, 2003; Boswell and Olyphant, 2007; Dimitrov et al., 2010; Shafroth et al., 2010), correlating flow regimes to hydroperiods, geomorphological and ecological changes (Bendix, 1997; Mertes, 1997; Cabezas et al., 2008; Shafroth et al., 2010), and evaluating flood response and restoration options (Springer et al., 1999; Rains et al., 2004; Acreman et al., 2007). In the present study, we focus on representing physical hydrologic processes to elucidate some of the mechanisms responsible for wetland formation and maintenance. This approach should help to make the results broadly applicable, although the detailed characteristics of individual model and restoration sites is expected to vary location by location (Schiemer et al., 1999). We have chosen to take a ‘‘soil water–groundwater’’ approach to wetland modeling because we wished to determine explicitly the connections between surface and subsurface water regimes, to understand which is most important for maintaining riparian wetland conditions, as

has been assessed in other settings (Bradley and Gilvear, 2000; Boswell and Olyphant, 2007; Staes et al., 2009; Dimitrov et al., 2010).

Our approach was to use moisture content data to quantify soil water retention and drainage characteristics, under a range of groundwater and flood scenarios, to assess the importance of competing processes. The movement and storage of soil water and groundwater were simulated using VS2DH, a variable saturation, transient, two-dimensional, porous medium model (Lapalla et al., 1987; Healy, 1990). VS2DH conserves water mass using the Richards equation for variably saturated flow (for which saturated groundwater flow is a special case):

$$\frac{\partial}{\partial x}\left[K(\psi)\frac{\partial h}{\partial x}\right] + \frac{\partial}{\partial z}\left[K(\psi)\frac{\partial h}{\partial z}\right] = C(\psi)\frac{\partial \psi}{\partial t} \qquad (1\text{-}3)$$

where x and z are spatial dimensions, K is hydraulic conductivity (m s^{-1}), ψ is pressure head (m), h is the total head (m), C is specific moisture capacity (m^{-1}), and t is time (s). The specific moisture capacity (C) is the slope of the moisture characteristic curve, $d\theta/d\psi$. The modeling domain was defined based on observations along the primary study transect, oriented perpendicular to the Tuolumne River near the downstream end of Poopenaut Valley riparian wetlands (Figure 1-3). The model domain extended from the middle of the river channel to the southeastern valley wall, 400 m away, and represented the upper 30 m of saturated aquifer and unsaturated soils above valley bedrock. The model contained 9295 grid cells with dimensions ranging from 0.1 x 1.5 m (height x width) near the ground surface in wetland areas, to

3 x 10 m at depth near the far field boundary. No-flow boundaries were assigned to the vertical side of the model domain in the middle of the river (based on symmetry) and the horizontal base of the domain. The far-field boundary opposite the river was set as a Dirichlet (constant head) boundary such that there was a pre-flood gradient resulting in groundwater flow to the river, consistent with pre-flood data from shallow wells. Initial conditions were determined from stream, groundwater, and soil water measurements made prior to flooding. A time-varying total head boundary was imposed on the ground surface of inundated areas during the flood, with the water level at the ground surface forced to follow the flood hydrograph. Water was allowed to ‘‘pond’’ on the ground surface, and the upper surface of the domain was made a potential seepage face throughout the simulations. The total head boundary representing the flood hydrograph had periods ranging from 1 to 7 days, and model time steps were 1 to 5 x 10^3 s, several orders of magnitude shorter than the periods used to model the flood hydrograph. The time steps were 1 s at the start of each boundary condition period, with a time step multiplier of 1.5 to allow a smooth system response, up to a maximum time step of 5000 s.

Unsaturated soil characteristics were modeled using the Brooks–Corey equations (Brooks and Corey, 1964), which relate soil moisture content, fluid pressure, and variably saturated hydraulic conductivity:

$$S = \frac{\theta - \theta_r}{\theta_s - \theta_r} = \left(\frac{\psi}{\psi_e}\right)^{-\lambda} \qquad (1\text{-}4)$$

$$\frac{K}{K_s} = S^{\eta} \quad (1\text{-}5)$$

where S is effective saturation (0–1), θ is volumetric water content, θ_r is residual volumetric water content, θ_s is saturated volumetric water content, ψ is pressure head (m), ψ_e is air entry pressure head (m), K is variably saturated hydraulic conductivity (m s^{-1}), and K_s is saturated hydraulic conductivity (m s^{-1}). λ and η are fitted parameters (determined for the present application by matching modeled and observed soil water contents) where λ is an index of pore size distribution and η is a function of λ. θ_r was inferred to be equal to the pre-flood soil moisture content (based on field observations, as described later), and porosity was determined from the maximum observed saturated soil moisture content. Calibrated hydraulic conductivities of saturated soils were also compared to standard relations based on grain size distributions (Carman, 1956; Bear, 1972; Shepherd, 1989; Fetter, 2001; Hazen, 1911).

The quality of the model fit to data was quantified as the root mean square error (RMSE) of 3000 soil moisture observations (n) from the shallowest water content sensor at L2 during the period of drainage following passage of the flood wave, where:

$$RSME = \sqrt{\frac{\sum(x_{obs} - x_{calc})^2}{n}} \quad (1\text{-}6)$$

The ability of the model to replicate the behavior of shallow groundwater, as measured with pressure transducers in wells along the primary transect, was also used to adjust simulation parameters, but it was determined that soil drainage characteristics were of greater importance for calibrating the model, particularly because these parameters had the greatest influence on the length of time during which shallow wetland conditions were maintained after passage of a flood wave. We explored fitting modeled to observed soil moisture values based on the Van Genuchten equation (Van Genuchten, 1980), but found that this resulted in drainage behavior that was less consistent with observed soil drainage behavior than did the Brooks–Corey equation.

1.5 Results

1.5.1 Controlled flood and extent of inundation

The Spring 2009 controlled flood in Poopenaut Valley began on 4 May (Flood Day 1, FD-1) and ended on 7 July (FD-65), with a total water release of 3.5×10^8 m^3. Prior to the flood, discharge in the Tuolumne River was 15 cubic meters per second (cms). There was a brief, intense precipitation event several days just prior to the start of the flood, and another brief precipitation event on FD-28 (Figure 1-5A), but these had little influence on channel discharge, particularly in comparison to the magnitude of the controlled flood. A rating curve for location TU, near the center of the Poopenaut Valley wetlands (Figure 1-3), was developed using stage data from this location and discharge data from USGS Gage number 11276500 (Figure 1-4A). This rating curve

was used with the DEM to calculate the extent of inundation of Poopenaut Valley wetlands as a function of stage (Figure 1-4B). The discharge hydrograph (Figure 1-5B) during the controlled flood was irregular in form, having three distinct peaks within a high-flow period lasting from 8 May to 8 June (FD-5 to FD-36). The peak of the flood occurred during 18–21 May (FD-15 to FD-18) with discharge reaching 220 cms, at which time the stage was >4 m above pre-flood conditions, and 90% of the riparian wetland area in Poopenaut Valley was inundated (Figure 1-4B).

1.5.2 Soil characteristics

Grain size analyses from soil samples collected along the primary transect are generally indicative of sandy loam, with texture varying with depth (Figure 1-6A–C). Shallower soils are more uniform (with a mean grain size of 56 lm), but there is a bimodal distribution of grain sizes between 100 and 180 cm-bgs, with modes of 78 and 140 lm. The organic carbon content of shallow soils vary between 0.7% and 7.1% by weight, with the highest values found near the ground surface at L1 and L2 (Figure 1-6D). Carbon concentrations are lower at depth at these two locations, but the pattern is reversed at location L3, with the highest values measured for the deepest samples. Measured organic carbon values are comparable to those seen in similar high-elevation wetlands that experience seasonal periodic inundation and variations in shallow water table elevation (Moorhead et al., 2000; Thompson et al., 2007). It was also apparent from visual inspection of soil samples that there were variations

with depth in soil texture and water content (finer grains retaining more moisture), consistent with expectations for layered flood-plain deposits.

Soil hydraulic conductivities were estimated using empirical relations based on grain size distribution (Hazen, 1911; Carman, 1956; Bear, 1972; Shepherd, 1989; Fetter, 2001), yielding values on the order of 10^{-7}–10^{-5} m s^{-1}. But as shown and discussed later in this paper, higher conductivity values were required for successful calibration of a numerical model of soil drainage response following passage of a flood wave.

1.5.3 Soil moisture content and water table dynamics

The soil moisture content at location L2 prior to the flood varied from 21% to 27% at depths of 40 to 100 cm-bgs, with higher values at greater depth (**Figure 1-4C**). There was a brief increase in soil moisture content associated with the precipitation event that preceded the flood, and a sustained increase in soil moisture once the flood began. Soil moisture rose abruptly to persistent values of 62–66%, interpreted to represent fully saturated conditions, as the leading edge of the flood wave passed. The soil sensor at 100 cm-bgs at L2 showed the earliest increase to saturated values, on 15 May (FD-12), 6 days before the ground surface became inundated. The soil sensor at 70 cm-bgs was next to approach saturated conditions on 17 May (FD-14), and finally the soil sensor at 40 cm-bgs indicated saturated conditions on 18 May (FD-15), coincident with ground inundation. This pattern illustrates the rising water table at 100 and 70 cm-bgs adjacent to the flooding river, and is consistent with water level

data from an adjacent shallow well. In contrast to the deeper sensors, the sensor at 40 cm-bgs became saturated immediately after the ground was inundated; it is not clear if saturation would have been achieved at this depth and location without inundation. Collectively, the data from these sensors illustrate two distinct mechanisms for saturating shallow soils below this riparian wetland: rising groundwater from below, and infiltrating floodwater from above. The relative importance of these two mechanisms for achieving and maintaining saturation is evaluated in modeling shown later.

Groundwater hydrographs and river stage data elucidate the patterns of surface water–groundwater interaction before, during, and after passage of the flood (Figure 1-7). Prior to the flood, groundwater gradients indicate flow across the southeastern riparian corridor from the valley wall towards the river, consistent with recharge occurring where the valley wall meets the valley bottom.

There was also a subtle groundwater gradient oriented from northeast to southwest, consistent with downstream flow along the Tuolumne River. However, the groundwater gradient is virtually perpendicular to the river near the southwestern end of the valley, where the valley alluvium abuts granitic bedrock and the wetland area and underlying shallow aquifer end.

Eight days after the start of the flood, the highest groundwater heads were found in the northeastern end of the aquifer (Figure 1-7B), and water flowed from the river into the aquifer throughout the field area, in a direction opposite to that before the flood. In addition, the water table gradient in the downstream direction of the river

was significantly larger, indicating a greater rate of groundwater flow through the shallow aquifer during the flood. On 28 May (FD-25), several days after the passage of the first flood peak (Figure 1-5), the water table gradient parallel to the river had decreased substantially, although river water continued to move into the aquifer. By 8 June (FD-36), after the main flood wave had passed, the primary groundwater gradient reversed again, and once more indicated flow from the aquifer to the river along the riparian corridor (Fig. 7D). However, water levels in the aquifer were elevated relative to pre-flood levels, indicating that the aquifer was still ‘‘charged’’ with flood water. This is consistent with flow through the aquifer being restricted laterally by bedrock along the valley walls and at the upstream and downstream valley ends. Groundwater levels remained highest at the southwestern end of the aquifer following passage of the flood wave, illustrating that the primary means for groundwater to leave the aquifer after being charged by the flood is subsurface discharge to the river.

1.5.4 Vertical seepage rates

Thermal data collected in the bottom of the Tuolumne River illustrate the dynamics of surface water – groundwater interactions in Poopenaut Valley (Figure 1-8). Prior to the flood, on 3 May, water seeped down into the streambed at the upstream end of the wetland study area, and up and into the river at the downstream end, consistent with the distribution of shallow groundwater heads. As river discharge increased during the flood, water was driven into the streambed at both thermal monitoring locations at

rates up to -0.5 m d^{-1} (negative = downward flow). By the time the thermal instruments were recovered in early July, streambed seepage was heading back towards pre-flood conditions. Streambed seepage patterns in the middle of the flood, when water levels in the river repeatedly moved rapidly up and down, are more difficult to interpret. The thermal time-series method is subject to greater errors when there are abrupt changes in flow rate and direction (Hatch et al., 2006), as was likely during the flood because of the complex nature of the hydrograph.

The thermal method was also applied to estimate infiltration rates using temperature data collected by the soil moisture sensors at location L2 (Figure 1-8C). Only a short segment of the thermal data collected in this location was analyzed to assess seepage rates because the time-series method, as currently developed, is applicable only under saturated conditions. Infiltration rates calculated at location L2 suggest that inundation caused an initial increase in downward flow (approaching -0.8 m d^{-1}), which subsequently reversed to upward flow once the flood wave passed, concurrent with the rise groundwater levels in the underlying aquifer.

1.5.5 Groundwater model calibration and behavior

Soil moisture data from location L2 were used to calibrate the transient, variably saturated soil and groundwater model from the time of the first inundation event at location L2 through the soil drainage following the passage of the flood wave, during 18 May to 19 June (FD-15 to -47). The complex flood hydrograph was approximated using 21 short periods of constant stage, with the total head surface boundary

condition corresponding to flood inundation levels as a function of local topography. The duration of each period depended on the period of time represented in the hydrograph. Residual and saturated soil water contents were fixed based on observations of pre-flood and mid-flood conditions (Figure 1-5C), and the remaining Brooks–Corey parameters (η, λ, and K_s) were adjusted to achieve a fit between observed and modeled soil moisture values (Figure 1-9; Table 1-1). The residual and saturation soil moisture values used for the model may seem high based on consideration of soil texture alone, but these values are similar to those found in shallow wetland soils in other settings (e.g. Sumner, 2007). We experimented with using lower residual moisture values but found a much poorer fit to field observations. We ran the model initially using homogeneous soil properties, and but added layered heterogeneity in order to achieve a satisfactory fit between observed and simulated soil water contents during the drainage period.

We found that replicating observed soil drainage behavior (Figure 1-10) at location L2 required a model with three soil layers (Figure 1-9A), with η, λ, and K_s having the highest absolute values in the shallowest soil layer (Table 1-1). Calibrated Brooks–Corey model parameters are consistent with soils comprising mainly fine sand and silt, as observed at the field site. Both K_s and λ (the pore size distribution index) appear to decrease with depth, consistent with the unimodal grain size distributions of surface soil samples, and bimodal distributions of samples at 100 cm and 180 cm depth. We do not suggest that this model stratigraphy is unique in replicating observed soil drainage behavior, or that this layering must apply

throughout the wetland area. Our preferred set of Brooks–Corey parameters generated a RMSE of 1.0% volumetric moisture content, based on comparison of 3000 model results and soil moisture data collected with the sensor at 40 cm-bgs. A sensitivity analysis of the Brooks–Corey parameters shows that k and K have the greatest impact on model results (Table 2). Changes in these parameters by ±10% increased the RMSE value by up to 370%.

Having calibrated for soil properties, we ran a series of simulations that included the entire controlled flood hydrograph to examine the importance of surface inundation versus groundwater rise in maintaining wetland conditions. Prior to the start of the flood, modeled groundwater flow was from the far field boundary towards the river, as observed (Figure 1-9B). The net flow from the aquifer to the river was 9.6×10^{-3} m^3 s^{-1} m^{-1} of river reach. If extrapolated along the reach of the Tuolumne River that flows through Poopenaut Valley, this would comprise a net gain to river discharge of 4.8×10^{-3} m^3 s^{-1}, a value too small to be resolved with confidence using standard stream gauging techniques, which have typical uncertainties that are the greater of 5–10% of gauged discharge or 0.04 m^3 s^{-1} (Schmadel et al., 2010). As the first part of the flood wave passes and river stage rises, but before the area adjacent to the river is inundated, water flows from the river into the adjacent aquifer, and the water table rises, causing a reversal in the lateral groundwater gradient (Figure 1-9C). As the river continues to rise and riparian wetlands are inundated, there is a zone of unsaturated soils that becomes temporarily trapped between infiltration from above and the rising water table from below (Figure 1-9D). Eventually the simulated

groundwater gradient reverses again after the flood wave passes, and groundwater flow is restored to the pre-flood direction, towards the river.

1.5.6 Modeling alternative flood scenarios

We explored alternative flood scenarios to evaluate options to benefit riparian wetlands while releasing less total water from the Hetch Hetchy Reservoir. The minimum acceptable wetland benefit was defined, following the USACE definition, as saturation for 14 consecutive days at 30 cm below ground surface. In the case of Hetch Hetchy flood releases, additional considerations include retaining sufficient water in the reservoir to meet anticipated municipal demand, and supplying downstream recreational benefits.

In addition, there are limitations on the rate of change of reservoir releases from Hetch Hetchy (how abruptly a flood wave can be initiated and ended) specified in the US Department of the Interior 1985 flow stipulation, and because of the mechanical operations needed to open and close valves in the O'Shaunessey Dam. At other sites where water is released from reservoirs, additional considerations could include power generation needs and restoring capacity for flood control by lowering reservoir levels.

Because there are so many considerations involved in designing a controlled flood release, we focus for illustrative purposes on three scenarios that emphasize surface water inundation of the wetland at location L2 (Figure 1-11). The extent to which any flood scenario will achieve wetland conditions will depend on soil

properties, local elevation and topography, and other factors, but we use location L2 for this analysis because achieving wetland conditions at this location by inundation should result in inundation of 90% of Poopenaut Valley riparian wetlands (Figure 1-4B). The characteristics of each flood scenario hydrograph, including stage, and duration of both inundating and non-inundating periods, have been adjusted specifically to reduce the total water requirement while meeting wetland conditions in the calibrated model.

The first scenario is a sustained release lasting 12 days, which results in 14 days of saturation at 30 cm-bgs. This is a reference case, with the water level set high enough to inundate the area of interest. The second scenario includes two days of higher stage, to inundate a larger initial area, followed by a somewhat lower stage for the remainder of a 12-day flood. Scenario 2 was intended to test whether it might be possible to delay drainage following the initially high flood stage, using a combination of inundation and raising the underlying water table, without discharging as much water as needed to maintain the higher stage throughout the flood. Scenario 3 comprises multiple cycles of higher and lower stage within a flood of the same 12 day duration, a "flood pulsing" approach that has proven useful in other restoration projects (Middleton, 1999; Tockner et al., 2000; Middleton, 2002).

Flooding during short periods, rather than constant discharge for long periods (Springer et al., 1999; Rains et al., 2004), allows for more efficient water releases that account for soil retention and drainage characteristics. In all scenarios presented, peak stages and durations were adjusted incrementally so as to achieve the minimal

saturation (wetland) objective at modeled location L2, releasing as little water as possible. Once this goal was achieved, we converted the individual stage hydrographs to discharge hydrographs based on a rating curve developed from data collected during the 2009 controlled flood (Figure 1-4). Integrating under these idealized discharge hydrographs allowed calculation of how much water would need to be released from the reservoir to achieve the desired result. Numerous alternative flood scenarios could also achieve the minimal hydrologic objective (14 days of continuous saturation down to 30 cm depth), but these three show a range of options and illustrate key issues that should be considered in designing a flood release plan.

All three flood scenarios were capable of meeting minimum wetland conditions at location L2, as did the 2009 controlled flood (Table 1-3). However, the modeled scenarios used only 28–40% of the total 2009 flood release, in part because the scenarios minimized the period of the flood that put river stage below the ground elevation at location L2 (before 19 May, after 7 June). The third flood scenario, based on cycling between higher and lower flood stage, was ideally timed to take advantage of the delayed drainage behavior of Poopenaut Valley soils, and so required the least river discharge to achieve minimal wetland goals.

We also attempted to achieve wetland conditions at location L2 with shallow saturation supported mainly by rising groundwater, but it proved to be impractical to extend wetland conditions far enough from the river in this way. In scenarios that achieved wetland conditions by shallow groundwater alone, the river discharge requirements associated with maintaining an elevated water table were far greater

than those of the other idealized flood scenarios, and were also greater than the observed total discharge during the 2009 controlled flood.

1.5.7 Alternative pre-flood groundwater conditions

Several climate studies have predicted large changes in annual precipitation and snowpack in the Sierra Nevada mountains over the next 50–100 years (Snyder and Sloan, 2005; IPCC, 2007). These changes would impact both the timing and quantity of water flowing into the Hetch Hechy reservoir, and the flow of water into Poopenaut Valley along the valley walls. The latter will have a significant influence on regional groundwater storage and flow conditions.

One of the primary considerations for riparian wetland restoration in Poopenaut Valley is the limited supply of water that can be released from Hetch Hetchy reservoir. As shown in the previous section, varying the flood duration and magnitude can be effective for meeting wetland restoration requirements while reducing the total amount of water released from the reservoir. But these scenarios were evaluated based on groundwater conditions observed in Spring 2009.

Additional simulations were run to assess how future hydrologic changes might impact saturation of wetland soils in response to flooding. We did not change the soil moisture retention parameters that were calibrated based on field observations, because these should be relatively insensitive to antecedent moisture, but focused instead on boundary and initial aquifer conditions consistent with wetter and dryer climate scenarios. If there were a larger fraction of precipitation in the

Tuolmne River Basin falling as rain rather than snow, this could result in a greater flow of water from higher elevations into Poopenaut Valley along the northwestern and southeastern valley walls earlier in the year, when much of the winter precipitation is currently stored at higher elevations as snow pack. This was represented in the model by raising the elevation of the water table at the far field boundary, bringing the water table closer to the surface below wetland areas and increasing the horizontal head gradient towards the river. Conversely, if there were less precipitation overall, or more of the current annual amount falling during a shorter winter rainy season, there could be less groundwater flowing into Poopenaut Valley, which would result in a lower water table and shallower gradient towards the river.

In all of the climate change simulations, the initial soil moisture content was the same as that measured prior to the controlled flood in 2009, 20–30%. This is based on the assumption that future controlled floods would continue to occur during the late Spring, when Poopenaut Valley is relatively warm and dry. We also assumed that the background stage (discharge) of the Tuolumne River would remain unchanged, being controlled mainly by releases from the reservoir prior to the flood.

Changes in the elevation of the water table at the far field boundary on the order of ±1 m had little influence on the duration of maintenance of wetland conditions, in comparison to results from the calibrated 2009 flood simulations (Figure 1-12). When the far field water table was lowered more than 1 m (dryer initial conditions), the constant flood and pulsed flood simulations (Scenarios 1 and 3)

provided the longest periods of wetland conditions. Even when the initial far field water table boundary was lowered by 3 m, wetland conditions were little changed in these scenarios, illustrating the importance of soil water retention relative to upflow of groundwater. Similarly, when the far field water table was elevated by >1 m (wetter initial conditions), the constant flood scenario showed no significant increase in wetland conditions. In contrast, the higher initial flood and pulsed flood simulations (Scenarios 2 and 3) showed much greater periods of saturation and wetland conditions. In these simulations, upflow of groundwater could play a much more important role in wetland hydrology. In fact, even a small increase in water table elevation would have a significant influence on the duration of soil saturation conditions in this setting.

1.6 Discussion

1.6.1 Hydrologic restoration of Poopenaut Valley wetlands

The first objective of this project was to evaluate the relative importance of inundation versus rising groundwater in establishing and maintaining riparian wetland conditions during and after controlled flooding. Observations and modeling suggest that, in the areas investigated, inundation is more efficient for this purpose than raising the water table, although a shallow water table can help to maintain soil saturation after a flood wave passes. The shallow aquifer in Poopenaut Valley is well connected to the Tuolumne River, and this means that flooding has strong short-term influence on groundwater conditions below riparian wetlands. But most of the time,

the river serves as a sink for groundwater that flows laterally from the edges of the valley. It may be that wetlands in this area were better supported by groundwater prior to installation of the O'Shaughnessy Dam, because the seasonal flood hydrograph was higher and longer (Fig. 2), and this should have helped to develop a shallow water table earlier in the season and to maintain this condition longer following the end of major rain and meltwater events.

The second objective of this study was to evaluate what kind of hydrograph might be most beneficial from a wetland restoration perspective, while simultaneously limiting the magnitude of total flood releases. A surface water–groundwater model was developed and calibrated using water content data from shallow wetland soils. Three soil layers were required to calibrate the model to the observed data. The properties of each layer agree with field observations of soil type and grain size distribution, but were optimized based on the hydrologic behavior rather than attempting to define soil properties solely based on cores. Model results indicate that "flood pulsing" is relatively efficient for improving the duration and area of wetland conditions. This approach depends on linking the timing of flood pulses to the timescale of soil drainage.

The flood scenario that is most successful in achieving a particular wetland restoration goal will also depend on initial groundwater and soil water conditions, and this will change year by year and with location in these heterogeneous systems. Modeling suggests that the flood pulsing scenario should be relatively robust for the monitored wetland even if groundwater levels are initially lower (dryer conditions)

than seen at present, and could result in a longer period of wetland saturation if groundwater levels are initially higher (wetter conditions) (Fig. 12). Wetter conditions would likely be accompanied by an increase of water availability from the Hetch Hetchy Reservoir, so there would be less need to conserve water during controlled flooding, and this could provide opportunities for inundating a larger area or maintaining saturation for a longer period of time.

Grain size and carbon analyses of shallow samples collected as part of the present study, along the primary transect, indicate significant variations in properties horizontally and with depth. Soils underlying adjacent wetland areas, identified initially on the basis of vegetation, are likely to have dissimilar wetting and drainage characteristics (Bradley et al., 2010). This suggests that there will be considerable spatial variability in wetland response to controlled flooding, making local soil characterization and monitoring important for both wetland delineation and flood management.

Our results also suggest that soil textural analysis may have limited use in characterizing hydrologic properties in the absence of in situ drainage measurements. We suspect that the hydraulic conductivity values estimated using in situ soil moisture data and model calibration (Table 1) are higher than values estimated based on grain size distribution because of preferential flow paths resulting from biological activity (burrowing, root tubules, etc.). This interpretation is consistent with soil moisture data indicating effective soil porosity >60%, considerably higher than would

be expected from a simple mixture of fine sand and silt, and is further supported by field observations of drainage into burrows during inundation.

The benefits of inundation to maintaining wetland conditions in Poopenaut Valley are likely to vary spatially along the Tuolumne River, independent of heterogeneity in soil and wetland types. At the southwestern end of the valley, where the river passes from alluvium to bedrock, groundwater that flows parallel to the river is forced to move upward and towards the river. Seepage rates calculated from temperature data collected with the soil moisture sensors at L2 show that water tends to seep upward through the wetland soils within a few days after the passage of a flood wave. This helps to extend the beneficial influence of seasonal and controlled flooding in this area; a similar benefit may not be achieved higher (upriver) in the valley.

Riparian wetlands in Poopenaut Valley are likely to be undergoing a period of transition, after decades of grazing on the valley floor, followed by installation of a large dam and associated modifications to the seasonal hydrograph of the Tuolumne River. Repeated flood events will help to establish wetland conditions for the short term, and should have longer term impacts by helping to deliver sediment to wetland areas. As wetland conditions develop and improve, leading to more obligate plants and hydric soils, wetland areas will slow the movement of floodwater, leading to the deposition and trapping of fine sediment, which should improve soil moisture retention in riparian areas. In addition to benefiting wetland conditions, controlled

flooding can also contribute to improved nutrient cycling and creation of more complex riverine habitats.

1.6.2 Study applicability and limitations

Results of this study show that a modest field instrumentation and sampling program can provide insights regarding surface water - groundwater interactions and the establishment of riparian wetland conditions. The simultaneous collection of shallow groundwater level and soil moisture data helped to quantifying the relative importance of rising groundwater versus inundation during flooding, and was essential for calibration of a numerical model. Additional field tests and sampling, including more extensive soil sampling and slug testing, would have provided additional benefit during model calibration. Time, budget, and access limitations required that this study be focused on a relatively small area, but results can be used to guide future field and numerical work if justified on the basis of restoration and water management goals. A much more extensive field and modeling effort would be required to account for the heterogeneity of shallow soils and the threedimensional nature of surface and subsurface fluid flow pathways throughout Poopenaut Valley wetlands.

There are numerous metrics for evaluating the success of wetland restoration. The USACE definition used in this study was observationally and computationally convenient, but satisfying this constraint should not be viewed as a de facto indication of wetland health. There would also be benefit in biological and biogeohemical

sampling and monitoring in order to quantify the success of wetland restoration efforts over time, ideally done simultaneously with hydrologic studies to link processes and conditions with confidence. When considering wetland restoration and health over even longer time periods, it could also be useful to incorporate larger floods at five or ten year intervals (Capon, 2003; Hughes and Rood, 2003), if water availability permits.

A saturated–unsaturated numerical model proved useful for interpreting field observations and testing a variety of flood scenarios. The model domain was cast in two dimensions, following careful selection of a focused field transect where this flow regime was expected (and subsequently confirmed). The representation of soil properties was layered, as needed to replicate observed drainage behavior, but was otherwise highly idealized. The code used for this analysis, VS2DH, represents transport of a single (liquid) phase, and as such does not simulate air that would be trapped in shallow soils between the rising water table and a wetting front extending downward following rapid flood inundation (Heliotis and DeWitt, 1987). This relatively simple model worked well to achieve the stated goals of this project, but a multiphase flow model might be helpful for resolving fine-scale flow paths of both water and air in the shallow soil. The model also neglected evapotranspiration, although VS2DH can represent this process, mainly because we were interested in a relatively short time period associated with flooding and drainage response. Modeling evapotranspiration is likely to be more important in studies that extend across several

seasons or multiple years, particularly in arid climates (Gerla, 1992), and would require collection of additional field data for calibration purposes.

The direct application of these results to restoration projects in other riparian wetlands and floodplains impacted by upstream flow regulation will depend on specific hydrologic conditions. But the overall approach taken in this study should be broadly useful. Simultaneous monitoring of shallow groundwater, soil moisture, stream discharge and stage, and streambed seepage throughout a controlled flood event provides information that is essential for resolving the relative importance of surface and subsurface hydrologic processes in saturation of wetland soils. A calibrated model is useful for evaluation of hypothetical controlled flooding and climate change scenarios, particularly where there are limitations to the water available for flood releases. Model results could be tested and extended through additional monitoring and analyses, including an evaluation of the importance of flood duration, rate of change of discharge during flooding, and the depth to a shallow water table (Nicol and Ganf, 2000; Sprenger et al., 2002; Siebentritt et al., 2004; Stromberg et al., 2007). Additional studies should be completed in riparian settings to help determine the typical importance of surface versus subsurface water in developing wetlands, and to assist in resource management for the benefit of environmental, agricultural, municipal, and recreational needs.

1.7 Conclusions

We completed a study of riparian wetland response to a controlled flood, combining soil sampling, analyses and in situ data collection; a two-dimensional saturated–unsaturated numerical model of flood response; and evaluation of flood scenarios capable of achieving a desired metric of wetland function based on soil saturation and drainage characteristics. Observations of soil moisture and groundwater levels were used for model calibration. The model was subsequently applied using several controlled flooding scenarios, with the goal of establishing wetland conditions (saturated soils at 30 cm depth for 14 consecutive days) while limiting total water released during the flood. Several model scenarios were capable of achieving the wetland metric while discharging considerably less water than was released during the 2009 controlled flood.

The ability of riparian soils to maintain wetland conditions in this setting depends mainly on: the height and duration of the flood wave (which determine the spatial and temporal extent of inundation), and soil drainage characteristics and the depth to the underlying water table (which determine the length of time following passage of a flood wave during which saturation is maintained).

In the riparian wetland monitored as part of the present study, inundation was found to be more important than a rising water table in establishing wetland conditions during a controlled flood, but this result depends, in part on the antecedent water table elevation. Model scenarios that included a higher initial water table achieved wetland conditions for a longer time based on the sample flood hydrograph.

In contrast, a lower initial water table resulted in a somewhat shorter period of shallow soil saturation, but in this case, soil drainage behavior was more important in determining the extent of wetland development.

Soil drainage characteristics during restoration will depend, in turn, on repeated short-term development of wetland conditions by controlled flooding, as this helps to move sediment out of the primary channel and into riparian areas, and contributes to an increase of organic carbon in shallow soils. Thus the benefits of controlled flooding to riparian wetlands should increase with time. Optimizing for multiple benefits from controlled flooding is likely to become increasingly important in future years, as hydrologic conditions become more variable and demand increases for limited fresh water resources. Future studies such as this one can help with developing a mechanistic understanding of links between river and wetland hydrology and associated ecosystem function.

Acknowledgements

This research was supported by the Committee on Research (University of California, Santa Cruz), the US National Science Foundation Graduate Fellowship Program, and the US National Park Service (Award J8CO790007). Critical lab and field support was provided by Dan Sampson, Lucas Beem, Kerri Johnson, Ted Baker, Brianne Davidson, Aaron Rinehart, Josh Baccei, and Roger Putnam. This manuscript benefited from thoughtful reviews by G. Stock and M. Buhler, and two anonymous reviewers.

References

Acreman, M.C., Fisher, J., Stratford, C.J., Mould, D.J., Mountford, J.O., 2007. Hydrological science and wetland restoration: some case studies from Europe. Hydrol. Earth Syst. Sci. 11, 158–169.

Ballantine, K., Schneider, R., 2009. Fifty-five years of soil development in restored freshwater depressional wetlands. Ecol. Appl. 19, 1467–1480.

Barbier, E.B., 1993. Sustainable use of wetlands – valuing tropical wetland benefits: economic methodologies and applications. Geogr. J. 159, 22–32.

Bayley, P., 1995. Understanding large river: floodplain ecosystems. BioScience 45(3), 153–158.

Bear, J., 1972. Dynamics of Fluids in Porous Media. American Elsevier, New York, NY.

Bendix, J., 1997. Flood disturbance and the distribution of riparian species diversity. Geogr. Rev. 87 (4), 468–483.

Blonquist, J.M., Jones, S.B., Robinson, D.A., 2005. Standardizing characterization of electromagnetic water content sensors: Part 2. Evaluation of seven sensing systems. Vadose Zone J. 4, 1059–1069.

Boswell, J.S., Olyphant, G.A., 2007. Modeling the hydrologic response of groundwater dominated wetlands to transient boundary conditions: implications for wetland restoration. J. Hydrol. 332, 467–476.

Bovee, K., Scott, M., 2002. Implications of flood pulse restoration for Populus regeneration on the upper Missouri River. River Res. Appl. 18 (3), 287–298.

Bradley, C., 2002. Simulation of the annual water table dynamics of a floodplain wetland, Narborough Bog, UK. J. Hydrol. 261, 150–172.

Bradley, C., Clay, A., Clifford, N.J., Gerrard, J., Gurnell, A.M., 2010. Variations in saturated and unsaturated water movement through an upland floodplain wetland, mid-Wales, UK. J. Hydrol. 393, 349–361.

Bradley, C., Gilvear, D.J., 2000. Saturated and unsaturated flow dynamics in a floodplain wetland. Hydrol. Process. 14, 2945–2958.

Brandt, S., 2000. Classification of geomorphological effects downstream of dams. Catena 40 (4), 375–401.

Brinson, M., Lugo, A., Brown, S., 1981. Primary productivity, decomposition and consumer activity in freshwater wetlands. Annu. Rev. Ecol. Syst. 12, 123–161.

Brock, M., Rogers, K., 1998. The regeneration potential of the seed bank of an ephemeral floodplain in South Africa. Aquat. Bot. 61 (2), 123–135.

Brooks, R.H., Corey, A.T., 1964. Hydraulic properties of porous media. Hydrology Paper No. 3, Civil Engineering Dept. Technical Report, Colo. State Univ., Fort Collins, Colo.

Brunke, M., 2002. Floodplains of a regulated southern alpine river (Brenno, Switzerland): ecological assessment and conservation options. Aquat. Conserv. 12 (6), 583–599.

Cabezas, A., Gonzalez, E., Gallardo, B., Garc´ıa, M., Gonzalez, M., Com´ın, F., 2008. Effects of hydrological connectivity on the substrate and understory structure of riparian wetlands in the Middle Ebro River (NE Spain): implications for restoration and management. Aquatic Sciences – Research Across Boundaries 70 (4), 361–376.

Capon, S., 2003. Plant community responses to wetting and drying in a large arid floodplain. River Res. Appl. 19 (5-6), 509–520.

Carman, P.C., 1956. Flow of Gases through Porous Media. Butterworths Scientific Publications, London.

Constantz, J., Thomas, C.L., 1996. The use of streambed temperature profiles to estimate the depth, duration and rate of percolation beneath arroyos. Water Resour. Res. 32, 3597–3602.

Costanza, R., dArge, R., de Groot, R., Farber, S., Grasso, M., Hannon, B., Limburg, K., Naeem, S., ONeill, R., Paruelo, J., Raskin, R., Sutton, P., van den Belt, M., 1997. The value of the world's ecosystem services and natural capital. Nature 387, 253–260.

Cowardin, L.M., 1978. Wetland classification in United-States. J. Forest. 76, 666–668.

Dahl, T.E., 1990. Wetlands Losses in the United States, 1780s to 1980s. Department of the Interior, Fish and Wildlife Service, Washington, DC.

Dimitrov, D.D., Grant, R.F., Lafleur, P.M., Humphreys, E.R., 2010. Modeling the subsurface hydrology of Mer Bleue Bog. Soil Sci. Soc. Am. J. 74, 680–694.

Dynesius, M., Nilsson, C., 1994. Fragmentation and flow regulation of river systems in the northern third of the world. Science 266, 753–762.

Fetter, C.W., 2001. Applied Hydrogeology. Prentice-Hall, NJ.

Gerla, P., 1992. The relationship of water-table changes to the capillary fringe, evapotranspiration, and precipitation in intermittent wetlands. Wetlands 12(2), 91–98.

Graf, W.L., 1999. Dam nation: a geographic census of American dams and their large-scale hydrologic impacts. Water Resour. Res. 35, 1305–1311.

Greene, L., 1987. Yosemite: The park and it's resources; A history of the discovery, management, and physical development of Yosemite National Park, California. Technical report, National Park Service.

Hatch, C.E., Fisher, A.T., Revenaugh, J.S., Constanz, J., Ruehl, C., 2006. Quantifying surface water–groundwater interactions using time series analysis of streambed thermal records: method development. Water Resour. Res., 42, W10410.

Hatch, C.E., Fisher, A.T., Ruehl, C., Stemler, G., 2010. Spatial and temporal variations in streambed hydraulic conductivity quantified with time-series thermal methods. J. Hydrol. 389, 276–288.

Hazen, A. In Discussion of 'Dams on sand foundations' by A.C. Koenig. Trans. AGU, 14th Ann. Mtg., 1911, pp. 446–460.

Healy, R.W., 1990. Simulation of solute transport in variably saturated porous media with supplemental information on modifications to the US Geological Survey's computer program VS2D. Technical report, US Geol. Surv. Water Resour. Invest. Rep.

Heliotis, F., DeWitt, C., 1987. Rapid water table responses to rainfall in a northern peatland ecosystem. J. Am. Water. Resour. Assoc. 23 (6), 1011–1016.

Henson, S.S., Ahearn, D.S., Dahlgren, R.A., Nieuwenhuyse, E.V., Tate, K.W., Fleenor, W.E., 2007. Water quality response to a pulsed-flow event on the Mokelumne River, California. River Res. Appl. 23, 185–200.

Huber, N.K., 1990. The late Cenozoic evolution of the Tuolumne River, Central Sierra-Nevada, California. Geol. Soc. Am. Bull. 102, 102–115.

Hughes, F.M.R., Rood, S.B., 2003. Allocation of river flows for restoration of floodplain forest ecosystems: a review of approaches and their applicability in Europe. Environ. Manage. 32, 12–33.

IPCC. Fourth Assessment Report of the Intergovernmental Panel on Climate Change, 2007.

Johansson, M., Nilsson, C., 2002. Responses of riparian plants to flooding in freeflowing and regulated boreal rivers: an experimental study. J. Appl. Ecol. 39 (6), 971–986.

Joris, I., Feyen, J., 2003. Modelling water flow and seasonal soil moisture dynamics in an alluvial groundwater-fed wetland. Hydrol. Earth Syst. Sci. 7 (1), 57–66.

Junk, W.J., Bayley, P.B., Sparks, R.E., 1989. The flood pulse concept in river floodplain systems. Can. Spec. Publ. Fish. Aqua. Sci. 106, 110–127.

Kondolf, G., 1997. Hungry water: effects of dams and gravel mining on river channels. Environ. Manage. 21, 533–552.

Lapalla, E., Healy, R., Weeks, E., 1987. Documentation of computer program vs2d to solve the equations of fluid flow in variable saturated porous media. Technical report, US Geol. Survey. Water Resour. Invest. Rep.

Mahoney, J.M., Rood, S.B., 1998. Streamflow requirements for cottonwood seedling recruitment: an integrative model. Wetlands 18, 634–645.

Mertes, L., 1997. Documentation and significance of the perirheic zone on inundated floodplains. Water Resour. Res. 33 (7), 1749–1762.

Michener, W.K., Haeuber, R.A., 1998. Flooding: natural and managed disturbances – a special issue of bioscience devoted to flooding as a disturbance. BioScience 48, 677–680.

Middleton, B., 1999. Wetland Restoration: Flood Pulsing and Disturbance Dynamics. John C. Wiley & Sons, Inc., New York.

Middleton, B., 2002. Flood Pulsing in Wetlands: Restoring the Natural Hydrologic Balance. John C. Wiley & Sons, Inc., New York.

Moorhead, K., Moynihan, R., Simpson, S., 2000. Soil characteristics of four southern Appalachian fens in North Carolina, USA. Wetlands 20 (3), 560–564.

Nicol, J., Ganf, G., 2000. Water regimes, seedling recruitment and establishment in three wetland plant species. Mar. Freshwater Res. 51 (4), 305–309.

Nilsson, C., Berggren, K., 2000. Alterations of riparian ecosystems caused by river regulation. BioScience 50 (9), 783–792.

Orr, C.H., Stanley, E.H., Wilson, K.A., Finlay, J.C., 2007. Effects of restoration and reflooding on soil denitrification in a leveed midwestern floodplain. Ecol. Appl. 17, 2365–2376.

Patten, D.T., Harpman, D.A., Voita, M.I., Randle, T.J., 2001. A managed flood on the Colorado River: background, objectives, design and implementation. Ecol. Appl. 11, 635–643.

Poff, N.L., Allan, J.D., Bain, M.B., Karr, J.R., Prestegaard, K.L., Richter, B.D., Sparks, R.E., Stromberg, J.C., 1997. The natural flow regime: a paradigm for river conservation and restoration. BioScience 47, 769–784.

Racz, A.J., Fisher, A.T., Schmidt, C.I., Lockwood, B., Huertos, M.L., 2011. Spatial and temporal infiltration dynamics during managed aquifer recharge. Ground Water, doi:10.1111/j.1745-6584.2011.00875.x

Rains, M., Mount, J., Larsen, E., 2004. Simulated changes in shallow groundwater and vegetation distributions under different reservoir operations scenarios. Ecol. Appl. 14 (1), 192–207.

Revenga, C., Brunner, J., Henninger, N., Payne, R., Kassem, K., 2000. Pilot analysis of global ecosystems. Freshwater systems. Technical report, World Resources Institute.

Robinson, C.T., Uehlinger, U., Monaghan, M.T., 2004. Stream ecosystem response to multiple experimental floods from a reservoir. Riv. Res. Appl. 20, 359–377.

San Francisco Public Utilities Commission: Water Enterprise, 2009. Water supply availability study for city and county of san francisco. Technical report.

Schiemer, F., Baumgartner, C., Tockner, K., 1999. Restoration of floodplain rivers: the Danube restoration project. Regul. River 15 (1-3), 231–244.

Schmadel, N., Neilson, B., Stevens, D., 2010. Approaches to estimate uncertainty in longitudinal channel water balances. J. Hydrol. 394 (3–4), 357–369.

Shafroth, P., Wilcox, A., Lytle, D., Hickey, J., Andersen, D., Beauchamp, V., Hautzinger, A., McMullen, L., Warner, A., 2010. Ecosystem effects of

environmental flows: modelling and experimental floods in a dryland river. Freshwater Biol. 55 (1), 68–85.

Shepherd, R.G., 1989. Correlations of Permeability and Grain Size. Ground Water 27, 633–638.

Siebentritt, M., Ganf, G., Walker, K., 2004. Effects of an enhanced flood on riparian plants of the River Murray, South Australia. River Res. Appl. 20 (7), 765–774.

Snyder, M., Sloan, L., 2005. Transient future climate over the western United States using a regional climate model. Earth Interact. 9 (11), 1–21.

Sparks, R.E., Nelson, J.C., Yin, Y., 1998. Naturalization of the flood regime in regulated rivers: the case of the upper Mississippi River. BioScience 48, 706–720.

Sprenger, M., Smith, L., Taylor, J., 2002. Restoration of riparian habitat using experimental flooding. Wetlands 22 (1), 49–57.

Springer, A.E., Wright, J.M., Shafroth, P.B., Stromberg, J.C., Patten, D.T., 1999. Coupling groundwater and riparian vegetation models to assess effects of reservoir releases. Water Resour. Res. 35, 3621–3630.

Staes, J., Rubarenzya, M.H., Meire, P., Willems, P., 2009. Modelling hydrological effects of wetland restoration: a differentiated view. Water Sci. Technol. 59, 433–441.

Stanford, J., Ward, J., Liss, W., Frissell, C., Williams, R., Lichatowich, J., Coutant, C., 1996. A general protocol for restoration of regulated rivers. Regul. River 12 (4), 391–414.

Stock, G.J., Roche, J., Butler, M., Della-Santina, D., Clor, L., Holmquist, J., Schmidt-Gengenbach, J., 2009. Looking downstream: ecological responses to an altered hydrologic regime downstream of Hetch Hetchy reservoir, yosemite national park 2007. Technical report, Yosemite National Park Division of Resources Management and Science.

Stromberg, J., Beauchamp, V., Dixon, M., Lite, S., Paradzick, C., 2007. Importance of low-flow and high-flow characteristics to restoration of riparian vegetation along rivers in arid south-western United States. Freshwater Biol. 52 (4), 651.

Sumner, D., 2007. Effects of capillarity and microtopography on wetland specific yield. Wetlands 27 (3), 693–701.

Thompson, Y., Sandefur, B., Miller, J., Karathanasis, A., 2007. Hydrologic and edaphic characteristics of three mountain wetlands in southeastern Kentucky, USA. Wetlands 27 (1), 174–188.

Tockner, K., Malard, F., Ward, J.V., 2000. An extension of the flood pulse concept. Hydrol. Process. 14, 2861–2883.

Turner, K., 1991. Economics and wetland management. Ambio, 59–63.

US Army Corps of Engineers, 2008. Interim regional supplement to the corps of engineers wetland delineation manual: Western mountains, valleys, and coast region. Technical report, Vicksburg, MS. ERDC/EL TR-08-13.

Van Genuchten, M.T., 1980. A closed-form equation for predicting hydraulic conductivity of unsaturated soils. Soil Sci. Soc. Am. J. 44, 892–898.

Ward, J., Tockner, K., Uehlinger, U., Malard, F., 2001. Understanding natural patterns and processes in river corridors as the basis for effective river restoration. Regul. River 17 (4-5), 311–323.

Whiting, G., Chanton, J., 2001. Greenhouse carbon balance of wetlands: methane emission versus carbon sequestration. Tellus B 53 (5), 521–528.

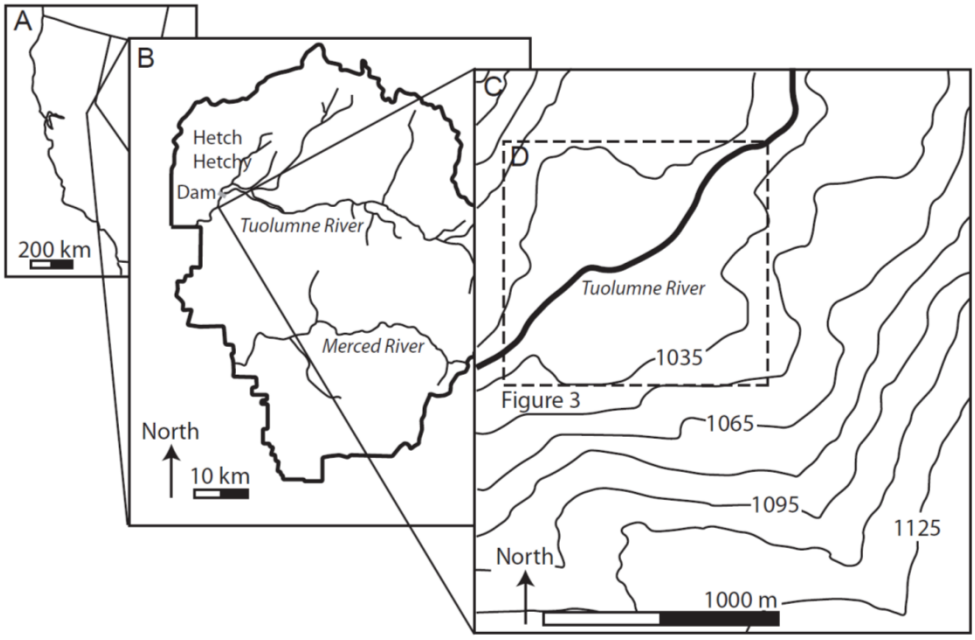

Figure 1-1 Site maps. (A) Index map showing location of field area in the Sierra Nevada range of California. (B) Field area is located approximately three kilometers downstream of the Hetch Hetchy Reservoir in Yosemite National Park, CA. (C) Riparian wetlands are located adjacent to the Tuolumne River, at the southwestern end of the Poopenaut Valley. Area labeled 'D' is shown in Figure 1-3 with instrument locations.

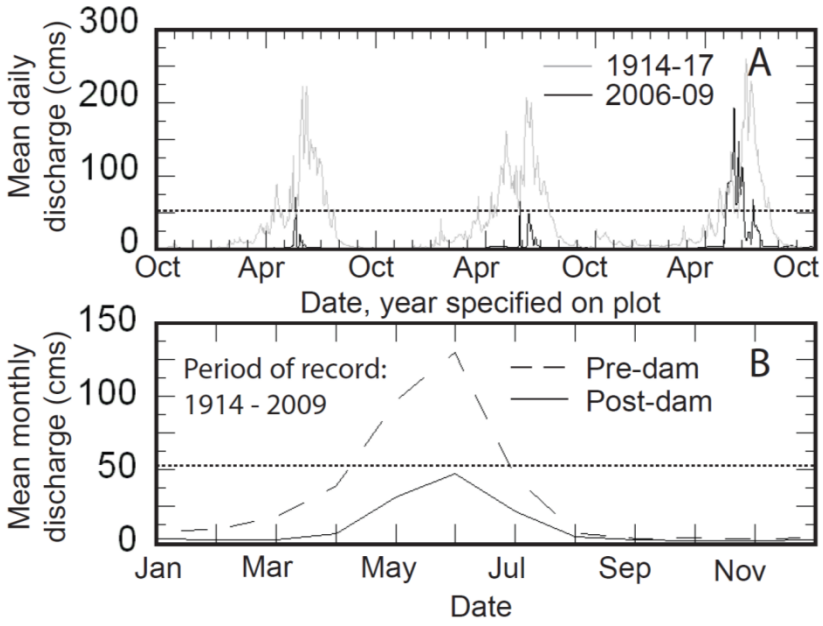

Figure 1-2 (A) Three years of average daily discharge on the Tuolumne River from pre-dam construction (1914–1917) and post-dam construction (2006–2009). This paper focuses on wetland soil response during and after the 2009 controlled flood release. (B) Average monthly discharge rates from pre-dam construction (1910–1923) and post-dam construction (1980–2010) periods. Data from USGS gaging station #11276500, downstream of the O'Shaughnessy Dam. The horizontal dotted line on each plot indicates the discharge required in inundate 50% of the wetland area within the valley.

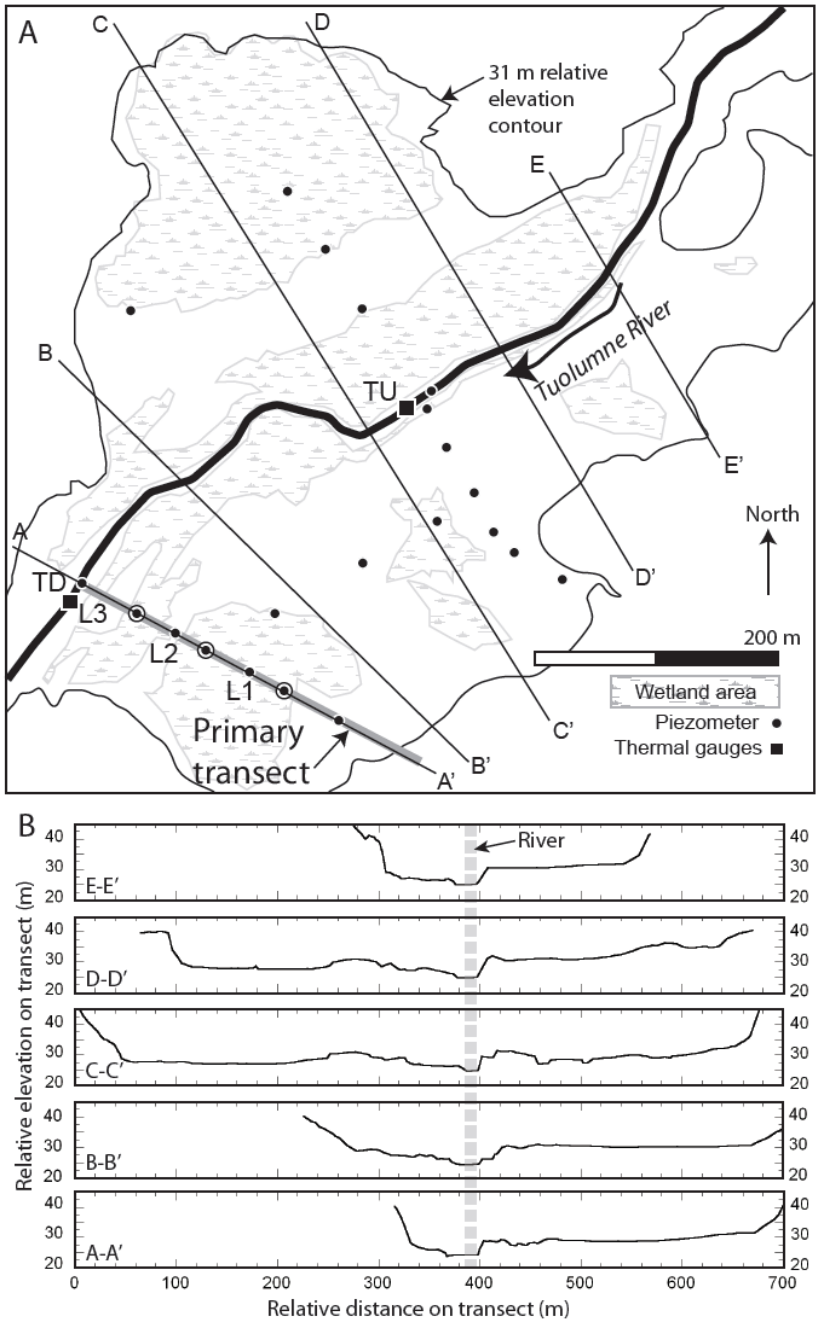

Figure 1-3 (A) The study area showing instrument and field test locations. The modeling study simulates conditions along the primary transect. (B) Five elevation transects perpendicular to the river.

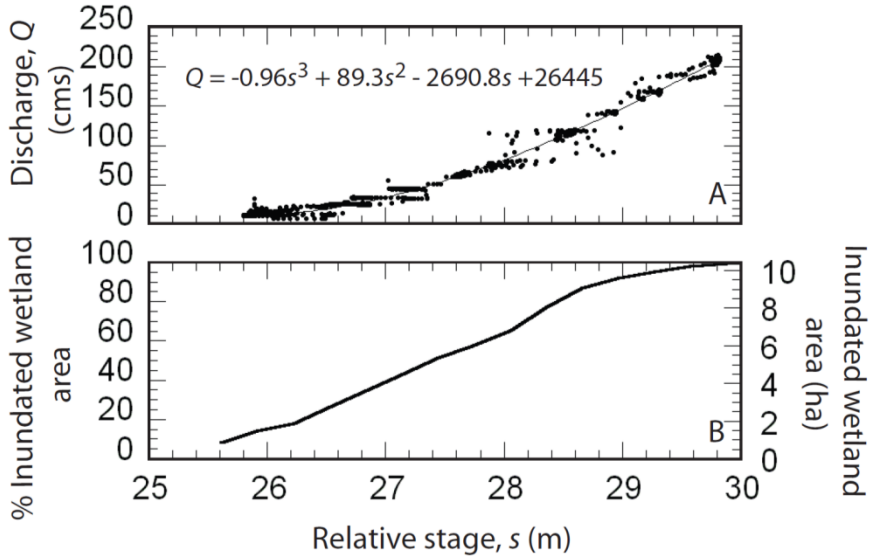

Figure 1-4 (A) Rating curve developed using river stage data from Poopenaut Valley and discharge measured at the USGS gaging station #11276500, (B) River stage and inundated wetland area, shown as percent of total wetland area and in hectares.

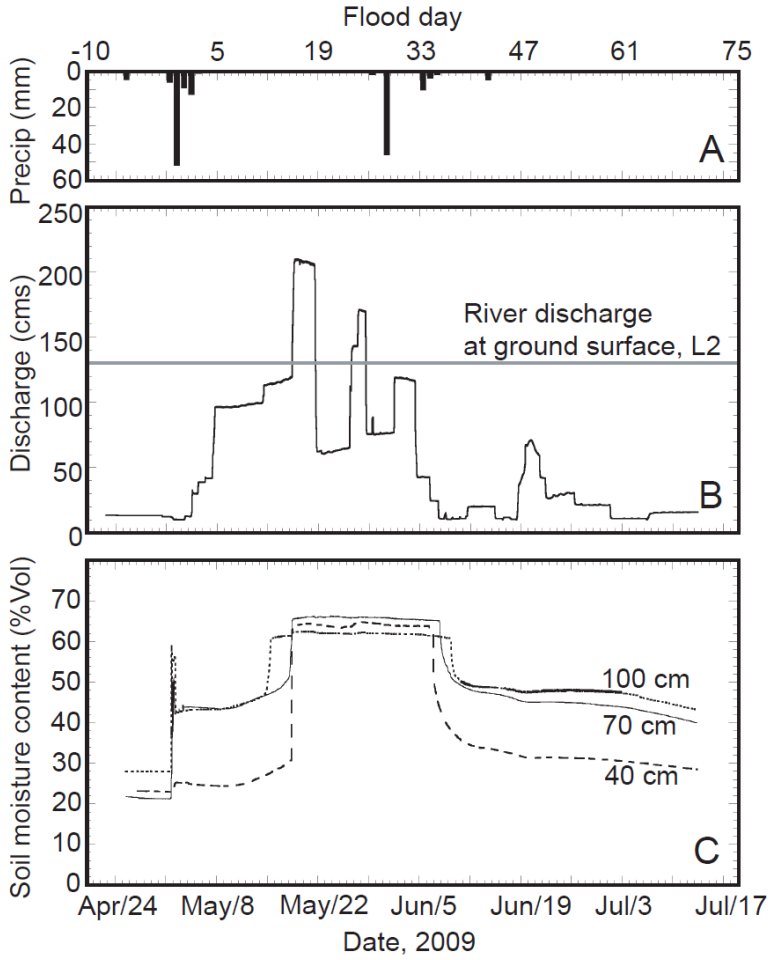

Figure 1-5 (A) Precipitation record, (B) discharge measured on the Tuolumne River at USGS gaging station #11276500. The discharge level where location L2 is inundated with flood water is shown at 130 cms, (C) volumetric soil moisture content observations from L2, measured at three depths: 40 cm, 70 cm, and 100 cm below ground surface, as indicated.

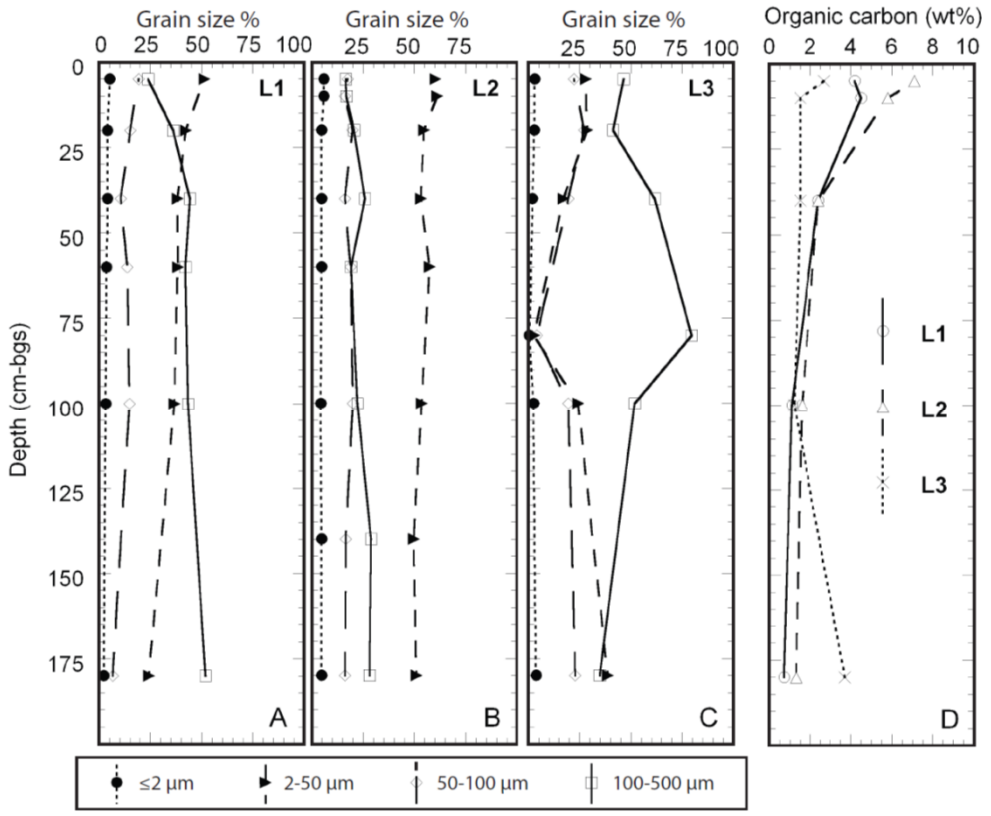

Figure 1-6 Soil properties. (A) Grain size at L1, (B) grain size at L2, (C) grain size at L3. Grain size data were analyzed at much higher resolution, but binned within the ranges shown. (D) Organic carbon content at L1, L2 and L3.

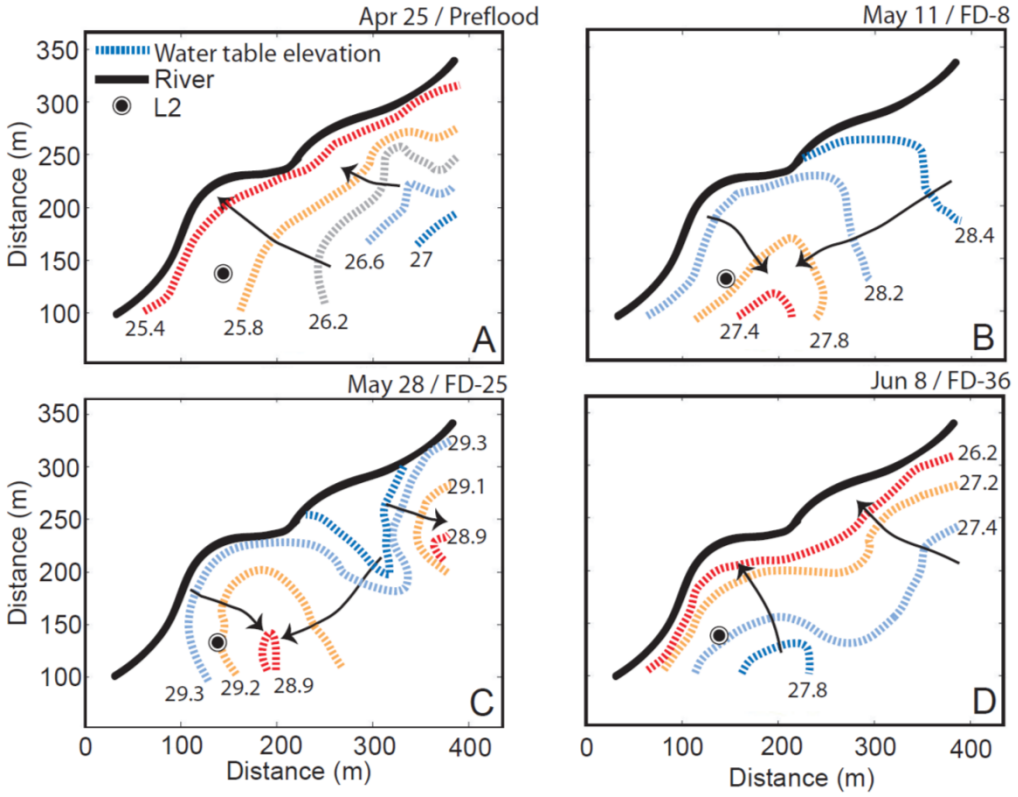

Figure 1-7 Contours of groundwater potential (meters relative elevation) south of the Tuolumne River, contoured by hand based on water level records collected in 19 water table wells (profiles indicated with dashed lines, locations shown in Figure 1-3). Location of monitoring and sampling site L2 shown with circle. Arrows indicate general trend of groundwater gradients. (A) April 25 (preflood), (B) May 12 (FD-8), (C) May 28 (FD-25), (D) June 8 (FD-36).

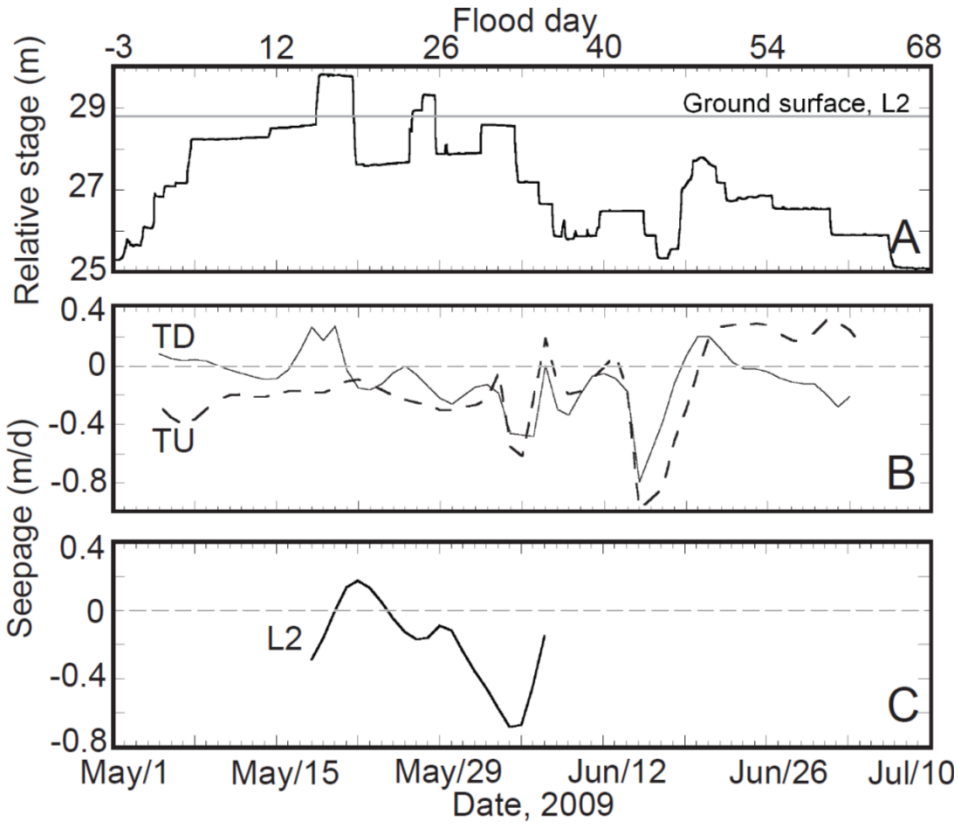

Figure 1-8 (A) Stage hydrograph of the Tuolumne River. Horizontal line indicates ground level at location L2. (B) Seepage calculated from thermal data collected at locations TU and TD in the streambed (shown on Figure 1-3). (C) Seepage calculated from thermal data during period of saturation at location L2. Positive values indicate upward flow, negative values indicate downward flow.

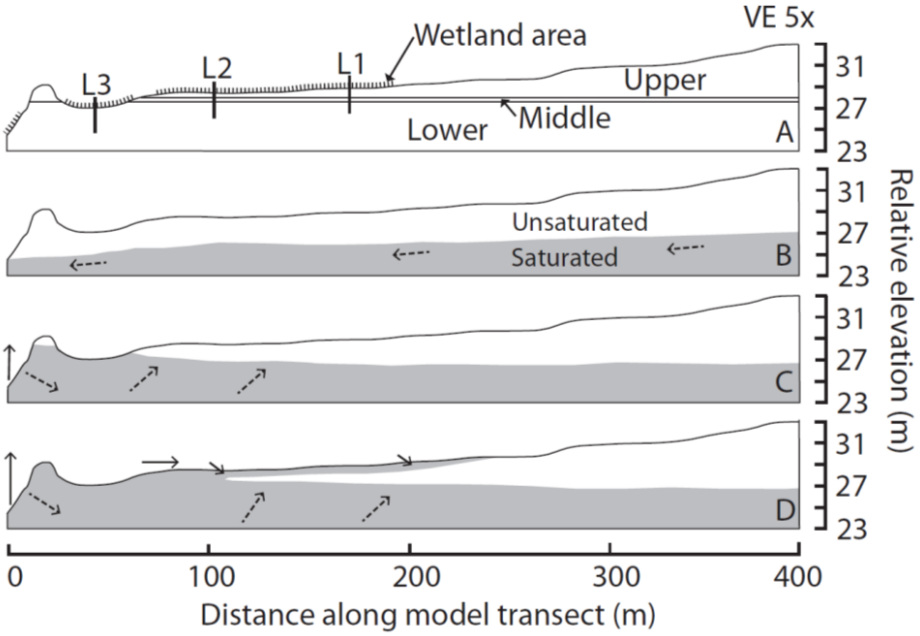

Figure 1-9 (A) The upper 10 m simulated by the model geometry showing three soil layers used to simulate Transect 1. L1, L2 and L3 are labeled and wetland locations shown. The model extends for an additional 22 m below what is shown. (B-D) Model results showing the dynamics of the saturated-unsaturated zone interface at FD-0, FD-10, and FD-15, respectively. Dashed arrows indicate direction of groundwater flow, and solid arrows indicate direction of surface water flow.

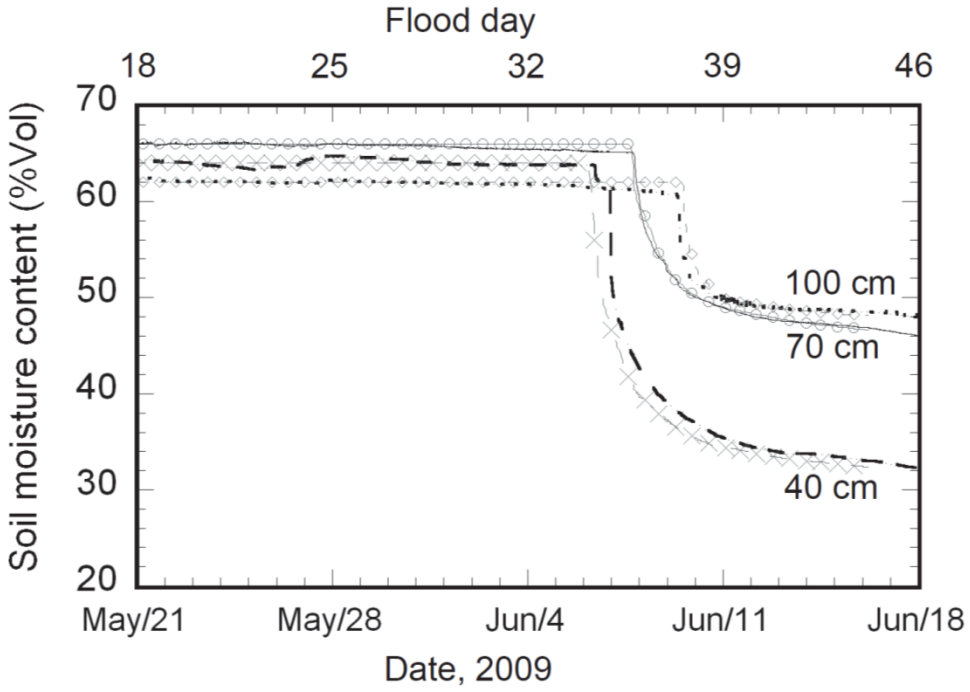

Figure 1-10 Calculated soil moisture content values are plotted with the observed values at L2. Calculated values are shown with marker symbols: diamonds for 100, circles for 70 and Xs for 40 cm-bgs.

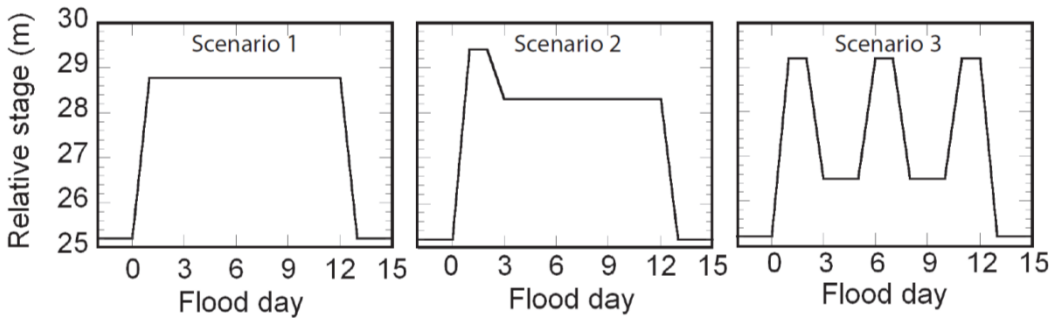

Figure 1-11 Three alternative flood scenarios tested with the model. All three scenarios will maintain saturation at 30 cm-bgs for 14 consecutive days, meeting wetland conditions specified by the USACE. Scenario 1: Constant stage reaching the ground at L2. Scenario 2: Brief period of inundation at L2, followed by a constant lower stage. Scenario 3: Multiple cycles of high and low stage.

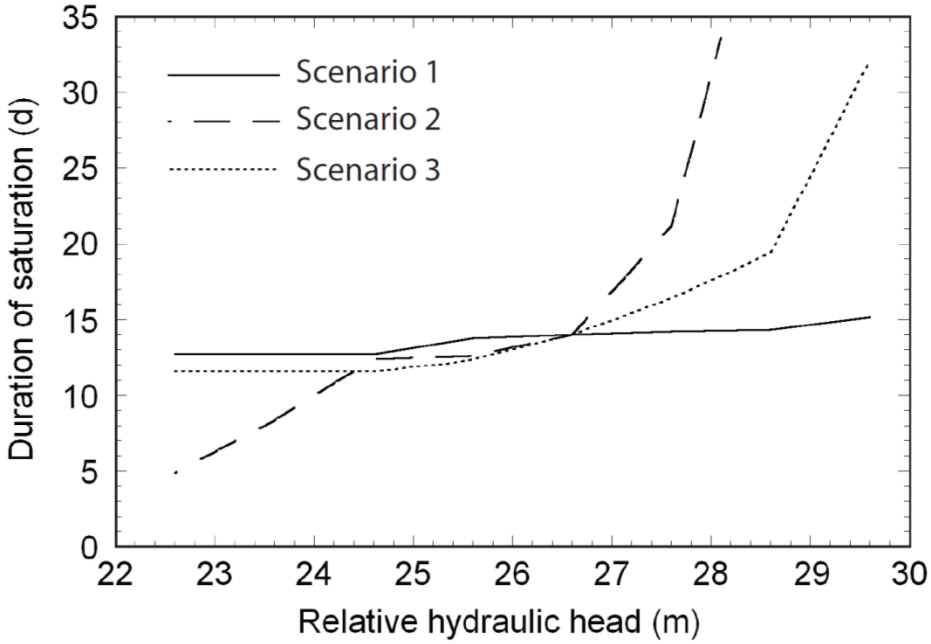

Figure 1-12 Days of saturation at 30 cm-bgs for three flood scenarios with varying antecedent water table depths.

Table 1-1 Model parameters

Layer	K_s (m/s)	θ_r	θ_s	η	λ
Shallow	8.0×10^{-4}	0.22	0.62	-0.15	0.8
Middle	2.5×10^{-4}	0.22	0.64	-0.05	0.25
Deep	1.0×10^{-4}	0.22	0.6	-0.01	0.12

K_s is saturated hydraulic conductivity

θ_r is residual moisture content

θ_s is saturated moisture content

η and λ are Brooks-Corey parameters

Soil saturation and conductivity parameters for three soil layers used in VS2DH to model surface water-groundwater flow on the primary transect of Poopenaut Valley.

Table 1-2 Model parameter sensitivity analysis results

Variation	K_s	η	λ
10% Increase	1.1	1.1	1.2
10% Decrease	2.9	1.7	3.8

The RSME between water content values measured during the drainage period and those calculated by the model, varying the Brooks-Corey parameters and saturated hydraulic conductivity by ±10%. The RSME for the original model parameters is 1.0% volumetric moisture content.

Table 1-3 Flood scenario results

Flood scenario	Q (m^3)	% of 2009 release
#1	1.4×10^8	40
#2	1.2×10^8	34
#3	9.7×10^7	28

Total water released and percent of water released in the 2009 controlled flood release for three scenarios. All scenarios meet the US Army Corps of Engineers wetland requirements.

Chapter Two

ASSESSING PLACEMENT OF MANAGED AQUIFER RECHARGE SITES WITH GIS AND NUMERICAL MODELING

Abstract

We completed a geographic information system (GIS) analysis to assess suitability for managed aquifer recharge (MAR) using the Pajaro Valley groundwater basin, central coastal California (PVGB) as a case study. We also used a groundwater model to assess the hydrologic impact of potential MAR operating scenarios, illustrating how a comprehensive analysis of MAR suitability can help with regional water supply planning. The GIS analyses used topographic, land use, surficial geology, soil infiltration capacity, aquifer and associated confining layer locations, properties, thicknesses, and historical changes in water levels. A map of MAR site suitability and comparison with an existing project suggests that about 8% (18 km^2) of the basin may be highly suitable for MAR. Results from the GIS analysis were used as input for a regional hydrologic model used to quantify the potential influences of different MAR scenarios. Model results show simulated MAR projects in locations identified as "highly suitable" for MAR reduce seawater intrusion more than projects simulated in "unsuitable" locations, supporting the GIS analysis results. Results from the model also illustrate the variability in seawater intrusion reduction and head level changes throughout the basin and over time, as simulated MAR project locations vary. Collectively, these studies help to evaluate management options for improving long-term groundwater conditions throughout the PVGB.

2.1 Introduction

Groundwater extraction exceeding natural recharge rates will result in basin overdraft, and in coastal aquifers, may induce seawater intrusion. Unsustainable groundwater use is rising as demand increases and is expected to continue to rise around the world, especially in developing nations, making groundwater management increasingly important [*Foster and Chilton*, 2003; *Konikow and Kendy*, 2005; *Giordano*, 2009; *Rosegrant and Cai*, 2009]. In many areas where groundwater use is unsustainable, overdraft can result in irreversible consequences such as pollution, including seawater intrusion, and land subsidence as a result of aquifer consolidation, leading to a permanent loss of groundwater storage.

Methods for mitigating groundwater overdraft include water conservation, pumping moratoriums, and enhancing recharge using injection wells, aquifer storage and recovery (ASR, with injection and extraction through the same wells) or managed aquifer recharge (MAR, using surface infiltration systems). Enhanced recharge has become a common and effective method for water resource management [*Ma and Spalding*, 1997]. ASR can help to reduce overdraft, [*Shammas*, 2007], but can have disadvantages such as energy usage and cost of pumping system operation and maintenance, as well as water quality issues [*Bouwer*, 2002]. In contrast, MAR can be part of a more passive operational system, potentially involving less engineering and lower operating costs. Water is diverted to a location, often a natural depression or constructed retention area, where it infiltrates into the subsurface over time. MAR projects have also

demonstrated improvements in water quality through denitrification during the infiltration process [*Ma and Spalding*, 1997; *Fryar et al.*, 2000; *Schmidt et al.*, 2011]. This can be particularly important for sites lacking reliable access to pristine surplus surface water supplies, such as basins with considerable agricultural development or numerous septic systems, resulting in elevated nutrient levels. The primary disadvantages of MAR include relatively large land area requirements, and the difficulty of identifying locations with amenable surface and subsurface properties for infiltration to an unconfined aquifer.

Identifying areas suitable for MAR projects and estimating the influence of these projects on groundwater levels and fluxes are challenging problems with numerous solutions. The first step is to locate regions where surface water infiltrates readily and is connected to a usable aquifer. These assessments are often required for large areas with complex geology and limited data availability. The second step is to determine how the benefits of managed recharge vary with project location and size, to help direct future recharge management efforts. This step will ultimately require field implementation, but computational models may be used initially to estimate MAR project effects on regional hydrology.

Early studies of the spatial distribution of recharge often focused on assessing groundwater vulnerability to contamination. Aller et al. [1987] developed a method for evaluating the potential for groundwater degradation, DRASTIC, which uses a relative ranking system. The method combines multiple datasets related to groundwater infiltration including net recharge, aquifer and soil properties, and impact of passage infiltrating water through the vadose zone on water quality. The parameters for each dataset are reclassified (generally to values

1 to 10), then multiplied by a parameter weight (1 to 5). The product of value and weight for each area (or subarea) are then summed for all the datasets, resulting in a relative vulnerability rank for each area in the study region. This method provides the basis for identifying recharge areas using geographic information system (GIS) based integration. We follow the general structure of this method, but use a different ensemble of datasets, different classification techniques, and different parameter weights.

Many hydrologic applications, including identification of locations for potential MAR projects, are well suited for GIS analysis [*Jha et al.*, 2007]. Several studies have used GIS-based integration of spatial coverages pertinent to groundwater recharge, with various data values being reclassified and weighted before combining [*Saraf and Choudhury*, 1998; *Shankar and Mohan*, 1998; *Piscopo*, 2001; *Murray and Mcdaniel*, 2003; *Jasrotia et al.*, 2007; *Chitsazan and Akhtari*, 2009; *Yeh et al.*, 2009; *Adham et al.*, 2010; *Chenini et al.*, 2010]. Methods used for reclassification and weighting generally differ from study to study, due to variations in data availability, local geology, and perceived level of dataset importance to groundwater recharge. As a practical matter, all classification schemes of this kind are somewhat arbitrary, but initial approaches and values can be refined over time as new data becomes available and individual recharge projects are tested and implemented. Chowdhury et al. [*Chowdhury et al.*, 2010] polled a group of geologists and hydrogeologists to determine a weighting system for their GIS-based recharge location assessment, and found that half the group thought equal weighting was appropriate while the other half agreed on a variable weighting method. Some studies have used GIS with a multi-

criteria decision analysis that accounts for local preferences, and attempt to reduce the arbitrary nature of weight assignment by using the analytical hierarchy process [*Chowdhury et al.*, 2010; *Rahman et al.*, 2012]. This method still requires (largely heuristic) estimation of the relative importance of each parameter.

Numerical modeling can also help to identify sites amenable for MAR, and be used for estimating the potential benefits of MAR projects on regional hydrologic conditions during a range of future climatic, water use, and management scenarios. Groundwater models may be combined with an optimization algorithm to test water management strategies, including artificial recharge [*Abarca et al.*, 2006]. These models tend to use simple governing equations and generalized aquifer properties. Another option for reducing computation time is to employ an ensemble of analytical models based on simplified lumped parameters [*Smith and Pollock*, 2012]. Combination of the GIS-based integration methods with numerical modeling allows a more detailed and quantitative assessment of MAR opportunities and impacts, and takes advantage of overlapping data requirements for GIS and numerical modeling studies (for example, aquifer geometry and depth and soil properties) [*Chenini and Mammou*, 2010]. The use of numerical modeling as a follow-up to a GIS-based study also provides an opportunity to assess the MAR location suitability analysis developed using GIS, and on time requirements to see specific improvements to resource conditions.

True assessment of MAR location suitability requires field testing to determine how project placement and operation influences local and regional hydrologic conditions and flows. Ultimately this requires field-scale

implementation of MAR projects, but budgetary and time constraints generally limit opportunities for large-scale installations purely for testing purposes. Thus numerical modeling has an important role to play in pre-implementation evaluation of project options, based on a MAR suitability analysis, helping to reduce the number of choices made in selecting appropriate management strategies. Similarly, evaluation of actual hydrologic responses to implementation of MAR projects can be used to "validate" individual and ensemble groups of groundwater models, contributing to a better understanding of system function and improved basin-wide management of scarce resources.

The present study combines GIS and numerical analyses to address the following questions, as applied to the Pajaro Valley Groundwater Basin (PVGB), central coastal California (**Figure 2-1**): 1) How should surface and subsurface information datasets be combined to assess MAR site suitability? 2) How does MAR suitability vary within the basin? 3) How might hypothetical MAR operating scenarios influence groundwater conditions in the basin over the 34 year model simulation? This project limits analysis to MAR options for the PVGB rather than exploring a more comprehensive assessment of basin management options and anticipated changes to water usage. An extensive technical and public process is currently underway in our study area to evaluate a wide range of supply and conservation options, and develop a new basin management plan, in an effort to improve groundwater conditions in the Pajaro Valley in coming decades. We limit analyses in this study to assessing the spatial distribution of MAR suitability and potential hydrologic impacts of several MAR options.

2.2 Study area

The Pajaro Valley Groundwater Basin (PVGB), central coastal California (**Figure 2-1**), is a 322 km^2 area delineated by the Pajaro Valley Water Management Agency (PVWMA) boundary. The region relies almost entirely on groundwater to satisfy agricultural and municipal/domestic needs (83% and 17%, respectively). Precipitation in the area averages ~50 cm/yr and is highly seasonal, with a majority falling between December and April, resulting in distinct dry and wet seasons.

Much of the PVGB corresponds to the lower drainage basin of the Pajaro River, which flows into the valley from the east at an average discharge of 1.3 x 10^8 m^3/yr (USGS Gage #11159000), after draining an upstream area of 3.1 x 10^3 km^2. Corralitos Creek, a tributary of the Pajaro River having a drainage area contained entirely within the PVGB, contributes an additional 1.4 x 10^7 m^3/yr of discharge (USGS Gage #11159200), and the Watsonville Sloughs also drain into the lower Pajaro River before it discharges into Monterey Bay (**Figure 2-1**).

The PVGB has six primary hydrologic units: alluvium, alluvial clay, the Upper Aromas Aquifer, the Aromas confining unit, the Lower Aromas Aquifer, and the Purisima Aquifer [*Muir*, 1972; *Dupre*, 1990; *Hanson*, 2003]. These layers are herein referred to as A1, C1, A2, C2, A3 and A4, respectively, where C signifies a confining unit and A signifies an aquifer (**Table 2-1**). The six layers are underlain by hydrogeologic basement rocks consisting of granite and Oligocene-aged deposits. Groundwater extraction from the basin is currently averages 6.8 to 7.4 x 10^6 m^3/yr, with the majority of water pumped from Layers A1 and A2 [*Hanson et al.*, 2012]. Over time, total groundwater outflows (including

extraction) have exceeded recharge and inflow rates; the current estimated overdraft in the PVGB is approximately 1.5 x 10^7 m^3/yr (~12,000 ac-ft/yr) [*Hanson et al.*, 2012]. This annual overdraft is approximately equivalent to 10% of the precipitation falling on the PVGB. Long-term monitoring over recent decades indicates that water levels within more than half of the PVGB are below sea level, particularly during the dry part of the water year, with the greatest depression of water levels below the City of Watsonville. A zone of seawater intrusion extends up to 5 km inland and is advancing at ~80 m/yr along much of the coastal region [*Hanson*, 2003; *Hanson et al.*, 2008; *Wallace and Lockwood*, 2009] (**Figure 2-1**).

The PVWMA is currently working with regional stakeholders to update their basin management plan in an effort to bring the basin back into hydrologic balance, and several projects have already been implemented. The Harkins Slough MAR system is permitted to divert up to 2.5 x 10^6 m^3/yr (~2,000 ac-ft/yr) from the wetland when flows and water quality are sufficiently high, pass the water through a sand pack filter, then pump it through a 1.5 km pipeline to an infiltration pond. Some of this percolated water is subsequently recovered and blended with other water supplies, then delivered using a coastal delivery pipeline to local farms and ranches. In addition, the PVWMA and the City of Watsonville jointly developed a water recycling plant that contributes water to the coastal delivery pipeline, as do inland groundwater wells, allowing project water to be blended to achieve quality and supply goals.

2.3 Methods

2.3.1 GIS analysis

We used GIS for data management, manipulation, and analysis of eleven surface and subsurface data sets in order to produce a basin-wide map of MAR suitability. As defined for this study, high MAR suitability indicates that, if a water supply of sufficient quantity and quality were available, surface and subsurface conditions could be favorable to developing one or more MAR projects. Surface and subsurface property data sets were analyzed separately initially, then were combined to produce a final map. For surface analyses, primary data included: (1) surficial geology, (2) soil infiltration capacity, (3) land use, (4) topographic slope, and (5) verified (measured) infiltration and recharge rates from observational studies. For subsurface analyses, primary data included: (6) aquifer layer thickness, (7) aquifer hydraulic conductivity, (8) confining layer thickness, (9) aquifer storativity, (10) unsaturated zone thickness, and (11) historical changes in water table height.

Surficial geology data were obtained from 1:62,500-scale geologic maps of Santa Cruz and Monterey Counties [*Brabb et al.*, 1997; *Clark et al.*, 1997]. Lithologic descriptions were used to classify individual geologic units in terms of whether or not they corresponded to PVGB aquifers, or if fine-grained sediment (clay and silt) would be likely to reduce direct connection to underlying aquifers. Soil infiltration capacity data were obtained from the Natural Resources Conservation Service SSURGO database [*NRCS*, 2010a, 2010b]. Infiltration capacity of basin soils was mapped in irregular polygons having values ranging from 0.2 to 12 m/d. Land classifications were developed by the PVWMA and the

USGS in collaboration with regional stakeholders, based on field visits and and parcel-specific reports of crops grown, as part of a broader effort to develop a regional hydrogeologic framework (Hanson, 2003; Hanson et al., 2012). Land use classifications include native vegetation, urban, and agricultural areas designated by crop type or presence of a nursery. Land surface slope values were calculated from the 10-m resolution USGS National Elevation Dataset (ned.usgs.gov). Locations of measured seepage rates along losing sections of the Pajaro River were reported in earlier studies based on differential gauging and streambed geothermometry [*Ruehl et al.*, 2006; *Hatch et al.*, 2010].

Subsurface data sets were prepared initially during development of a regional hydrogeologic model [*Hanson*, 2003; *Hanson et al.*, 2012], and modified as needed for use in our GIS-based analysis. Aquifer properties, including layer thicknesses, hydraulic conductivity, and storativity were assembled using data from >300 well logs distributed throughout the basin, and compiled on a grid having horizontal resolution of 250 x 250 m and variable cell thickness. The unsaturated zone thickness was calculated by subtracting the interpolated water table elevations, using data collected in 2010, from the ground elevation. Water levels in the basin were compared using 1998 and 2010 data sets, two times for which there is widespread information on water levels across the basin, yielding a coverage that shows the extent of water level changes during this time.

The GIS-based integration generally involves reclassifying relevant datasets to a common scale (e.g. values of 1 to 5) and then assigning a weight to each dataset. For grid cell in the analysis, an index is calculated by summing the products of value and weight for each dataset.

$$Index(x,y) = \sum_{i=1}^{n} v(x,y)_i w_i \qquad (2\text{-}1)$$

where n is the total number of datasets, v is the reclassified value at (x,y) and w_i is the weight assigned to dataset i. We defined a weighting scheme based on (a) a review of published recharge mapping studies of other regions, and (b) inferences as to how groundwater recharge in this region might be influenced by a variety of coexisting factors (**Figure 2-2**).

Our approach differed in several respects from methods used in earlier GIS-based studies of MAR suitability. Most significantly, we evaluated surface data (1 to 4) and subsurface data (6 to 11) independently, with the former indicating the ease of surface water infiltration, and the latter indicating the ease of subsurface transport and extent of available storage. In addition, we used some data sets as modifiers for other data sets, rather than as independent indicators, before combining individual coverages to derive a final assessment of MAR suitability. Locations having direct measurements of recharge rates were subsequently assigned MAR suitability values based entirely on field observations.

2.3.1.1 Data classification

We standardized several of the datasets by classifying values or properties on a scale of 1 to 5, where 1 represents an unfavorable (or negative) attribute for MAR suitability, and 5 represents a favorable attribute. The main approach was to link MAR suitability to measured or known physical hydrologic properties and

relationships, and to combine related values (e.g., topographic slope and land use) as part of data integration, rather than simply adding all attributes as if they were independent indicators.

Both numerical and non-numerical datasets (e.g., soil infiltration capacity and surficial geology, respectively) were used in this study, requiring different approaches for classification. We used three approaches for classifying numerical datasets: (1) classify values based on knowledge of field properties and MAR operations, (2) classify values using the Jenks optimization method based on the distribution of property values in the study area, and (3) operate on raw data. The first method was applied to soil infiltration capacity and locations with stream seepage rates measured in the field (**Table 2-2**). The second Method was applied to specific yield, unsaturated zone thickness, historical changes in water table height. The third method was applied to surface slope values. Non-numerical datasets, including surficial geology and land use, were classified based on interpretation of properties. For surficial geology, we assigned each lithologic unit a value based on whether the mapped lithology and texture [*Brabb et al.*, 1997; *Clark et al.*, 1997] corresponded to a known aquifer or would likely be connected to a known aquifer. For land use, we classified descriptions based on associated roughness coefficient values [*Chow*, 1959] (**Table 2-2**), where roughness coefficients range from 14 to 100, for nursery/pavement to forested/native vegetation.

2.3.1.2 Data integration

We used a modification of the relation between slope and land roughness from the Manning equation to characterize relative runoff, then combined this information with soil infiltration capacity to calculate an effective infiltration (I_E) value:

$$I_E = I_C + ln\left[\frac{n/\sqrt{s}}{(n/\sqrt{s})_{max}}\right] \qquad (2\text{-}2)$$

where I_C is infiltration capacity, n is a surface roughness coefficient (with values ranging from 14 to 100), and s is slope in radians. Theoretically, the second term in **Eqn. 2-2** is proportional to the quantity of water that will not infiltrate, and because the relation between slope and surface roughness is normalized by the maximum (optimal) conditions for the region, the term is ≤ 0. Effective infiltration values are therefore dependent on the soil infiltration capacity, but modified by the relative likeliness of runoff based on surface slope and roughness. For example, if the soil infiltration capacity is low, the influence of low-slope and native vegetation (high roughness coefficient), which might be optimal for infiltration through a more permeable soil, becomes negligible. Likewise, a high soil infiltration capacity located in a region with high slope and a land use of turf grass (low roughness coefficient), will have an I_E value that is lower than the I_C value associated with the land use alone. The I_E value will be equal to I_C for optimal surface and slope conditions (the second term goes to 0 as the term in brackets goes to 1), but otherwise the I_C value will be reduced by the second term,

so that $I_E < I_C$. An example of how this construction influences I_E values is shown in **Figure 2-3**, where separate traces are drawn for different surface slope values.

Transmissivity (T) is in important subsurface parameter and can be difficult to estimate across a large spatial area. For operating a MAR system, high transmissivity is necessary for avoiding excessive mounding (or even flooding), and for allowing infiltrated water to flow to nearby recovery wells. The primary constraints on transmissivity with respect to MAR are aquifer hydraulic conductivity (K) and thickness (b) and the presence or absence of confining layers. To account for spatially variable K and b and the presence of confining layers in the subsurface, we use the following equation to calculate an effective transmissivity (T_E) as it applies to MAR suitability:

$$T_E = K_{A1}b_{A1} + K_{C1}b_{C1} + F_1[K_{A2}b_{A2} + K_{C2}b_{C2} + F_2(K_{A3}b_{A3} + K_{A4}b_{A4})] \quad (2\text{-}3)$$

$$F_1 = 1 - \frac{b_{C1}-1}{9} \text{ for } 1 \leq b_{C1} \leq 10 \quad (2\text{-}4)$$

$$F_2 = 1 - \frac{b_{C2}-1}{9} \text{ for } 1 \leq b_{C2} \leq 10 \quad (2\text{-}5)$$

where F_1 and F_2 are confining unit factors that affect the influence of underlying aquifer units. F_1 and F_2 scale linearly between 1 and 0 for confining unit thicknesses ranging between 1 and 10 m, respectively. Thus, the transmissivities of multiple aquifer layers are combined (at least in part), provided that any confining layers between the aquifer layers are <10 m in thickness. This accounts for noncontinuity of thin confining layers that was readily apparent in hundreds of

well logs and drilling records from across the basin. T_E values were classified on a scale of 1 to 5 per Method 2, described in §*3.1.1*.

Available storage space was assessed as part of the MAR suitability analysis, by multiplying aquifer specific yield by the unsaturated thickness of each cell. There may be additional storage capacity in confined aquifers, but this is likely to be negligible in comparison to storage available in unconfined aquifer units. MAR suitability was additionally enhanced in areas where there has been a large drop in water levels during the period of 1998 to 2010.

Following calculations and reclassifications, each dataset was assigned a weight based on the perceived importance to groundwater recharge. The normalized weights used in this study are comparable to those obtained from a review of similar peer-reviewed studies (**Figure 2-2**), although there is considerable variability depending on the number and type of available datasets and local hydrogeology for each study. We note that in all of the earlier studies shown for comparison, individual parameters were added as independent variables on a cell by cell basis. As described earlier, we used land use and topographic slope data to modify the MAR suitability implied by soil property data sets, rather than applying land use and slope data independently. Values shown for these parameters in **Figure 2-2** are the means of weights applied in the present study when calculating effective infiltration (Equation 2-2).

A final map of MAR suitability was created by summing the weighted, classified values for every 10-by-10 m polygon in the basin for which all data sets existed, using this equation:

$$MAR\ suitability\ index = 5I_E + 4G + 5V + 4T + 2D \quad (2\text{-}6)$$

$$\text{If } L \text{ exists, } MAR\ suitability\ index = L \quad (2\text{-}7)$$

where: G is surficial geology, V is available storage, T_E is effective transmissivity, D is an historic change in water table height, and L is the index for a losing stream reach within which recharge rates have been measured and indicate high MAR suitability. The full process was constructed using ArcGIS ModelBuilder, which can be modified as additional datasets become available or weighting methods are changed based on new information or understanding.

2.3.2 Numerical modeling of MAR scenarios

To model the relative hydrologic impact of MAR projects, we modified a hydrogeologic model developed recently to assess a range of conditions and management options for the Pajaro Valley [*Hanson et al.*, 2012]. Surface and subsurface hydrologic processes were simulated using MODFLOW-2005 [*Harbaugh*, 2005]. The model domain extends from the back of the basin to >10 km offshore (**Figure 2-4A**), with grid resolution of 250 x 250 m. The six model layers vary in thickness across the basin, corresponding to aquifer and confining layer thicknesses (**Figure 2-4B**). The model incorporates the Farm Process [*Schmid and Hanson*, 2009; *Hanson et al.*, 2010] which modifies agricultural groundwater pumping rates during the simulation based on changes in land-use, climate, and groundwater availability. The simulations used in the present study represent 34 years modeled with 408 stress periods having two time steps each. The details of developing and hydrogeologic framework for the Pajaro Valley, and

creating and applying a complex model for assessing historical groundwater extraction and conditions in the Pajaro Valley, are described elsewhere [*Hanson*, 2003; *Hanson et al.*, 2012]. In the present paper, we focus on how this model was used with the GIS analysis to assess hydrologic impacts of potential MAR project placement.

We worked with a Baseline simulation, developed to represent a 34 year time period beginning nominally in 2006. Climate conditions for the Basecase simulation were assumed to be a "mirror image" of climate during the preceding 34 years, and land use in the simulation was fixed to be that as of 2006. After this simulation was completed, we ran 31 additional simulations, each with a different combination of hypothetical MAR projects adding water in different locations and at different rates around the basin (**Table 2-3**).

MAR projects were simulated by adding water to shallow aquifer layers using a head-independent boundary condition. It was assumed that each MAR project existed within a single model cell. Adding water to the subsurface in a prescribed way did not allow evaluation of how surface properties (slope, land use, and soil infiltration capacity) influenced recharge dynamics, but subsurface storativity, transmissivity and the presence of confining units did govern flow after infiltration. However, surface properties did influence how MAR projects were placed based on the GIS-based suitability analysis.

MAR project scenarios had four variables: (1) MAR project location(s), (2) number of MAR projects, (3) quantity of applied water per project (and in total), and (4) duration of activity during each year. We evaluated the influence of locating MAR projects in four general regions: coastal area (CO), the back (eatern

side) of the basin (BB), areas identified as being particularly suitable for MAR ("GIS-good", GG) and areas identified as being considerably less suitable for MAR ("GIS-poor" GP). We expected that the distance from the coast would have a significant influence on MAR project impact, so locations for GG and GP simulations were selected in pairs such that the sites in each pair were equidistant from the coast. MAR sites in each location group recharge to different layers, depending on how aquifer layers are distributed across the basin. For example, sites used for MAR in the back of the basin (simulation group BB) recharge directly to aquifer layer A4 (Purisima Formation), whereas sites used for MAR projects based on the most suitable conditions (simulation group GG) are located over a mix of aquifer layers A1, A2 and A4.

Each modeling scenario had either 5 or 10 MAR projects. The rate of MAR-associated recharge applied at individual project sites ranged from 6.2×10^4 m^3/yr (50 ac-ft/yr) to 1.5×10^6 m^3/yr (1200 ac-ft/yr). Water was applied evenly during periods of either 4 or 12 months/yr. The 4-month MAR operation was intended to represent projects that run only during the wet season, when runoff, or diversion from other surface water supplies might be appropriate. MAR projects that use water supplied by the local water recycling plant, or water conveyed from higher in the basin using the Pajaro River, might theoretically operate throughout the water year. This set of model scenarios was not intended to be exhaustive, but gives a good sense of how MAR project number, placement, and operations could influence groundwater conditions over the long term.

To analyze MAR scenario results, we compared model output of head levels and flows from the coastal region into the aquifer below the Pajaro Valley.

Changes in head levels can be quantified in two ways: 1) at a given time over the entire basin, and 2) or over the duration of the model simulation at a given location. The first method was applied to compare head levels from layer A2 during the final time-step to the respective head levels in the Basecase simulation. Using the second method, we selected a single grid cell and extracted the head values in each aquifer layer during six stress periods. Flux of water from the offshore zone to coastal zones was classified as seawater intrusion. With seawater intrusion as an active concern in the study region, it was natural to use coastal flux as a metric for comparing MAR scenarios to the Basecase model. Model calculated coastal flux values were calculated for each stress period, and then summed to provide flux per year over the entire duration of the model run. Flux values are given for the six model layers combined either as seawater intrusion or flow to the offshore zone.

2.4. Results

2.4.1 Assignment of MAR suitability index values

Results from classification of six of the surface and subsurface properties are shown in **Figure 2-5**. The majority of the surficial geology in the PVGB indicates connectivity to the local aquifers, except the flood plains which have significant silt and clay layers (**Figure 2-5A**). Classified soil infiltration capacity values are similar to classified surficial geology values, with generally favorable conditions (infiltration capacity >1.2 m/d) for over 85% of the PVGB area and less favorable conditions in the river floodplain (**Figure 2-5B**). The roughness coefficient, which is a function of land use, varies throughout the basin, with urban and turf areas

concentrated in the center of the basin in Watsonville, CA (**Figure 2-5C**). Urban and turf areas account for 21% of the total area, whereas agricultural fields and pastures account for 41%. The remaining 38% is native vegetation and unfarmed land, predominately located in the higher sloped northern and north-western edges of the basin (**Figure 2-5D**). Classified values of effective transmissivity are highly variable across the basin (**Figure 2-5E**). These values represent three datasets: aquifer layer thickness, aquifer hydraulic conductivity, and confining layer thickness. Variability in historical changes in groundwater levels appears to have a North-South trend, most notably with a decrease in water levels along the coast (**Figure 2-5F**).

The normalized weights used to integrate the reclassified datasets are generally low compared to weights used in other peer-reviewed studies (**Figure 2-2**). This is primarily due to including more datasets than the other studies, which tends to reduce the influence of each individual dataset. The final map of MAR suitability has a nominal resolution of 10 x 10 m (**Figure 2-6**), although resolution of the individual datasets varies considerably (**Figure 2-5**). In addition, the full spatial extent of the MAR suitability map is limited by the intersection of the extents of each of the data sets used in the analyses (228 km^2).

Calculated MAR suitability index values from across the PVGB range from 2 to 40 and appear to follow a (roughly) normal distribution, with a mean of 22 and a standard deviation of 6.5 (**Figure 2-7**). The upper quartile of this range, comprising land areas being the most suitable for MAR, accounts for 13% of the analyzed land area in the PVGB (29 km^2). These areas are located throughout the basin, particularly along the coast north and south of the Pajaro River, inland

south of the Pajaro River, and along the back of the basin (**Figure 2-6**). The site of the Harkins Slough MAR project (**Figure 2-6**), which recharges approximately 10^6 m^3/yr diverted water to a perched aquifer, has a MAR suitability index of 32.

2.4.2 Influence of MAR projects on head levels and seawater intrusion

All simulations of MAR scenarios (**Table 2-3**) show that MAR projects can help to raise water levels in basin aquifers and may reduce (or reverse) seawater intrusion, relative to Basecase model conditions. The difference in conditions from the Basecase will herein referred to as MAR "benefit". In general, benefits due to MAR increase with time, but the extent and nature of benefit varies with MAR project location and amount of water applied (**Figure 2-8**).

Unsurprisingly, simulated groundwater levels increased the most in areas closest to MAR project (**Figure 2-9**). The GG location scenario (**Figure 2-9A**) shows the greatest increase in the Northwest region of the PVGB, and produces >1 m head level increase in over 80% of the onshore area. The CO location scenario (**Figure 2-9B**) raises the head levels mostly along the coast, and produces a >1 m head level increase in ~60% of the onshore area. There are significantly greater head level increases offshore with MAR projects located in CO positions, compared to GG positions.

Simulated benefits to water levels within the aquifer layers vary based on MAR location because water is applied to the exposed surface layer, which differs throughout the basin. In general, and at the mid-basin location (**Figure 2-1**), head levels increase by similar amounts in layers A1 and A2 (**Figure 2-10A and 2-10B**), with variation due to simulated MAR location. Benefit to head levels in the

deepest aquifer, A4, are similar for the four groups of MAR locations (**Figure 2-10C**), and show a smaller groundwater level increase than in the upper aquifers.

For all tested scenarios, simulated MAR projects reduced seawater intrusion compared to the Basecase, with the difference increasing on average over time. The location of simulated MAR projects has a notable effect on the magnitude of reductions in seawater intrusion. The greatest benefit is achieved by simulating MAR projects in the GG locations, followed by BB, GP, and CO, in order of decreasing benefit (**Figure 2-11A**). Though the rate of change of benefit varies with time, the benefit in the GG scenarios increase approximately twice as quickly as that for the CO scenario over the 34 year simulation. MAR project location also affects the quantity of flux in the offshore direction, and the rate of change over time (**Figure 2-11B**). Flux offshore was greatest early in the model runs and decreased over time, suggesting that head levels rose and/or more water was extracted by pumping. The CO scenario results in the greatest increase in flux offshore compared to the Basecase, followed by GG, GP and BB scenarios, in that order.

The reduction of seawater intrusion varies with the amount of water applied in simulated MAR projects, and with project location and time. In general, model output shows that increasing water applied to the system through simulated MAR projects results in larger reductions of seawater intrusion along the coast (**Figure 2-12**). Increasing the amount of MAR water applied at CO locations (**Figure 2-12A**) produces a smaller reduction in seawater intrusion than MAR water applied at GG locations (**Figure 2-12B**). The difference in benefit between the two MAR project locations groups is minimal for the lowest applied water rate

(1.5×10^6 m^3/yr), and increases to ~50% greater benefit at the GG MAR locations for the highest applied water rate (1.5×10^7 m^3/yr).

We use the reduction in seawater intrusion divided by the total applied water as a measure of MAR efficiency (**Figures 12-C and 12-D**). For a given MAR location group, the efficiency is approximately equal for the full range of applied water quantities at time = 1 yr. In other words, the initial benefit is linearly related to the amount of MAR water applied to the surface. For example, with MAR projects in GG locations, the seawater intrusion reduction efficiency is approximately 1.5% of the total water applied for any given amount of water (**Figure 2-12D**). Over time, the efficiency increases at a rate dependent on the amount of applied water, where scenarios with less applied water show the greatest increase in efficiency.

Changing the number of MAR projects from 5 to 10 appears to have a similar effect as doubling the total applied water, although locations of the additional 5 MAR projects are likely to influence specific results. If the added projects have a different average proximity to the coast, then the effect on seawater intrusion will be different than simply doubling the total applied water.

The duration of MAR operation has minimal effect on the reduction of seawater intrusion over the full (34 year) simulations. The scenarios active for 4 months and 12 months per year have nearly identical influence on seawater intrusion for the first 20 years of the model simulation, then the projects active year-round tend to have an impact ~5 to 8% greater than the projects operating only 4 months per year.

2.5. Discussion

2.5.1 Integration of GIS and numerical modeling

This study assessed MAR suitability in the PVGB using GIS-based integration, followed by numerical analysis to determine the relative influence of MAR placement on groundwater hydrologic conditions. The eleven datasets used to assess site suitability for MAR have implications for either surficial or subsurface recharge dynamics. Five of the datasets were also used to define properties in the numerical model: land use, aquifer and confining unit thinknesses, hydraulic conductivity, and storativity values. This commonality in the construction of the two project components supports subsequent usage of GIS results as input for the model.

This study used a unique approach to the common method of integrating multiple datasets with GIS. We allowed specific properties to operate directly on the total value of other properties, thus more accurately reflecting the relationships between geology, hydrology, and groundwater recharge. Effective infiltration encompasses the relationship between soil infiltration, ground slope, and land surface roughness, and the ultimate quantity of water entering the subsurface, which may not be best estimated by summing properties. Because ground slope and surface roughness can only detract from soil infiltration capacity, areas with already low soil infiltration capacities have low effective infiltration values. Effective transmissivity was calculated by summing all (or part of) the transmissivity values from the surface-down, until a significant confining unit was reached. This contrasts the traditionally calculated aggregate transmissivity which would under-represent the value of areas with deep confining units. Results show

the highest transmissivity values are located south of the Pajaro River on the coast and farther inland, and in the Northern and Northeastern areas in the back basin. The latter regions have high effective transmissivity because layer A4 is several hundred meters thick and relatively permeable.

The arbitrary nature of classification and integration was a concern with using the GIS-based integration method for identifying recharge locations. Every published paper using this method that we found had a different weighting system for a different collection of datasets. The inclusion of datasets depended on availability, local geologic and hydrologic conditions, and other site-specific concerns. One determination of a reasonable weighting system could be a uniform- to normal-distribution of MAR suitability throughout the study area. This provides relative information about MAR suitability, which can later be calibrated to field observations. Until field verification exists for MAR suitability or natural recharge maps, it might be correct to assume that the weighting system should be site-specific, as long as the results appear reasonable and are interpreted as relative values of MAR suitability.

Modification of the PVGB model to include MAR projects serves to evaluate the relative influence of major MAR parameters including project location, number of projects, amount of water applied, and duration of operation through the year. The model was calibrated to PVGB conditions under normal agricultural and municipal water use conditions. Though Harkins Slough MAR project was included in the original model, note that the model response to additional MAR projects has not been calibrated. The results should therefore be

interpreted as relative hydrologic responses due to the addition of MAR projects, and not exact projections of groundwater level or seawater intrusion changes.

The ~8 year increase in seawater intrusion reduction starting in model year 20 for all MAR scenarios (**Figures 2-11 and 2-12**) was a product of modeled climate and water use parameters. Model year 20 represented the beginning of a decrease in pumping across the PVGB. This decrease in demand was accompanied by a wet climate period which lasted from water year 23 to 28. The events were likely related as farmers did not have to irrigate as much during wet years, though must also represent an independent decrease in pumping because it proceeded the wet period. Reduction in pumping and an increase in natural recharge during wet years appear to compound the benefit provided by simulated MAR projects.

2.5.2 Implications for MAR in the Pajaro Valley

MAR suitability values are variable throughout the PVGB due to variations in physical characteristics across the region (**Figure 2-6**). The most prominent feature in the final MAR suitability map is the Pajaro River floodplain, which has relatively low suitability primarily due to soil infiltration and surficial geology classifications. This is not surprising given that floodplain lithology tends to comprise silt and clay layers which impede surface infiltration. According to the final map, the active streambed appears similarly unsuitable for MAR projects, however measurements of streambed infiltration rates suggest that certain reaches lose on the order of 1 m/d. This discrepancy might originate from interpolating floodplain soil properties into streambed areas.

We were able to assess the GIS results with respect to an active MAR project in the PVGB operated by the PVWMA which recharges approximately 10^6 m^3/yr during the wet season [*Racz et al.*, 2011; *Schmidt et al.*, 2011]. We define this as a successful MAR project, and therefore characterize the location as highly suitable. The projected MAR suitability index based on the GIS analysis for this site is in the 81st percentile (**Figure 2-6**). Using this location as a calibration point, we see that 8% of the basin area (18 km^2) has an equal or higher projected MAR suitability index. These highly suitable areas are distributed throughout the basin. We would need approximately 15 similarly performing MAR projects to offset annual overdraft in the PVGB. This would equate to approximately 2.3% of the land area that was classified as equal to or more suitable for MAR than the Harkins Slough recharge project, or 0.19% of the total analyzed area. Realistically, MAR will not be the only method used to restore groundwater conditions, though knowing that the potential for MAR is significant and requires relatively little land area could assist the restoration planning process.

Model results showed that MAR project location, amount of applied water, and years of operation affect the reduction of seawater intrusion. Projects along the coast provided the greatest immediate benefit, however after ~3 years, seawater intrusion reduction was greatest for scenarios with MAR projects distributed throughout the PVGB or located in the back-basin. As the amount of water recharged increases, the overall efficiency of the project decreases due to losses offshore that do not contribute to seawater intrusion reduction.

Results show that the benefit from MAR projects varies depending on which evaluation metric is used (groundwater rise or seawater intrusion

reduction), and for the former, where the metric is applied in the basin. MAR projects located at CO sites result in the largest groundwater head increase along the coast (**Figure 2-9**), but also the lowest long-term seawater intrusion reduction (**Figure 2-11A**). GG MAR projects are most effective at reducing seawater intrusion, though on average are farther from the coast than CO MAR projects. This exemplifies the importance of including subsurface hydrologic properties and conditions when assessing locations for MAR projects.

Comparing results from the GG and GP scenarios provides a level of support for the GIS MAR suitability map. There was negligible difference in aquifer head levels for the two simulated location groups of MAR projects. However, on average, there was a 25% greater reduction of seawater intrusion for MAR projects located in areas identified as highly suitable in the GIS analysis (**Figure 2-11**). The inefficiency of GP MAR projects located in unsuitable locations might be partially because they only recharge to layer A1. Because seawater intrusion is occurring in all aquifer layers in the PVGB, it might be beneficial to distribute MAR projects among the regions where each aquifer is unconfined, in addition to selection by suitability index. For example, if all MAR projects recharge to layer A1, where the presence of underlying confining units restrict downward flow, reduction of seawater intrusion might be limited in layers A2 to A4. Note that GP sites were not intentionally selected in areas where layer A1 is unconfined, but happened because the alluvial layer contains low permeability flood plains that are poorly suited for MAR projects, which met the selection criteria.

To assess the issue of flow between geologic layers, we reference model groundwater head calculations which indicate that confining units do not restrict all flow between aquifer layers. Though groundwater head levels increase the most in the layer being recharged, head increases are calculated to a lesser extent in under- and over-lying aquifers. For example, the BB MAR projects recharge to A2, A3 and A4, however the head levels increase approximately 0.3 m in A1 over the 34 year model simulation (**Figure 2-10A**). This was calculated for a cell in the City of Watsonville, and does not reflect head level increases for the entire PVGB. With the majority of groundwater extraction occurring in layer A2 [*Hanson et al.*, 2012], having discontinuous confining units to accommodate fluid flow between aquifers is critical because it allows MAR projects in all areas of the basin.

When comparing applied water scenarios in the CO MAR locations, we note the anomalous behavior of benefit achieved with the largest quantity of applied water. The benefit calculated for the largest amount of applied water in the CO MAR locations is similar to, and sometimes lower, than the benefit from the 2nd largest amount of applied water (**Figure 2-12A**). The largest amount, which is equal to the annual overdraft of the PVGB, was modeled as an upper limit, and likely exceeded the realm of practical input values for the model. Therefore, the significance of the deviation from the general trend in this case may be negligible.

The duration of MAR activity through the year had little impact on seawater intrusion, and the difference of ~5 to 8% increase in benefit observed with year-round projects may be within the error of the model results. We consider this effect to be negligible compared to the other variables tested in the MAR scenarios, and therefore conclude that seasonally operating MAR projects

show equal benefit to those projects recharging the same amount of water while operating year-round.

2.5.3 Study limitations and next steps

Several critical factors are not accounted for in the GIS and modeling analyses, including water availability, solute (salt) transport, unsaturated zone transport, land-owner cooperation, and proximity to seawater intruded area. These factors should be considered in next step where GIS results are used to identify locations for field and pilot testing. As such, considering uncertainty in the recharge related spatial datasets and integration method, the GIS analysis results are not intended to be used alone for identifying potential MAR project sites.

This study does not include analysis of water availability for MAR projects, however we speculate about water sources in regions with high MAR suitability index. We show many areas in the PVGB as highly suitable for MAR projects, especially the coast, which coincides with the recycle water plant distribution system, and the back of the basin where runoff from adjacent hills could serve as a recharge water source. The wide distribution of areas amenable for MAR projects may encourage more landowners to participate in distributed recharge enhancement efforts, not just those who are experiencing the consequences of aquifer overdraft.

Numerical model results suggest that placement of MAR projects according to the GIS suitability index provides the greatest reduction of seawater intrusion along the coast. The quantity of water applied using MAR is proportional to the long-term benefit. However, in this water-stressed area, it will

be necessary to optimize the quantity of water applied with respect to desired reduction in seawater intrusion. Larger applied quantities of water will provide a greater benefit, though at a lower efficiency than smaller applied quantities of water. Water availability will likely govern the quantity of applied water on an annual basis.

The current model does not include solute advection, and therefore cannot estimate the influence of recharge on the salinity of the seawater intruded areas. The study would benefit from a more detailed solute transport model, especially with respect to MAR location within the PVGB. For example, placing MAR projects within the seawater intruded area might be a feasible option for impeding further intrusion, but provide minimal water quality benefit to the already saline-contaminated areas. Conversely, recharging onto a local perched aquifer above the seawater intruded area can provide an alternate source for users, allowing coastal farming to continue and reducing demand on the overdraft aquifers below [*Racz et al.*, 2011; *Schmidt et al.*, 2011].

The model does not solve unsaturated groundwater flow equations, which is an important factor in aquifer recharge. Water applied to the surface moves immediately down to the uppermost saturated model cell which can introduce errors in the time between surface infiltration and reaching the water table. Results from the Harkins Slough MAR project suggest that recharge water travels primarily through preferential flow paths in the vadose zone at a rate of ~4 m/d [*Schmidt et al.*, 2011], therefore instantaneous transport is appropriate given the month-long stress periods. This might present an issue for MAR projects situated

in poorly suited areas where infiltration rates are slow and confining units impede flow pathways to the aquifer.

The model includes a relatively new MODFLOW package called the Farm Process [*Schmid and Hanson*, 2009], which varies the amount of water pumped based on land use and water supply. As MAR water recharges the aquifer, groundwater supply increases, therefore potentially increasing pumping in scenarios that result in more recharge to the aquifer. This does not pose an issue in this study because the rate at which pumping increases is less than the rate of recharge, so we assume that making relative comparisons between model scenarios is appropriate. Overall, if increased head levels due to MAR cause pumping in the model to increase beyond realistic projections, then the estimations of seawater intrusion reduction are conservative. Due to the potential sources of uncertainty described above, the model results are intended to represent the relative influence of various MAR scenarios, not necessarily the true physical response.

The next step in determining where to implement MAR projects is field testing soil infiltration properties at locations that have been identified as suitable for MAR by the GIS analysis. Areas with a high MAR suitability index would be more appropriate locations to focus initial field testing efforts. However, if an area with a low MAR suitability index is amenable for other reasons (e.g. water availability, land-owner interest, etc.), investigation of infiltration properties may still be appropriate, given uncertainties in the index calculation.

Assessing sites for MAR is a complicated problem, as evidenced by the number of studies and variety of methods. We produced a MAR suitability index

map, and show relative impacts on seawater intrusion and groundwater levels, though this must be an iterative process. Field testing and MAR implementation are required both to reduce groundwater overdraft and to help calibrate the suitability mapping method. With more field data, and comparisons to similar results from other study areas, the GIS-based integration method will become more robust for assessing MAR site suitability.

2.6 Conclusions

MAR likely will become increasingly important for sustaining groundwater supply in future years; however, identifying areas amenable to MAR, and estimating the groundwater response remain challenging. This paper proposed a physically based, GIS integration method for identifying locations for MAR projects, and quantified the relative benefit of such projects using a numerical model. We developed a method that allows specific properties to operate directly on the total value of other properties to calculate the effective infiltration and relative transmissivity terms. Compared to the standard reclassification and weighting system, this method more accurately reflects the relationships between geology, hydrology, and groundwater recharge. Results suggest that ~30 km^2 of the PVGB may be highly suitable for MAR projects. If MAR were the only solution for groundwater overdraft, this would require implementation of projects on 1.4% of the highly suitable land area. Using a numerical model to simulate MAR projects, we show that project sites on high MAR suitability areas reduce seawater intrusion to a greater extent than other areas. Reducing seawater

intrusion is achieved most efficiently with MAR projects distributed throughout the PVGB in highly suitable locations, rather than located along the coast.

Groundwater development is expected to continue increasing around the world, providing significant economic benefits especially in developing nations. Unfortunately, the financial returns from increased agriculture and industrial development are rarely used towards water management, resulting in declining water tables, reduction in groundwater storage, and water quality issues. MAR projects may contribute towards sustainable groundwater use as a low-cost, low-maintenance, and potentially distributed method. This paper illustrates a simple method for identifying suitable locations for MAR projects, and determining the relative effect of various recharge project scenarios using numerical modeling.

Acknowledgements

We would like to thank Mike Cloud, Michael Cahn, and Marc Los Huertos for their thoughtful contributions. This work was supported by the National Science Foundation Graduate Research Fellowship Program (ID# 2009083666), the National Institute for Water Resources (Grant 08HQGR0054), and The Recharge Initiative (rechargeinitiative.org).

References

Abarca, E., E. Vázquez-Suñé, J. Carrera, B. Capino, D. Gámez, and F. Batlle (2006), Optimal design of measures to correct seawater intrusion, *Water Resources Research*, *42*(9), 1-14, doi:10.1029/2005WR004524.

Adham, M., C. Jahan, Q. Mazumder, M. Hossain, and A.-M. Haque (2010), Study on groundwater recharge potentiality of Barind Tract, Rajshahi District, Bangladesh using GIS and Remote Sensing technique, *Journal of the Geological Society of India*, *75*(1), 432-438.

Aller, L., J. Lehr, and R. Petty (1987), *DRASTIC: A Standardized System to Evaluate Ground Water Pollution Potential using Hydrogeologic Settings*, EPA 600/2-87-035:622.

Bouwer, H. (2002), Artificial recharge of groundwater: hydrogeology and engineering, *Hydrogeology Journal*, *10*, 121-142, doi:10.1007/s10040-001-0182-4.

Brabb, E. E., S. Graham, C. Wentworth, D. Knifong, R. Graymer, and J. Blissenbach (1997), *Geologic map of Santa Cruz County, California*.

Chenini, I., and A. B. Mammou (2010), Groundwater recharge study in arid region : An approach using GIS techniques and numerical modeling, *Computers and Geosciences*, *36*(6), 801-817, doi:10.1016/j.cageo.2009.06.014.

Chenini, I., A. Mammou, and M. El May (2010), Groundwater recharge zone mapping using GIS-based multi-criteria analysis: a case study in Central Tunisia (Maknassy Basin), *Water Resources Management*, *24*, 921-939, doi:10.1007/s11269-009-9479-1.

Chitsazan, M., and Y. Akhtari (2009), A GIS-based DRASTIC model for assessing aquifer vulnerability in Kherran plain, Khuzestan, Iran, *Water Resources Management*, *23*, 1137-1155, doi:10.1007/s11269-008-9319-8.

Chow, V. (1959), *Open-Channel Hydraulics*, McGraw-Hill, New York.

Chowdhury, A., M. Jha, and V. Chowdary (2010), Delineation of groundwater recharge zones and identification of artificial recharge sites in West Medinipur district, West Bengal, using RS, GIS and MCDM techniques, *Environmental Earth Sciences*, *59*, 1209-1222, doi:10.1007/s12665-009-0110-9.

Clark, J., W. Dupre, and L. Rosenberg (1997), *Geologic map of Monterey County, California*.

Dupre, W. (1990), Quaternary geology of the Monterey Bay region, California, in *Geology and tectonics of the Central California Coast region, San Francisco to Monterey*, edited by R. Garrison, H. Greene, K. Hicks, G. Weber, and T. Wright, p. 314, American Association of Petroleum Geologists, Bakersfield, CA.

Foster, S. S. D., and P. J. Chilton (2003), Groundwater: the processes and global significance of aquifer degradation., *Philosophical transactions of the Royal Society of London. Series B, Biological sciences*, *358*(1440), 1957-72, doi:10.1098/rstb.2003.1380.

Fryar, A. E., S. a. Macko, W. F. Mullican III, K. D. Romanak, and P. C. Bennett (2000), Nitrate reduction during ground-water recharge, Southern High Plains, Texas, *Journal of Contaminant Hydrology*, *40*(4), 335-363, doi:10.1016/S0169-7722(99)00059-5.

Giordano, M. (2009), Global Groundwater? Issues and Solutions, *Annual Review of Environment and Resources*, *34*(1), 153-178, doi:10.1146/annurev.environ.030308.100251.

Hanson, R. (2003), *Geohydrologic framework of recharge and seawater intrusion in the Pajaro Valley, Santa Cruz and Monterey Counties, California*, US Geological Survey, Sacramento, CA.

Hanson, R., W. Schmid, J. Lear, and C. Faunt (2008), Simulation of an Aquifer-Storage-and-Recovery (ASR) System using the Farm Process in MODFLOW for the Pajaro Valley, Monterey Bay, California, in *Modflow and More - Ground Water and Public Policy*, pp. 501-505, Golden, CO.

Hanson, R., W. Schmid, C. Faunt, J. Lear, B. S. Lockwood, and S. Predmore (2012), *Hydrologic Model of Pajaro Valley, Santa Cruz and Monterey Counties, California*, US Geological Survey, In Review.

Hanson, R. T., W. Schmid, C. Faunt, and B. Lockwood (2010), Simulation and analysis of conjunctive use with MODFLOW's farm process, *Ground Water*, *58*(5), 674-689.

Harbaugh, A. W. (2005), *MODFLOW-2005, The U.S. Geological Survey modular ground-water model—the Ground-Water Flow Process: U.S. Geological Survey Techniques and Methods 6- A16*.

Hatch, C. E., A. T. Fisher, C. R. Ruehl, and G. Stemler (2010), Spatial and temporal variations in streambed hydraulic conductivity quantified with time-series thermal methods, *Journal of Hydrology*, *389*(3-4), 276-288, doi:10.1016/j.jhydrol.2010.05.046.

Jasrotia, A., R. Kumar, and A. Saraf (2007), Delineation of groundwater recharge sites using integrated remote sensing and GIS in Jammu district, India, *International Journal of Remote Sensing*, *28*(22), 5019-5036, doi:10.1080/01431160701264276.

Jha, M., A. Chowdhury, V. Chowdary, and S. Peiffer (2007), Groundwater management and development by integrated remote sensing and geographic information systems: prospects and constraints, *Water Resources Management*, *21*, 427-467, doi:10.1007/s11269-006-9024-4.

Konikow, L. F., and E. Kendy (2005), Groundwater depletion: A global problem, *Hydrogeology Journal*, *13*(1), 317-320, doi:10.1007/s10040-004-0411-8.

Ma, L., and R. Spalding (1997), Effects of artificial recharge on ground water quality and aquifer storage recovery, *Journal of the American Water Resources Association*, *33*(3), 561-572.

Muir, K. (1972), *Geology and ground water of the Pajaro Valley area, Santa Cruz and Monterey Counties, California*, US Geological Survey, Menlo Park, CA.

Murray, J., and P. A. Mcdaniel (2003), Development of a GIS database for ground-water recharge assessment of the Palouse Basin, *Soil Science*, *168*(11), 759-768, doi:10.1097/01.ss.0000100474.96182.5f.

NRCS (2010a), National Resources Conservation Service, Soil Data Mart, *Santa Cruz County, CA*.

NRCS (2010b), National Resources Conservation Service, Soil Data Mart, *Monterey County, CA*.

Piscopo, G. (2001), *Groundwater vulnerability map explanatory notes: Castlereagh Catchment*.

Racz, A. J., A. T. Fisher, C. M. Schmidt, B. S. Lockwood, and M. L. Huertos (2011), Spatial and Temporal Infiltration Dynamics During Managed Aquifer Recharge., *Ground water*, 1-9, doi:10.1111/j.1745-6584.2011.00875.x.

Rahman, M. A., B. Rusteberg, R. C. Gogu, J. P. Lobo Ferreira, and M. Sauter (2012), A new spatial multi-criteria decision support tool for site selection for implementation of managed aquifer recharge., *Journal of Environmental Management*, *99*, 61-75, doi:10.1016/j.jenvman.2012.01.003.

Rosegrant, M. W., and X. Cai (2009), Global Water Demand and Supply Projections Global Water Demand and Supply Projections Part 2 . Results and Prospects to 2025, , (April 2012), 37-41.

Ruehl, C., a. T. Fisher, C. Hatch, M. L. Huertos, G. Stemler, and C. Shennan (2006), Differential gauging and tracer tests resolve seepage fluxes in a strongly-losing stream, *Journal of Hydrology*, *330*(1-2), 235-248, doi:10.1016/j.jhydrol.2006.03.025.

Saraf, A., and P. Choudhury (1998), Integrated remote sensing and GIS for groundwater exploration and identification of artificial recharge sites, *International Journal of Remote Sensing*, *19*(10), 1825-1841.

Schmid, W., and R. T. Hanson (2009), *The Farm Process Version 2 (FMP2) for MODFLOW-2005—Modifications and Upgrades to FMP1: U.S. Geological Survey Techniques and Methods 6-A-32, 102 p.*

Schmidt, C., A. Fisher, and A. Racz (2011), Rapid nutrient load reduction during infiltration of managed aquifer recharge in an agricultural groundwater basin: Pajaro Valley, California, *Hydrological Processes*, doi:10.1002/hyp.

Shammas, M. I. (2007), The effectiveness of artificial recharge in combating seawater intrusion in Salalah coastal aquifer, Oman, *Environmental Geology*, *55*(1), 191-204, doi:10.1007/s00254-007-0975-4.

Shankar, M. N. R., and G. Mohan (1998), A GIS based hydrogeomorphic approach for identification of site-specific artificial-recharge techniques in the Deccan Volcanic Province, *October*, (1997).

Smith, A. J., and D. W. Pollock (2012), Assessment of Managed Aquifer Recharge Potential Using Ensembles of Local Models, *Ground Water*, *50*(1), 133-143, doi:10.1111/j.1745-6584.2011.00808.x.

Wallace, M., and B. S. Lockwood (2009), *Pajaro Valley Water Management Agency Annual Report*.

Yeh, H.-F., C.-H. Lee, K.-C. Hsu, and P.-H. Chang (2009), GIS for the assessment of the groundwater recharge potential zone, *Environmental geology*, *58*, 185-195, doi:10.1007/s00254-008-1504-9.

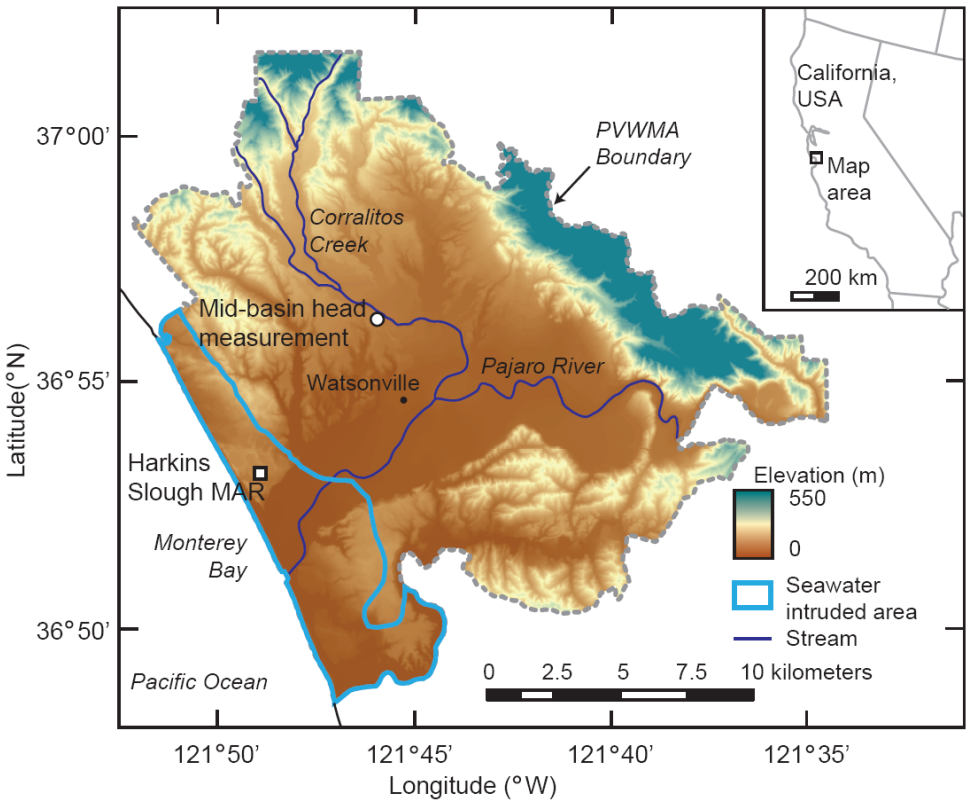

Figure 2-1 Location of the Pajaro Valley, CA, with extent of seawater intrusion measured in 2001[*Hanson*, 2003], elevation and major streams. Area shown is the local water management's (Pajaro Valley Water Management Agency) boundary of operation.

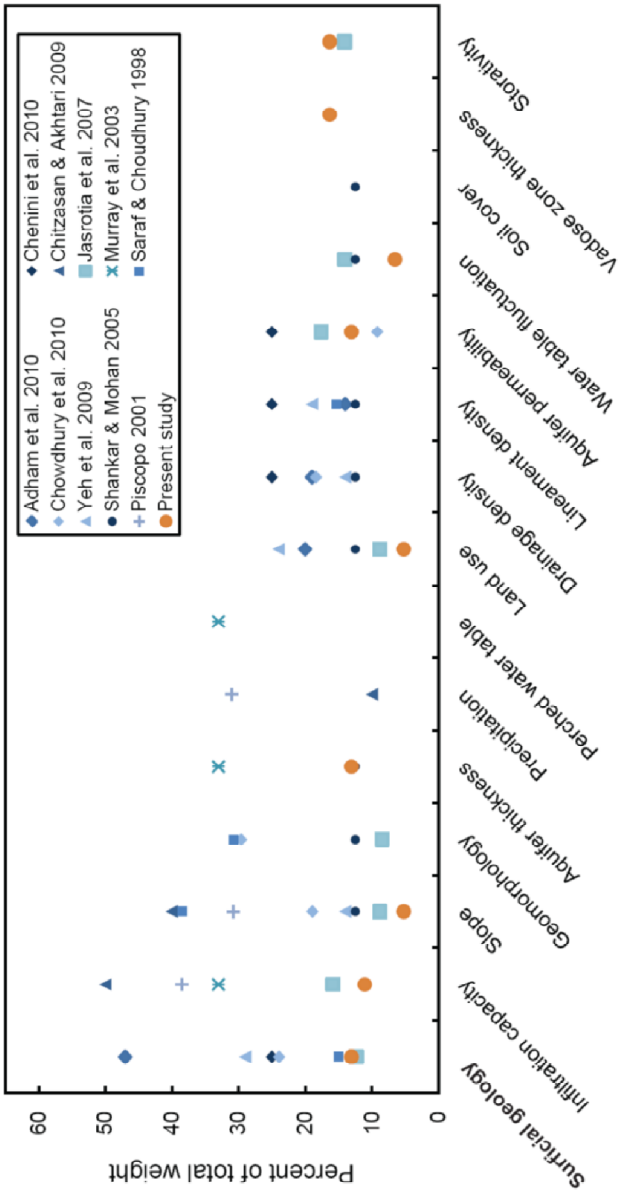

Figure 2-2. Comparison of dataset weights used in other studies to map groundwater recharge with a GIS. The normalized weights used in this study are shown in orange. Values shown for land use and slope are calculated means of values used, because these data sets were used as modifiers for other data sets, as discussed in the text.

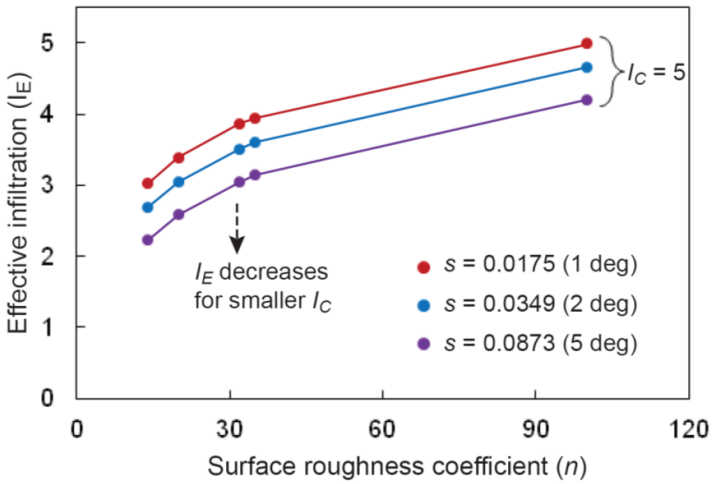

Figure 2-3 Example calculated effective infiltration (I_E) values for 5 roughness coefficients and three slope values, given an infiltration capacity (I_C) value of 5. The I_E curve will move down for larger slopes and smaller I_C values.

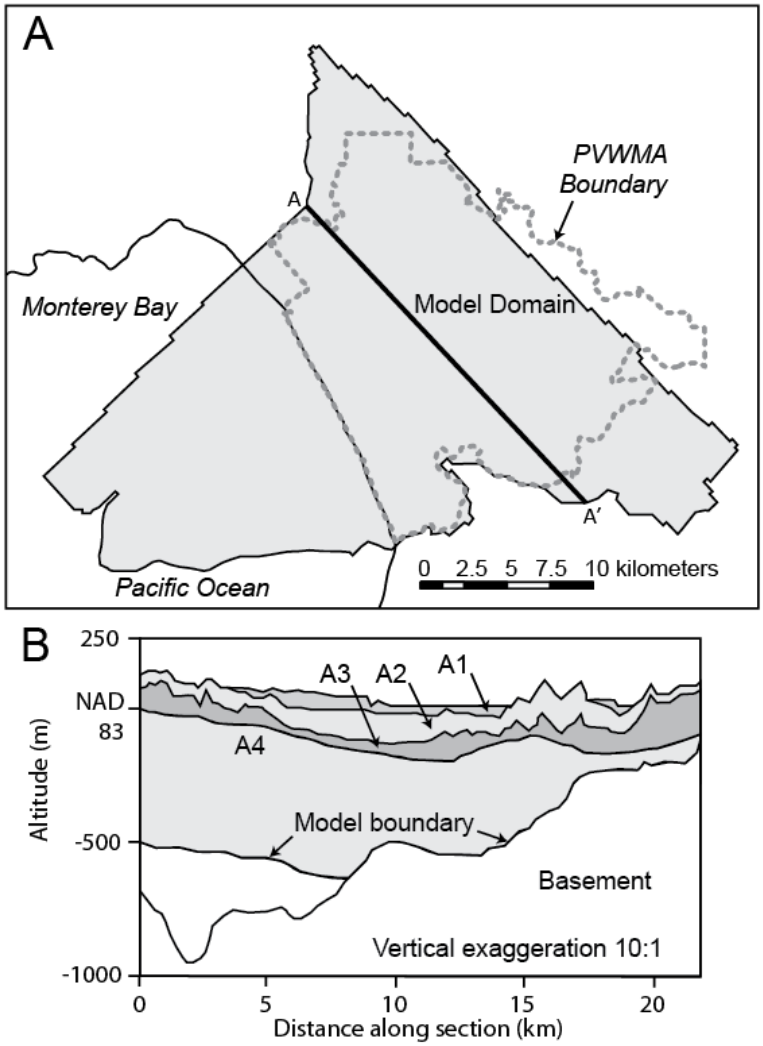

Figure 2-4 Pajaro Valley Hydrologic Model (PVHM), (A) map view of model domain showing grid cells, (B) cross section showing model layers along transect A-A'. Modified from [*Hanson et al.*, 2012].

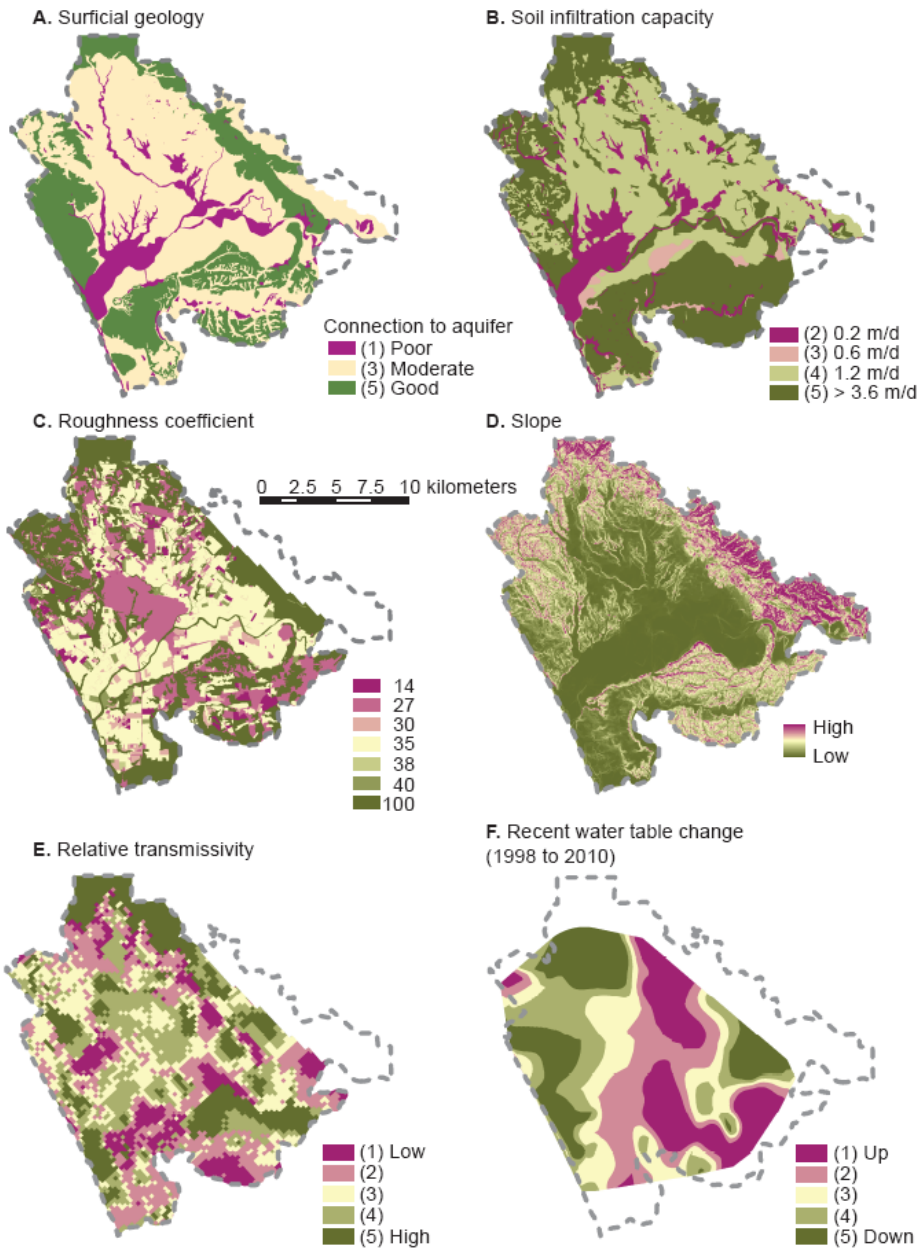

Figure 2-5 Reclassified surface and subsurface properties used to determine relative MAR suitability. (A) surficial geology, (B) soil infiltration capacity, (C) land use, (D) slope, (E) relative transmissivity, (F) change in water table elevation.

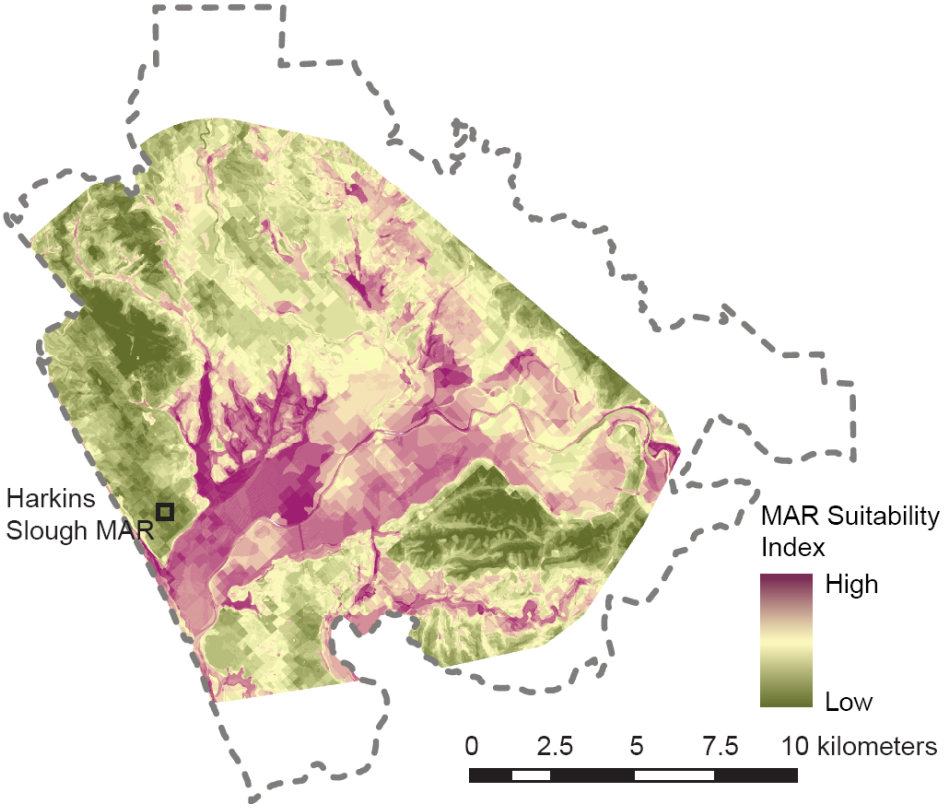

Figure 2-6 Map of relative MAR suitability determined by GIS-based integration. The location of the existing Harkin Slough MAR project is indicated with an arrow.

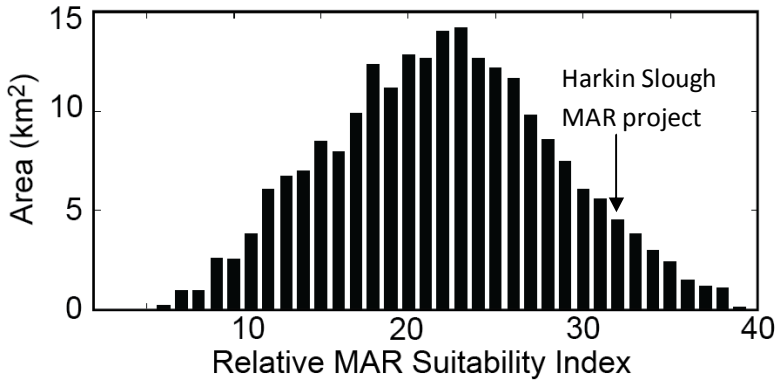

Figure 2-7 Histogram of the MAR suitability index values for the PVGB. The suitability index value of the Harkin Slough project is 32 (81st percentile), which represents field tested managed recharge of approximately 10^6 m^3/yr. Thirteen percent (30 km^2) of the PVGB has similar or higher suitability index values.

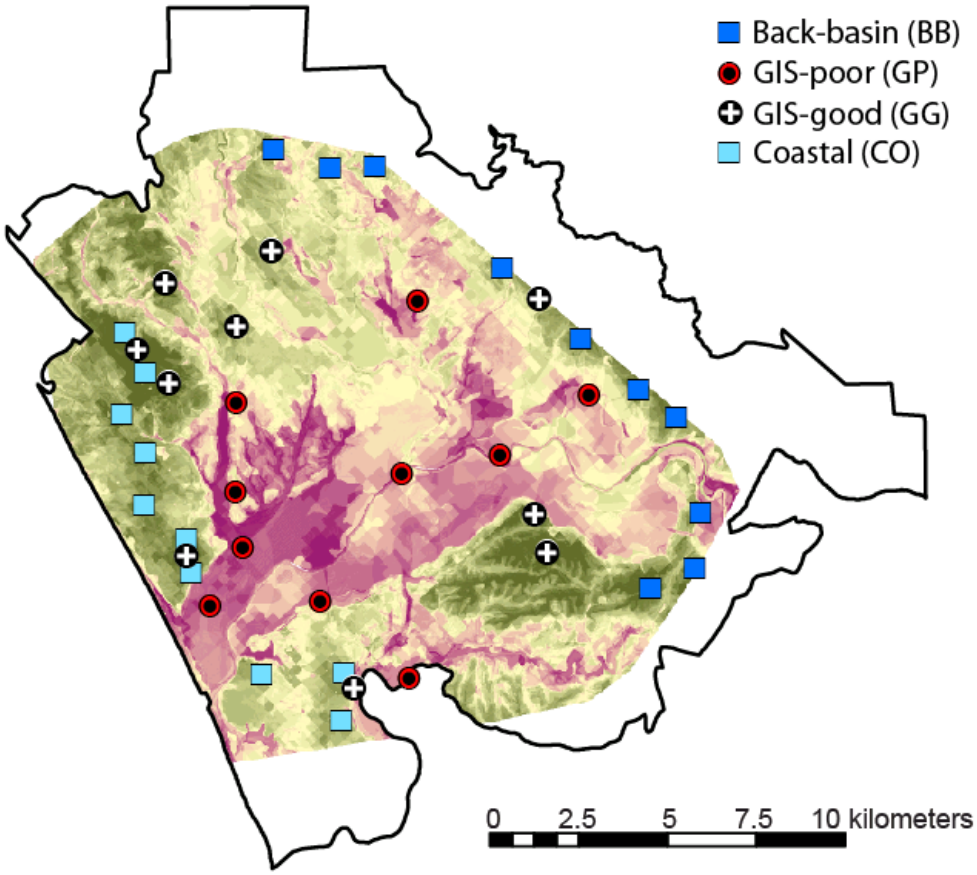

Figure 2-8 MAR scenario location groups shown on the MAR suitability index map. Ten site locations are shown for each of the four groups: Coastal (CO), Back-basin (BB), GIS-good (GG), and GIS-poor (GP). Head levels were compared to the Basecase simulation at a location in Watsonville (**Figure 2-10**), indicated with a filled black circle.

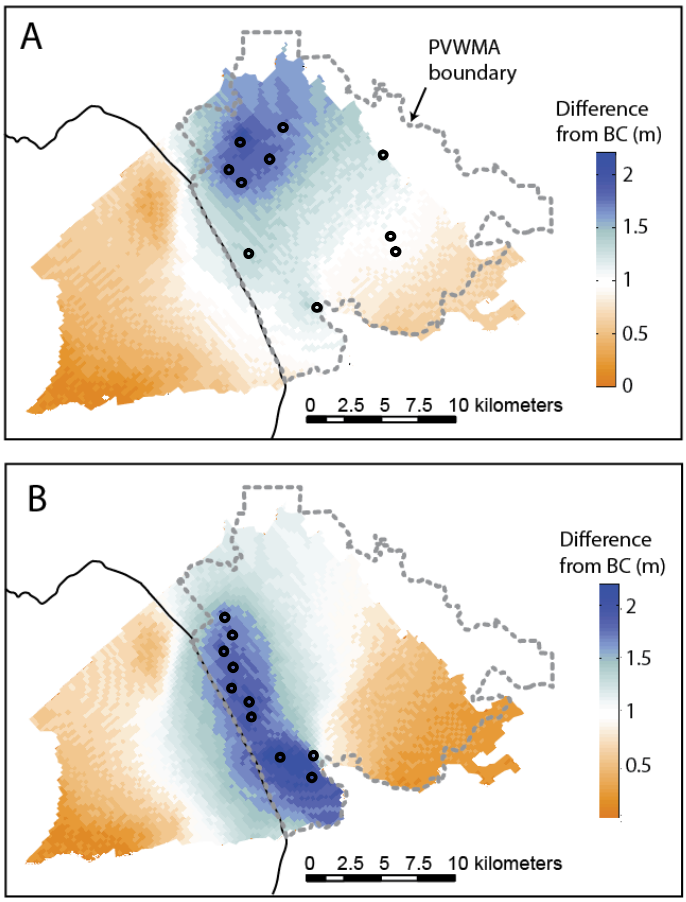

Figure 2-9 Increase in head levels in Layer A2 at model yr-34 relative to the Basecase due to MAR projects simulated in GG Run-22 (A) and CO Run-8 (B) locations. Both scenarios have 10 MAR projects applying 4.6 x 10^5 m^3/y each indicated by black open circles.

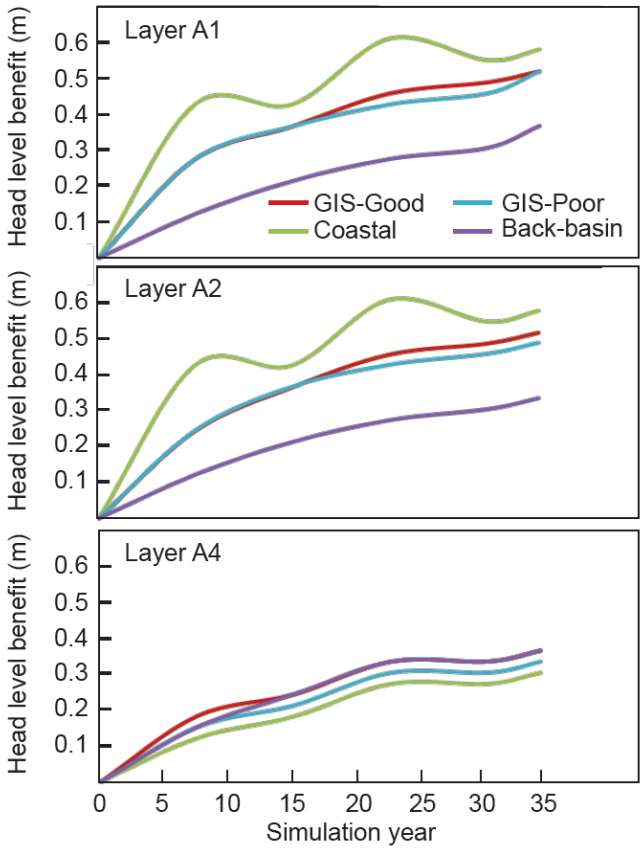

Figure 2-10 Increase in head levels at a point in the middle of the basin (Figure 2-1) relative to the Basecase due to MAR projects simulated in four regions of the basin, (A) in Layer A1, (B) in Layer A2, and (C) in the Layer A4.

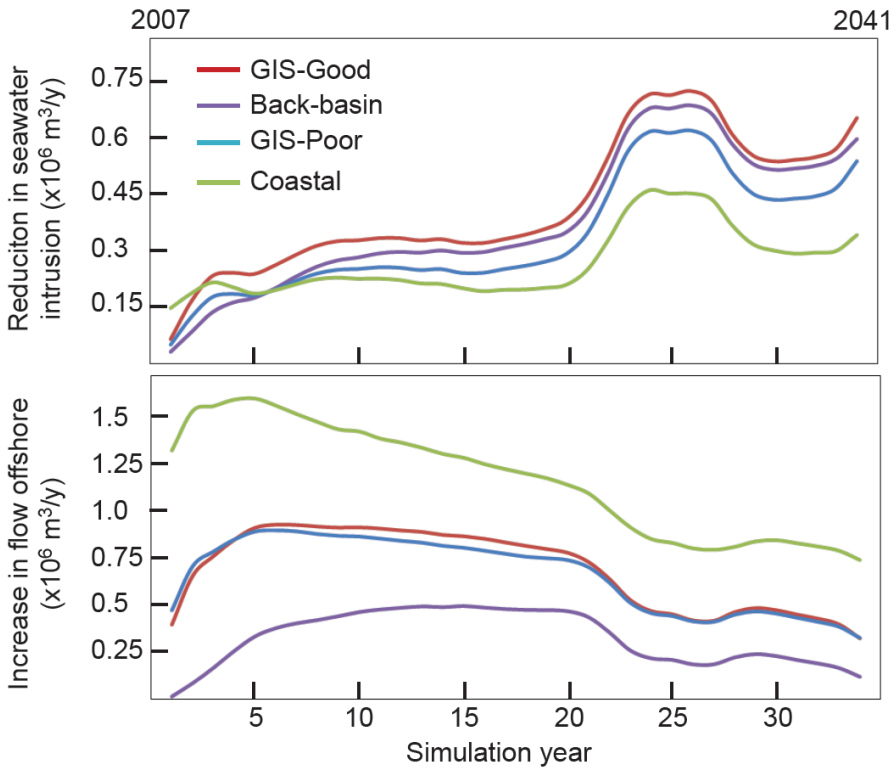

Figure 2-11 Benefits relative to the Basecase due to MAR projects simulated in four regions of the basin, respectively, for (A) Reduction of seawater intrusion shown versus time, and (B) Increase in flow to offshore zone shown versus time. Each scenario has 5 MAR projects, applying 9.8 x 10^5 m^3/y each, and operating 12-mo/y.

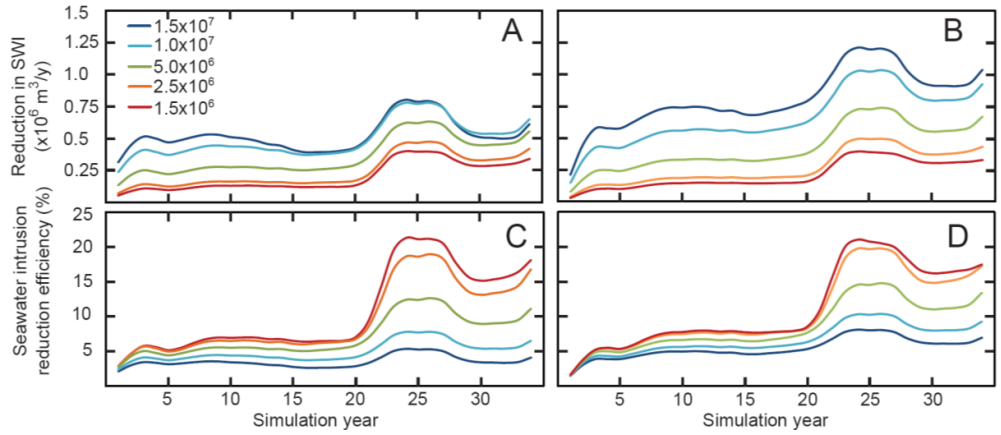

Figure 2-12 seawater intrusion reduction relative to the Basecase due to simulated MAR projects with varying rates of total applied water. Each scenario uses 10 MAR projects operating 12-mo/yr, located at (A) CO sites, and (B) GG sites. The efficiency, with respect to seawater intrusion, is shown for MAR projects located at (C) CO sites, and (D) GG sites.

Table 2-1 Model layer IDs and geologic information

Layer ID	Layer Name	Thickness[1] (m)	Aquifer lithology[2]
A1	Alluvial aquifer	0 to 116	Unconsolidated, moderately sorted silt, sand, and gravel with discontinuous lenses of clay and silty clay
C1	Alluvial clay	0 to 16	--
A2	Upper Aromas aquifer	0 to 153	Sequence of eolian and fluvial sand, silt, clay and gravel
C2	Aromas clay	0 to 35	--
A3	Lower Aromas aquifer	0 to 319	Semiconsolidated, fine-grained, oxidized sand and silt
A4	Purisima aquifer	0 to 500	Thick bedded tuffaceous and diatomaceous siltstone with interbeds of fine-grained sandstone

[1]Layer thickness obtained from the Pajaro Valley Hydrologic Model [*Hanson et al.*, 2012]

[2]Aquifer lithology summarized from USGS geologic maps [*Brabb et al.*, 1997; *Clark et al.*, 1997]

Table 2-2 Classification of data based on physical properties

Soil infiltration capacity		Stream seepage		Surficial geology		Land use	
Rate (m/d)	Value	Rate (m/d)	Value[1]	Connection to aquifer	Value	Description	Roughness coefficient[2]
12	5	>1	40	Good	5	Forest/ Nat. veg.	100
3.6	5	0.2 to 1	34	Moderate	3	Pasture	40
1.2	4			Poor	1	Field crop	38
0.6	3					Row crop	35
0.2	2					Fallow	30
						Turf	27
						Pavement	14

[1]Note that stream seepage rates are field measured and are assigned values that represent highly suitable locations for MAR. For locations where L is measured, the MAR suitability index = L (Eq. 2-7)

[2]Roughness coefficients modified from Chow [1959] are used in Eq. 2-2

Table 2-3 Description of MAR scenario model simulations

Run #	Location	Inf. Rate (m^3/d)	Inf. Rate (ac-ft/y)	Quantity	Active (mo/y)	Total MAR Water (m^3/y)	Total MAR Water (ac-ft/y)
1	Coastal	505	50	5	4	3.1E+05	250
2	Coastal	505	50	10	4	6.2E+05	500
3	Coastal	169	50	10	12	6.2E+05	500
4	Coastal	8085	800	5	4	4.9E+06	4000
5	Coastal	8085	800	10	4	9.9E+06	8000
6	Coastal	505	150	10	12	1.9E+06	1500
7	Coastal	674	200	10	12	2.5E+06	2000
8	Coastal	1347	400	10	12	4.9E+06	4000
9	Coastal	2695	800	10	12	9.9E+06	8000
10	Coastal	4043	1200	10	12	1.5E+07	12000
11	Back-basin	505	50	5	4	3.1E+05	250
12	Back-basin	505	50	10	4	6.2E+05	500
13	Back-basin	8085	800	5	4	4.9E+06	4000
14	Back-basin	8085	800	10	4	9.9E+06	8000
15	Back-basin	2695	800	10	12	9.9E+06	8000
16	GIS-good	505	50	5	4	3.1E+05	250
17	GIS-good	505	50	10	4	6.2E+05	500
18	GIS-good	505	150	10	12	1.8E+06	1500
19	GIS-good	674	200	10	12	2.5E+06	2000
20	GIS-good	8085	800	5	4	4.9E+06	4000
21	GIS-good	2695	800	5	12	4.9E+06	4000
22	GIS-good	1347	400	10	12	4.9E+06	4000
23	GIS-good	8085	800	10	4	9.9E+06	8000
24	GIS-good	2695	800	10	12	9.9E+06	8000
25	GIS-good	4043	1200	10	12	1.5E+07	12000
26	GIS-poor	505	50	5	4	3.1E+05	250
27	GIS-poor	505	50	10	4	6.2E+05	500
28	GIS-poor	8088	800	5	4	4.9E+06	4000
29	GIS-poor	2695	800	5	12	4.9E+06	4000
30	GIS-poor	8085	800	10	4	9.9E+06	8000
31	GIS-poor	2695	800	10	12	9.9E+06	8000

Chapter Three

REGIONAL AND LOCAL INCREASES IN STORM INTENSITY IN THE SAN FRANCISCO BAY AREA BETWEEN 1890 AND 2010

Russo, T. A., A. T. Fisher and D. M. Winslow, Regional and local increases in storm intensity in the San Francisco Bay Area, USA, between 1890 and 2010. *Journal of Geophysical Research: Atmospheres,* **In Review.**

Abstract

Studies of extreme precipitation have documented changes at the continental scale during the 20th century, but few studies have quantified changes at small to regional spatial scales during the same time. We analyze historic data from over 1000 precipitation stations in the San Francisco Bay Area (SFBA), California, to assess whether there have been statistically significant changes in extreme precipitation between 1890 and 2010. An exceedence probability analysis of extreme precipitation events in the SFBA, coupled with a Markov Chain Monte Carlo algorithm, reveals an increase in the occurrence of large events. The depth-duration-frequency characteristics of maximum annual precipitation events having durations of 1 hour to 60 days indicate an increase in storm intensity in the last 120 years, with the intensity of the least frequent (largest) events increasing the most. Mean annual precipitation (MAP) also increased during the study period, but the relative increase in extreme event intensity exceeds that of MAP, indicating that a greater fraction of precipitation fell during large events. Analysis of data from subareas within the SFBA region indicates considerable heterogeneity in the observed nonstationarity. Urban areas show disproportionate increases in storm intensity relative to rural areas. These results emphasize the importance of analyzing local data for accurate risk assessment, emergency planning, and resource management.

3.1 Introduction

Climate change is expected to increase the frequency and intensity of extreme weather events [*Trenberth et al., 2007*], but few studies have explored the nature of hydrologic change occurring on local to regional scales. Evaluating temporal changes in precipitation requires examination of a range of spatial dimensions, from local studies that capture the scales of many extreme storms, to regional and continental studies that quantify large-scale variations in evapotranspiration, moisture transport, and cloud formation [e.g., *Booij*, 2002; *Smith et al.*, 2005]. Some recent research suggests that the regional signal of observable precipitation change will not exceed the natural variability until the late 21st century or beyond [*Giorgi and Bi*, 2009; *Mahlstein et al.*, 2012]. However, significant local changes in precipitation quantity and patterns have been observed over the last 100 years [*Tomozeiu et al.*, 2000; *Douglas and Fairbank*, 2011]. Local studies are particularly important for understanding the mechanisms leading to changes to precipitation patterns, which are needed for the creation and calibration of accurate regional climate models. Local studies are also essential for risk assessment, municipal planning and resource management. Large-scale analyses may not be as directly relevant for policy makers and other stakeholders, although these analyses provide broader context and can indicate where evaluation of local data may be especially important.

Several continental and country-scale precipitation studies of data from the 20th century suggest that the largest storms increased in intensity at rates that exceeded those of annual or seasonal precipitation increases [*Karl and Knight*, 1998;

Groisman et al., 1999, 2005; *Fowler and Kilsby*, 2003]. In some cases, annual to decadal variability in large-scale precipitation patterns correlates with global climate phenomena, including the Pacific Decadal Oscillation (PDO) and El Niño–Southern Oscillation (ENSO) cycles [*Hanson et al.*, 2006; *Higgins et al.*, 2007; *Arriaga-Ramírez and Cavazos*, 2010], or with higher atmospheric moisture content due to increasing temperatures [*Trenberth et al.*, 2003; *Trapp et al.*, 2007; *Allan and Soden*, 2008; *Min et al.*, 2011]. Some assessments of the 20th century North American observational record do not clearly show systematic changes in the intensity of large storms [*Kunkel*, 2003a, 2003b], but this does not preclude significant changes in hydrologic conditions and processes at local to regional scales.

Continental-scale studies of 20th century precipitation that include the San Francisco Bay Area (SFBA), California, have generated disparate results. Studies have shown an increase in the magnitude of extreme precipitation events across the western United States ranging between ~0.5 and 1.5%/decade, [*Karl and Knight*, 1998; *Groisman et al.*, 2004; *Kunkel et al.*, 2010]. Other studies found a decrease in winter (wet season) precipitation [*Weare and Du*, 2008], or changes that are statistically insignificant [*Snyder and Sloan*, 2005; *Barnett et al.*, 2008; *Peterson et al.*, 2008]. Most studies of North America indicate that storm intensity has increased in the last century, although the frequency of storms may have decreased [*Brommer et al.*, 2007] or increased [*Karl and Knight*, 1998].

The present study was motivated by the wide range of results noted above, and by the recognition that long (>100 year), high-quality observational data sets are

available for many areas of interest, including centers of industry, agriculture and urban population such as the SFBA (**Figure 3-1**). Rantz [1971] presented the last comprehensive depth-duration-frequency (DDF) analysis of precipitation in the SFBA, using data collected from 1906 to 1956. These results have been used for decades for technical analysis, planning, and risk assessment [e.g., *Tait and Revenaugh*, 1998; *Keefer*, 2000; *Crovelli and Coe*, 2009], although the observational record Rantz [1971] used was relatively short and is now more than 50 years old.

The present study addresses three main questions: 1) Was there a statistically significant change in the intensity of extreme precipitation in the SFBA during the past 120 years, locally and in comparison to large-scale analyses? 2) Did the magnitudes of extreme events change relative to changes in mean annual precipitation (MAP) during this time? 3) How do local changes in the magnitude of extreme events compare within the SFBA region? This paper does not assess the mechanism(s) responsible for changes in precipitation intensity over the last 120 years, but focuses instead on quantifying the magnitudes of changes apparent in the observational record. Additional work will be required to assess causality and mechanisms, and to quantify the hydrologic implications of documented changes, as discussed later.

3.2 Data Sources

Precipitation data were gathered by the California Department of Water Resources, and include records from the California Data Exchange Center (CDEC), California Irrigation Management Information Systems (CIMIS), and Remote Automatic

Weather Stations (RAWS). Historical data used for depth-duration-frequency (DDF) analyses were obtained from 1015 SFBA precipitation monitoring stations (**Figure 3-2a**) at hourly and daily intervals (336 and 679 stations, respectively). These stations are located within a region of 31,000 km^2, extending from Pacific Ocean coastal areas to the western side of the Central Valley. We split the complete data record into two time periods for comparison: 1890 to 1955 (referred to herein as the "early period") and 1956 to 2010 ("late period"). Data used for DDF analysis had at least 15 years of data in one or both of the study time periods. Data used for individual station statistical analyses came from 111 stations that had at least 15 years of daily data within both time periods. Of the stations in this data set, 40.5% were urban and 59.5% were rural. Data used for decadal DDF analysis came from 33 stations having at least 100 years of data.

3.3 Methods

3.3.1 Regional depth-duration-frequency analysis

We applied a standard metric for quantifying the probability of recurrence of large storms: the annual exceedance probability, p. The annual exceedence probability is the probability that, for a particular duration, an event of a given size or larger will be the largest event in a year. The recurrence interval of such an event, which has an intensity of depth/duration, is calculated as $RI = 1/p$. Exceedance probability analysis is advantageous for quantifying hydrologic conditions because it is widely applied for a variety of data types, is simple to implement, benefits from availability of relatively

long data sets, and produces DDF values that are readily interpreted and understood by researchers, resource managers, industry, and the public at large.

Using observational records from 1890 to 2010 (**Figures 3-2b and 3-2c**), the largest annual event depth at each station was extracted for 17 durations ranging from 1 hour to 60 days. The exceedence probability was calculated for each time period using a Pearson type III distribution fitted to the annual maximum depth data, with skew and kurtosis calculated for individual stations. We report results for six recurrence interval (*RI*) values: 2, 5, 10, 25, 50, and 100 years. Event depth was calculated for every duration–*RI* pair, resulting in 102 characteristic storm intensities.

The time period over which the DDF is calculated may impact resulting values. In this study, the early and late time periods were defined based on the objective of determining whether exceedance depths had changed in the SFBA during two time periods, corresponding roughly to the time period applied in the previous analysis [*Rantz*, 1971], and a time period of roughly equal length that followed. Using 33 stations with at least 100 years of data, the DDF analysis was repeated for 11 decadal time periods between 1890 and 2000, to assess if there are long-term trends apparent across the full time period of the study. Breaking the data set into shorter time intervals makes it less reliable for assessing variations in long-*RI* events, so the decadal analysis was restricted to *RI* values of 2 and 5 years. This analysis was also restricted to event durations of 1 to 60 days, because the decadal records of hourly data were relatively sparse.

3.3.2 Markov Chain Monte Carlo algorithm

We followed Rantz [1971] in completing DDF analyses for the entire SFBA, then identified the linear best-fit model for each duration-*RI* pair, based on regressing storm exceedance depth against MAP, for the two main time periods defined in this study. To test whether the linear best-fit models for the early time periods were consistent with data from the late time period, we conducted a Bayesian analysis using a Markov Chain Monte Carlo (MCMC) approach.

The MCMC method develops a distribution of model parameters (in this case, slope and intercept from a regression of exceedance depth versus MAP) generated from a random ensemble of proposals. Each proposal is accepted or rejected based on known constraints, in the form of prior distributions and the resultant model's misfit from accepted data. The resulting ensembles of modeled parameters are interpreted as data-conditioned probability distributions. We determined the distribution of linear models that fit exceedance depth versus MAP data for early and late time periods, based on 10,000 trials drawn from the population of data available from each applicable weather station. We ran the MCMC analyses for 72 daily duration-*RI* pairs (duration = 1 to 60 days, *RI* = 2 to 100 years). Event durations <1 day were omitted from the MCMC analyses because there are fewer stations having continuous records of this type, particularly for the early time period. The MCMC approach generates an estimate of uncertainty in the slope relating exceedence depth to MAP, and allows for fitting to actual distributions of annual precipitation data for each station, rather than assuming that interannual variations in annual precipitation are normally distributed

around the MAP (as is often done with a traditional least-squares fit). This method extends that used by Rantz [1971] by generating a distribution of slope values, rather than a single best-fit value, relating precipitation exceedence depth to MAP for each duration-*RI* pair.

We used two nonparametric methods to compare the distributions of best fitting linear models from early and late time periods for each duration-*RI* pair subjected to MCMC analysis: Mann-Whitney and Kolmogorov-Smirnov tests. The Mann-Whitney test uses rank analysis, whereas the Kolmogorov-Smirnov test compares cumulative density functions, to determine the probability that data from two sample sets are drawn from a single data set.

3.3.3 Individual station analysis

One hundred and eleven stations with >15 years of data in each time period were used to compare storm intensity differences to MAP differences for individual stations. After calculating differences in exceedence depths for individual stations between the two time periods, we calculated the percent difference in depth, and the normalized difference for each station (the percent difference in exceedance depth divided by the percent difference in MAP at the same station). The normalized difference value is 1.0 if the percent difference of event exceedence depth is the same as the percent difference in MAP. Calculated change plotted by station location illustrates the scale of precipitation change variability. Data from three urban subregions (San Francisco,

San Jose and Napa) in the SFBA were compared to quantify the nature of variations within the area of regional analysis.

The average normalized change for each station was analyzed to assess whether there were quantitative differences in exceedance probabilities between urban and rural stations and on the basis of elevation. We calculated the average and standard deviation of the normalized change values for every station and all duration-*RI* pairs. Normalized change values >4 were classified as "high," whereas values <2 were classified as "low." A similar classification was made for the standard deviation of normalized values, using cutoff values of 3 and 1. Data from all stations were combined to assess whether normalized changes classified as "high" and "low" at urban and rural stations differed from the regional average. Percent anomalies in results from urban and rural setting were defined as the percent differences between setting-specific and full SFBA results classified as "high" or "low." Finding no anomaly would indicate that the aggregates of normalized changes from urban and rural stations were similar to those from the overall SFBA analysis. Similarly, normalized changes were regressed against station elevation. A null result from this analysis would indicate that there is no apparent dependence of change in exceedence probability as a function of station elevation.

3.4 Results

3.4.1 Changes in Mean Annual Precipitation (MAP) and exceedance depth

MAP in the SFBA changed by +4.5% between early and late time periods, although there is considerable variability between stations (**Figure 3-3**). In contrast, for the State of California overall, there was a change in MAP of -4.2% between the same two time periods [*NOAA*, 2012b]. The increase in MAP in the SFBA was accompanied by even larger changes in storm exceedance depth for most duration-*RI* pairs.

As shown by Rantz [1971], the relationship between exceedance depth and MAP for SFBA stations during the early time period was often linear, with greater variability in event depths where MAP was greater. In the later time period, we found greater variability, increased storm intensity (e.g. **Figure 3-4a**), and steeper slopes relating storm exceedance depth to MAP (e.g. **Figure 3-4b**). Coefficients for equations relating exceedence depth to MAP for all duration-*RI* pairs in the late time period are presented in Appendix **A3-3.** Mann-Whitney and Kolmogorov-Smirnov tests of the two slope distributions show that early period data and late period data comprise separate data sets for all 72 duration-*RI* pairs ($\alpha < 0.01\%$).

To illustrate the difference in storm intensity between the two time periods, we compare average exceedance depths for 1, 3, and 10 day storm durations (**Figure 3-5a**). The increase in average exceedance depth between early and late time periods is 0.46 to 6.1 cm/event, corresponding to significant decreases in the *RI* of large storms. For example, a 10-day, 50-yr event during the early time period became the

10-day, 10.3-yr event during the late time period. Similarly, the exceedence depths for 25-yr *RI* storms during the late time period are equal to or greater than equivalent depths for 50-yr *RI* storms during the early time period, for all durations of 1 to 30 days, indicating a ≥100% increase in the exceedance probability of a given event (**Figure 3-5b**). Average exceedance depths calculated over decadal time periods illustrate long-term increasing trends over the past 120 years, although there is considerable decade-to-decade variability (**Figure 3-6**). Nevertheless, every duration-*RI* pair shows a positive trend of exceedance depth versus time based on decadal analysis (**Table 3-1**).

3.4.2 Changes in storm intensity relative to MAP

The increase in the intensity of extreme storms in the SFBA is greater than the increase in annual precipitation, with the largest storms showing the most disproportionate increase. These results are consistent with some large-scale analyses [*Karl and Knight*, 1998; *Groisman et al.*, 1999, 2005; *Fowler and Kilsby*, 2003]. For storm durations of 1 hr to 60 d, the median normalized change ranges from 1.01 to 1.52. On average across the SFBA, ~50% of the precipitation intensity increase can be attributed to an increase in MAP, whereas the rest of this change results from a concentration of a greater fraction of annual precipitation into a smaller number of larger events. More than 20% of SFBA stations show a percent increase in storm intensity four times larger than the percent increase in MAP. Storm intensity changes are often inconsistent with long-term trends in MAP, as seen in some earlier studies

[*Alpert et al.*, 2002; *Goswami et al.*, 2006; *Leahy and Kiely*, 2010; *Douglas and Fairbank*, 2011]. We also found that the relation between storm intensity and MAP varied greatly between stations in a relatively small geographic region, as discussed in the next section.

3.4.3 Local variability

Differences in annual precipitation and in the most intense storms were highly localized within the SFBA (**Figure 3-7**). The spatial scale of changes in extreme storm events appears to occur at ~20 to 50 km, consistent with spatial scale studies of extreme precipitation [*Booij*, 2002; *Smith et al.*, 2005], and >10 times finer than the spatial resolution of previous precipitation change studies. The MAP (**Figure 3-7a**) and change in MAP (**Figure 3-7b**) vary greatly across the region. A majority of the stations show increases in MAP, as shown using 100 yr records (**Figure 3-7b**), though with distinct decreases in the dryer Central Valley. The percent change in storm intensity (**Figure 3-7c**) is generally the same sign as change in MAP, but has a greater magnitude for many stations, indicated by normalized change values >1 (**Figure 3-7d)**.

For three urban subregions, we found that event intensity tended to increase more in San Francisco and Napa than in the San Jose metropolitan area (**Table 3-2**), with the largest local differences being associated with the largest events. For 2-, 5-, and 10-d events having RI = 50 yr, the intensity increase for San Jose was 8 to 19% (~0.7 to 1.6%/decade). In contrast, the same duration-RI events had an intensity

increase of 30 to 42% (~2.5 to 3.5%/decade) in Napa, corresponding to exceedance depth increases of 4.5 to 11 cm.

We found the average and standard deviation of normalized change values to depend, in part, on the urban versus rural setting of individual stations. Seventy one percent of stations with low normalized change values were located in rural settings, whereas 59% percent of stations with high normalized change values were located in urban settings. Thus we found that stations in rural settings were 20% more likely to have less change in extreme precipitation relative to the full SFBA analysis, whereas stations in urban settings were 45% more likely to have a greater change in extreme precipitation. Similarly, rural stations had lower variability in storm intensity, whereas urban stations had greater variability, both relative to the SFBA overall (by 25% and 49%, respectively). We found no correlation between normalized changes in precipitation intensity and elevation across the SFBA.

3.5 Discussion and Conclusions

Our analyses indicate that there have been significant changes in both the frequency and magnitude of extreme precipitation events around the SFBA over the last 120 years. On average, increases in storm intensity are greater than previously estimated for the same area based on analysis of larger regions [*Groisman et al.*, 2004; *Kunkel et al.*, 2010]. In addition to identifying a significant change in storm intensity within the SFBA, we found greater variability than was suggested from previous analyses [*Rantz*, 1971; *Abatzoglou et al.*, 2009], particularly for the largest events. For

example, 25% of the stations in our study show >5%/decade increase in 25 yr *RI* storm magnitude, more than three times that suggested by large-scale analyses. Collectively, these results suggest that municipal planning, infrastructure design, and risk assessment should be updated in response to observed historical (and likely ongoing) trends, and in many cases should emphasize local historical observations.

The mechanism(s) responsible for increased precipitation intensity observed during the late time period were not assessed in this study, but could include greater atmospheric moisture transport and/or storage due to atmospheric warming, or changes to wind patterns or speeds, perhaps in association with annual and decadal-scale global climate phenomena. There are likely to be many factors involved, as indicated by the irregularity of decadal variations in exceedence probability values for *RI*=2 and 5 years (**Figure 3-6**). But the finding of positive slope values for exceedance depth versus time for all 24 duration-*RI* pairs in the decadal analysis (**Table 3-1**) suggests that the increase in storm intensity shown in this study is not an artifact of the time periods selected.

Some studies have suggested that urban development may increase convective precipitation [*Jauregui and Romales*, 1996; *Shepherd*, 2006; *Mote et al.*, 2007]. Our results provide circumstantial support for this interpretation, with urban stations showing disproportionate increases in precipitation intensity compared to MAP relative to the SFBA overall. This suggests that changes in MAP may not be an accurate proxy for estimating changes in the intensity of extreme precipitation events, especially in urban areas. Urban stations in the SFBA also showed greater variability

in extreme storm intensity during the late time period. In contrast, rural areas tended to have increases in storm intensity that were more consistent with changes in MAP, and had less year-to-year variability in the intensity of large events. Identifying the mechanisms responsible for observed differences in temporal trends in extreme precipitation events between urban and rural areas will require further study.

Greater intensity in extreme precipitation, and an associated increase in runoff in urbanized areas, are likely to contribute to more frequent and extensive flooding, erosion, sediment transport, and other geomorphologic changes [e.g., *Baker, 1977*; *Mulligan, 1998*; *Osterkamp and Friedman, 2000*]. Urban planners, resource managers, homeowners, first-responders, and other stakeholders need to reassess whether infrastructure, land-use policies, and agricultural practices are adapted for current and anticipated future hydrologic conditions. Historical daily precipitation records are available for many areas (**Figure 3-1**), which would allow analyses similar to those reported herein to be applied elsewhere. Large-scale studies demonstrating changes in extreme precipitation, combined with results emphasizing the importance of local heterogeneity, suggest that other municipal regions should undertake similar analyses and assessments.

The nonstationarity seen in records from the last 120 years of extreme precipitation events in the SFBA shows how historical analyses tend to lag current conditions. Thus consideration should be given to using trends from precipitation records to project the future probability of major events. Updated records of major event frequency and intensity are also important for assessing how the global

hydrologic system continues to respond to anthropogenic forcing [*Zhang et al.*, 2007; *Barnett et al.*, 2008; *Min et al.*, 2011], and for creating data sets needed to test and calibrate the next generation of regional and global climate models.

References

Abatzoglou, J. T., K. T. Redmond, and L. M. Edwards (2009), Classification of Regional Climate Variability in the State of California, *Journal of Applied Meteorology and Climatology*, *48*(8), 1527–1541, doi:10.1175/2009JAMC2062.1.

Allan, R. P., and B. J. Soden (2008), Atmospheric warming and the amplification of precipitation extremes, *Science*, *321*(5895), 1481–4, doi:10.1126/science.1160787.

Alpert, P., T. Ben-Gai, A. Bahrahad, and Y. Benjamini (2002), The paradoxical increase of Mediterranean extreme daily rainfall in spite of decrease in total values, *Geophysical Research Letters*, *29*(0), 1-4, doi:10.1029/2001GL013554.

Arriaga-Ramírez, S., and T. Cavazos (2010), Regional trends of daily precipitation indices in northwest Mexico and southwest United States, *Journal of Geophysical Research*, *115*(D14), 1–10, doi:10.1029/2009JD013248.

Baker, V. R. (1977), Geological Society of America Bulletin Stream-channel response to floods , with examples from central Texas, *Geological Society Of America Bulletin*, *88*, 1057–1071, doi:10.1130/0016-7606(1977)88<1057.

Barnett, T. P. et al. (2008), Human-induced changes in the hydrology of the western United States, *Science*, *319*(5866), 1080–3, doi:10.1126/science.1152538.

Booij, M. J. (2002), Extreme daily precipitation in Western Europe with climate change at appropriate spatial scales, *International Journal of Climatology*, *22*(1), 69-85, doi:10.1002/joc.715.

Brommer, D. M., R. S. Cerveny, and R. C. Balling (2007), Characteristics of long-duration precipitation events across the United States, *Geophysical Research Letters*, *34*(22), 2–6, doi:10.1029/2007GL031808.

Crovelli, R. A., and J. A. Coe (2009), Probabilistic estimation of numbers and costs of future landslides in the San Francisco Bay region, *Georisk: Assessment and Management of Risk for Engineered Systems and Geohazards*, *3*(4), 206–223, doi:10.1080/17499510802713123.

Douglas, E. M., and C. A. Fairbank (2011), Is Precipitation in Northern New England Becoming More Extreme? Statistical Analysis of Extreme Rainfall in Massachusetts, New Hampshire, and Maine and Updated Estimates of the 100-Year Storm, *Journal of Hydrologic Engineering*, *16*(3), 203–217, doi:10.1061/(ASCE)HE.1943-5584.0000303.

Fowler, H. J., and C. G. Kilsby (2003), Implications of changes in seasonal and annual extreme rainfall, *Geophysical Research Letters*, *30*(13), 1999-2002, doi:10.1029/2003GL017327.

Giorgi, F., and X. Bi (2009), Time of emergence (TOE) of GHG-forced precipitation change hot-spots, *Geophysical Research Letters*, *36*(6), 1-6, doi:10.1029/2009GL037593.

Goswami, B. N., V. Venugopal, D. Sengupta, M. S. Madhusoodanan, and P. K. Xavier (2006), Increasing trend of extreme rain events over India in a warming environment, *Science*, *314*(5804), 1442–5, doi:10.1126/science.1132027.

Groisman, P. Y. et al. (1999), Changes in the probability of heavy precipitation: Important indicators of climatic change, *Climatic Change*, *42*(1), 243–283, doi:10.1023/A:1005432803188.

Groisman, P. Y., R. W. Knight, T. R. Karl, D. R. Easterling, B. Sun, and J. H. Lawrimore (2004), Contemporary changes of the hydrological cycle over the contiguous United States: Trends derived from in situ observations, *Journal of Hydrometeorology*, *5*(1), 64–85, doi:10.1175/1525-7541(2004)005<0064:CCOTHC>2.0.CO;2.

Groisman, P. Y., R. W. Knight, D. R. Easterling, T. R. Karl, G. C. Hegerl, and V. N. Razuvaev (2005), Trends in intense precipitation in the climate record, *Journal of Climate*, *18*(9), 1326–1351, doi:10.1175/JCLI3339.1.

Hanson, R. T., M. D. Dettinger, and M. W. Newhouse (2006), Relations between climatic variability and hydrologic time series from four alluvial basins across the southwestern United States, *Hydrogeology Journal*, *14*(7), 1122–1146, doi:10.1007/s10040-006-0067-7.

Higgins, R. W., V. B. S. Silva, W. Shi, and J. Larson (2007), Relationships between Climate Variability and Fluctuations in Daily Precipitation over the United States, *Journal of Climate*, *20*(14), 3561–3579, doi:10.1175/JCLI4196.1.

Jauregui, E., and E. Romales (1996), Urban effects on convective precipitation in Mexico City, *Atmospheric Environment*, *30*(20), 3383–3389, doi:10.1016/1352-2310(96)00041-6.

Karl, T. R., and R. W. Knight (1998), Secular trends of precipitation amount, frequency, and intensity in the United States, *Bulletin of the American Meteorological Society*, *79*(2), 231–241, doi:10.1175/1520-0477(1998)079<0231:STOPAF>2.0.CO;2.

Keefer, D. K. (2000), Statistical analysis of an earthquake-induced landslide distribution — the 1989 Loma Prieta, California event, *Engineering Geology*, *58*, 231–249, doi:10.1016/S0013-7952(00)00037-5.

Kunkel, K. E. (2003a), North American trends in extreme precipitation, *Natural Hazards*, *29*, 291–305, doi:10.1029/2003GL018052.

Kunkel, K. E. (2003b), Temporal variations of extreme precipitation events in the United States: 1895–2000, *Geophysical Research Letters*, *30*(17), 1–4, doi:10.1029/2003GL018052.

Kunkel, K. E., K. Andsager, and D. R. Easterling (2010), Long-term trends in extreme precipitation events over the conterminous United States and Canada, *Journal of Climate*, *12*, 2515–2527, doi:10.1175/1520-0442(1999)012<2515:LTTIEP>2.0.CO;2.

Leahy, P. G., and G. Kiely (2010), Short Duration Rainfall Extremes in Ireland: Influence of Climatic Variability, *Water Resources Management*, *25*(3), 987–1003, doi:10.1007/s11269-010-9737-2.

Mahlstein, I., R. W. Portmann, J. S. Daniel, S. Solomon, and R. Knutti (2012), Perceptible changes in regional precipitation in a future climate, *Geophysical Research Letters*, *39*(February), 1-5, doi:10.1029/2011GL050738.

Mantua, N. J., S. R. Hare, Y. Zhang, J. M. Wallace, R. C. Francis, and others (1997), A Pacific interdecadal climate oscillation with impacts on salmon production, *Bulletin of the American Meteorological Society*, *78*(6), 1069–1080, doi:10.1175/1520-0477(1997)078<1069:APICOW>2.0.CO;2.

Min, S.-K., X. Zhang, F. W. Zwiers, and G. C. Hegerl (2011), Human contribution to more-intense precipitation extremes, *Nature*, *470*(7334), 378–381, doi:10.1038/nature09763.

Mote, T. L., M. C. Lacke, and J. M. Shepherd (2007), Radar signatures of the urban effect on precipitation distribution: A case study for Atlanta, Georgia, *Geophysical Research Letters*, *34*(20), 2-5, doi:10.1029/2007GL031903.

Mulligan, M. (1998), Modelling the geomorphological impact of climatic variability and extreme events in a semi-arid environment, *Geomorphology*, *24*(1), 59–78, doi:10.1016/S0169-555X(97)00101-3.

NOAA (2012a), Global Historical Climatology Network - Daily, www.ncdc.noaa.gov/oa/climate/ghcn-daily/.

NOAA (2012b), State of California, average precipitation, www.ncdc.noaa.gov/temp-and-precip/.

Osterkamp, W. R., and J. M. Friedman (2000), The disparity between extreme rainfall events and rare floods -- with emphasis on the semi-arid American West, *Hydrological*

Processes, *14*, 2817–2829, doi:10.1002/1099-1085(200011/12)14:16/17<2817::AID-HYP121>3.0.CO;2-B.

Peterson, T. C., X. Zhang, M. Brunet-India, and J. L. Vázquez-Aguirre (2008), Changes in North American extremes derived from daily weather data, *Journal of Geophysical Research*, *113*(D7), 1–9, doi:10.1029/2007JD009453.

Rantz, S. E. (1971), *Precipitation depth-duration-frequency relations for the San Francisco Bay region, California*, US Geological Survey, Prof. Paper 750-C, 237-241.

Shepherd, J. M. (2006), Evidence of urban-induced precipitation variability in arid climate regimes, *Journal of Arid Environments*, *67*(4), 607–628, doi:10.1016/j.jaridenv.2006.03.022.

Smith, D., A. Gasiewski, D. Jackson, and G. Wick (2005), Spatial scales of tropical precipitation inferred from TRMM microwave imager data, *Geoscience and Remote Sensing*, *43*(7), 1542-1551, doi:10.1109/TGRS.2005.848426.

Snyder, M. A., and L. C. Sloan (2005), Transient Future Climate over the Western United States Using a Regional Climate Model, *Earth Interactions*, *9*(11), 1–21, doi:10.1175/EI148.1.

Tait, J. F., and J. Revenaugh (1998), Source-transport inversion: An application of geophysical inverse theory to sediment transport in Monterey Bay, California, *Journal of Geophysical Research*, *103*(C1), 1275–1283, doi:10.1029/97JC01909.

Tomozeiu, R., A. Busuioc, V. Marletto, F. Zinoni, and C. Cacciamani (2000), Detection of changes in the summer precipitation time series of the region Emilia-Romagna , Italy, *Journal of Geophysical Research*, *200*, 193-200.

Trapp, R., N. Diffenbaugh, H. Brooks, M. Baldwin, E. Robinson, and J. Pal (2007), Changes in severe thunderstorm environment frequency during the 21st century caused by anthropogenically enhanced global radiative forcing, *Proceedings of the National Academy of Sciences of the United States of America*, *104*(50), 19719-19723, doi:10.1073/pnas.0705494104.

Trenberth, K. E., A. Dai, R. M. Rasmussen, and D. B. Parsons (2003), The Changing Character of Precipitation, *Bulletin of the American Meteorological Society*, *84*(9), 1205–1217, doi:10.1175/BAMS-84-9-1205.

Trenberth, K. E., P. D. Jones, P. Ambenje, R. Bojariu, D. Easterling, A. Klein Tank, D. Parker, F. Rahimzadeh, J.A. Renwick, M. R., and B. S. and P. Zhai (2007), *Observations: Surface and Atmospheric Climate. In: Climate Change 2007: The Physical Science Basis.*, Cambridge University Press.

Weare, B., and H. Du (2008), Modelling regional climate changes: influences of recent global warming and irrigation in California, *International Journal of Climatology*, *28*, 1201–1212, doi:10.1002/joc.

Zhang, X., F. W. Zwiers, G. C. Hegerl, F. H. Lambert, N. P. Gillett, S. Solomon, P. a Stott, and T. Nozawa (2007), Detection of human influence on twentieth-century precipitation trends, *Nature*, *448*(7152), 461–5, doi:10.1038/nature06025.

Acknowledgments: We thank Jim Goodridge (California Department of Water Resources) for providing thorough and organized precipitation records extending back more than a century. This work was supported by the National Science Foundation Graduate Research Fellowship Program (ID# 2009083666), the National Institute for Water Resources (Grant 08HQGR0054), and The Recharge Initiative.

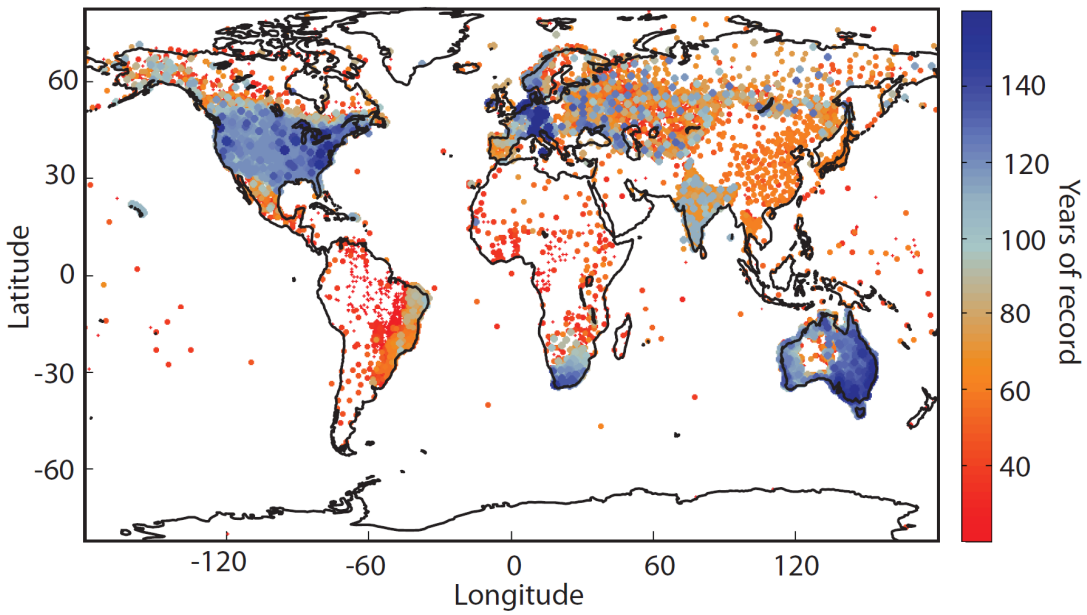

Figure 3-1 Length of worldwide historical daily precipitation records [*NOAA*, 2012a]. Station record lengths are represented with a color gradient, from 20 years (red) to >160 years (blue).

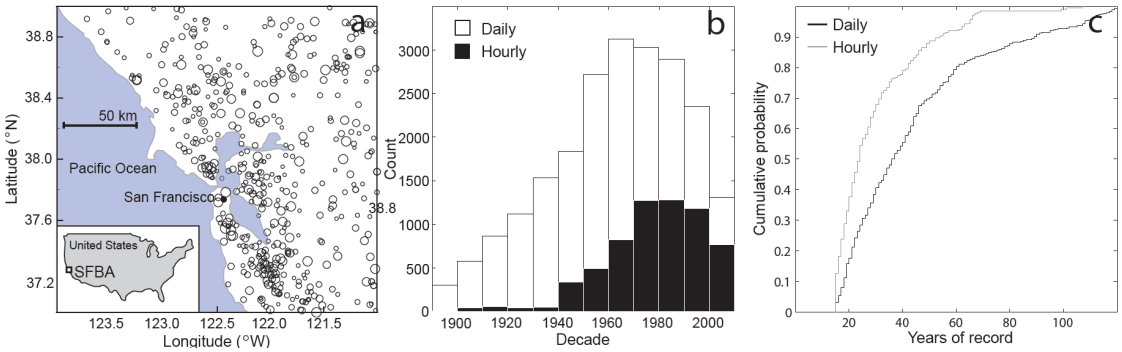

Figure 3-2 (a) Locations of precipitation stations in the SFBA used in this study. Size of the station marker indicates the record duration for that station, ranging from 15 years to 120 years. Total number of daily and hourly records shown as a (b) histogram for each decade, daily data in white, hourly data in black, and (c) cumulative density function, daily data in black, hourly data in gray.

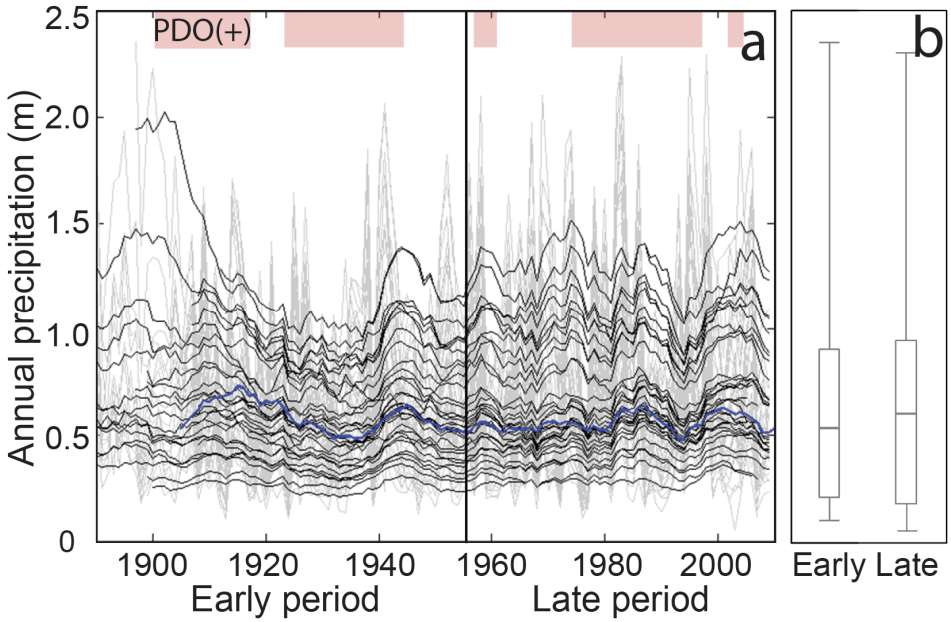

Figure 3-3 (a) Annual total precipitation from 33 SFBA stations with a record longer than 100 years (grey), 10 year running average for each station (black), and 10 year running average for State of California (blue) [*NOAA*, 2012b]. Periods with positive average PDO index [*Mantua et al.*, 1997] are shown highlighted in pink. (b) Median annual precipitation for the early and late time periods, 1890 to 1955 and 1956 to 2010, respectively. Boxes represent one standard deviation with whiskers at maximum and minimum values for each period.

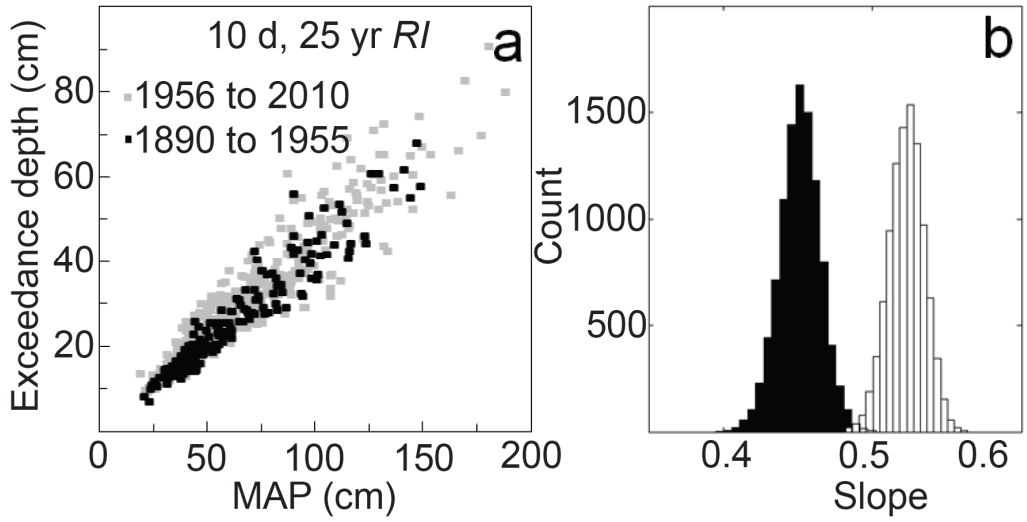

Figure 3-4 Example of exceedence depth versus MAP and distribution of slopes for 10-d, 25-yr events, calculated for early and late time periods. (**a**) Exceedence depth versus MAP, with early time data (1890-1955) in black and late time data (1956-2010) in gray. The early time result is essentially that calculated by Rantz [1971], whereas the late time data show more variability, greater storm intensity, and a steeper slope, (**b**) The distribution of linear model slopes that fit the data from plot 3A based on an MCMC analysis, with early time data (1890-1955) in black, and late time data (1956-2010) in white. This histogram shows visually what was revealed through nonparametric statistical analyses: data from the two time periods comprise separate data sets.

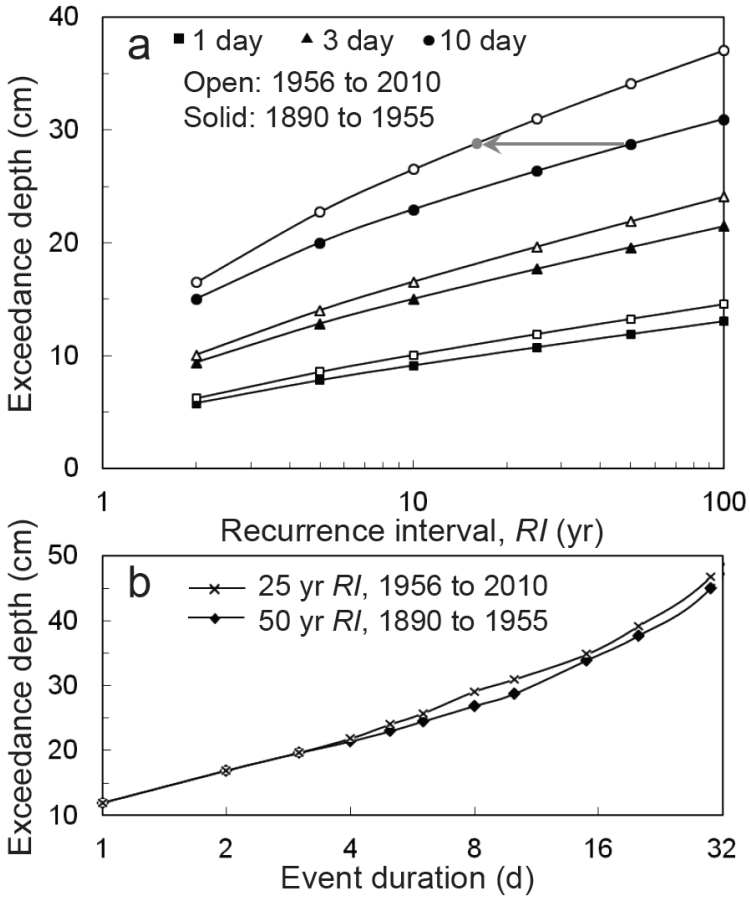

Figure 3-5 Exceedance depths from early and late time periods shown for (**a**) 1-, 3- and 10-d storms plotted for *RI* = 2 to 100 yr, and (**b**) *RI* = 50-yr storm in the early period, and the *RI*=25 yr *RI* storm in the late period. Arrow in (a) shows that the 10-d, 50-yr storm exceedance depth in the early time period is equal to the 10-d, 10.3-yr *RI* storm in the late period.

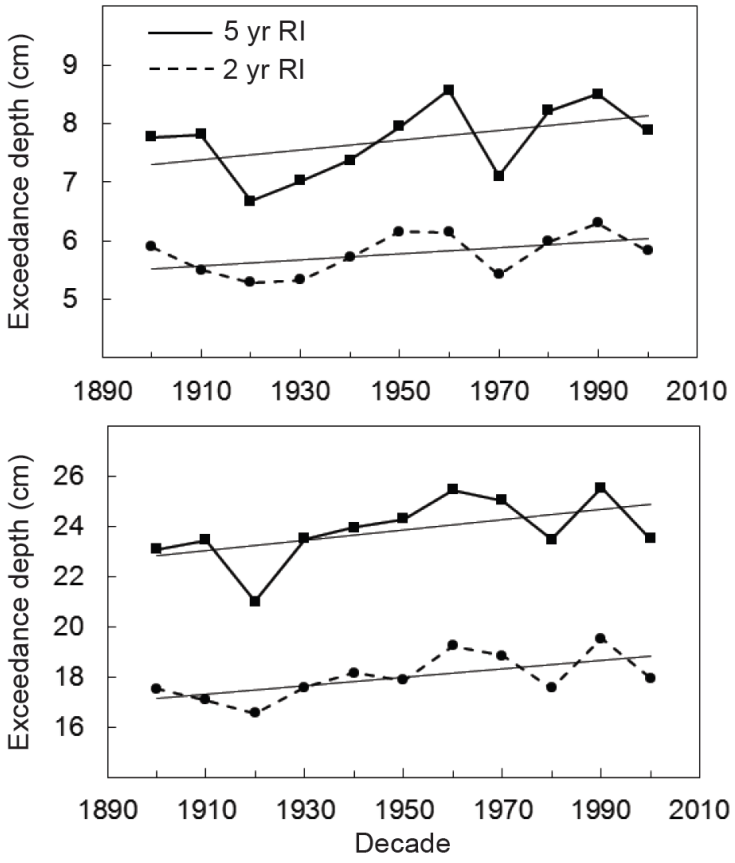

Figure 3-6 Event magnitudes calculated for 1 and 15 day storms (a and b, respectively), with 2 year (dashed-line) and 5 year (solid-line) recurrance intervals, for each decade of the 20th century. The slope and the R^2 value are given for all daily storm durations in Table 1.

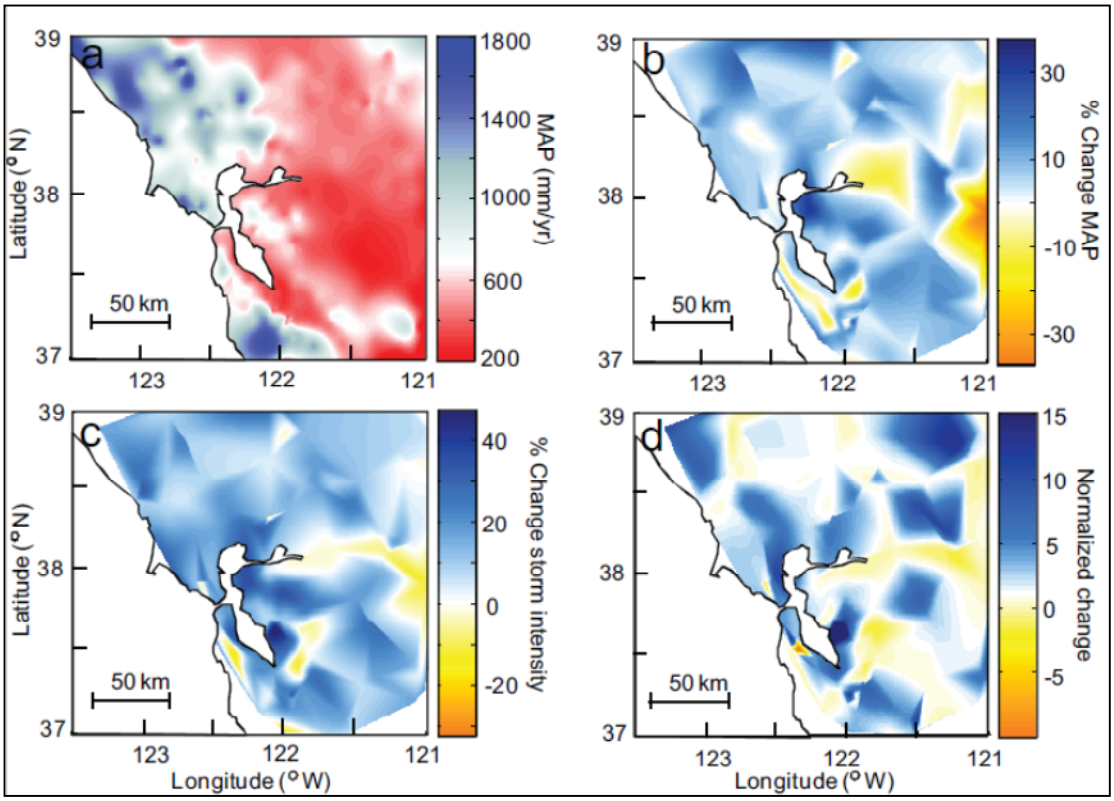

Figure 3-7 Individual station analysis results showing (a) MAP from the later period, (b) MAP percent change between the early and late periods, (c) average percent change of daily storm exceedance depths between the early and late periods, and (d) normalized storm intensity change.

Table 3-1. Slope of linear regression showing change between exceedence depth and mean annual precipitation analysed over decadal time periods. [1] Decadal data and trends for 1 and 15 day storms are shown in Figure 3-2.

Duration (d)	*RI* (yr)	*m*	R^2
1	2	0.0051	0.21
1	5	0.0084	0.23
2	2	0.0065	0.16
2	5	0.012	0.13
3	2	0.0068	0.14
3	5	0.011	0.10
4	2	0.0084	0.25
4	5	0.013	0.15
5	2	0.0066	0.15
5	5	0.012	0.14
6	2	0.0066	0.12
6	5	0.012	0.11
8	2	0.0068	0.11
8	5	0.014	0.18
10	2	0.0088	0.13
10	5	0.017	0.20
15	2	0.017	0.38
15	5	0.020	0.28
20	2	0.023	0.46
20	5	0.023	0.27
30	2	0.040	0.40
30	5	0.037	0.15
60	2	0.053	0.31
60	5	0.057	0.14

[1] Regression equations for the change in precipitation exceedance depth calculated using decadal time periods for 2- and 5-yr *RI* storms.

Table 3-2. Average changes in storm exceedance depth[1]

Location		San Jose						San Francisco						Napa					
RI (yr)		50	25	10	5	2		50	25	10	5	2		50	25	10	5	2	
2 d Event	Change (cm)	0.6	0.8	0.9	0.9	0.5		3.9	3.1	2.1	1.3	0.4		4.5	4.0	3.2	2.6	1.4	
	% Change	8.1	9.6	12	14	10		42	35	26	19	7.1		31	29	26	22	15	
5 d Event	Change (cm)	0.8	1.0	1.1	1.1	0.7		4.2	3.3	2.3	1.5	0.5		11	8.4	5.6	3.6	1.1	
	% Change	8.2	9.6	11	13	11		31	26	19	14	6.0		43	36	27	20	8.6	
10 d Event	Change (cm)	3.0	2.6	2.1	1.7	0.9		6.3	4.9	3.1	1.8	0.4		11	9.2	6.4	4.4	1.9	
	% Change	19	18	17	15	11		34	28	20	13	4.0		33	29	24	19	11	
Mean Normalized change in depth[2]		2.0	2.0	1.9	1.8	1.2		4.4	3.8	3.0	2.3	1.4		2.4	2.2	1.9	1.6	1.6	

[1] Examples for three cities in the SFBA

[2] Percent change in event depth divided by the percent change in MAP at each station, respectively

CONCLUSIONS

Environmental changes are influencing hydrologic and other Earth systems at an unprecedented rate, and in many cases with detrimental results. This thesis quantified hydrologic system behavior and response to environmental change as part of three case studies, which is required for the development of effective restoration practices. Changes to most hydrologic systems have consequences for ecologic or human development and safety, therefore restoration practices are often considered to improve hydrologic conditions. Some anthropogenic-based changes (as in the first two case studies) can be mitigated, either by altering the current practices or by initiating some form of restoration. For the third case study on extreme rainfall, the objective was not restoration but rather to quantify the nature of extreme precipitation event changes.

The three thesis chapters are disparate in study area and objectives, but all include quantification of hydrologic system behavior. In Chapter 1, we monitored wetland soil response to a controlled flood, then used this information to calibrate a numerical model. Based on subsequent modeling, we concluded that surface inundation is more efficient for establishing wetland conditions than lateral and upward groundwater transport in this setting. This information can be used in flood release optimization, where multiple factors including limiting water use for wetland restoration are considered. In Chapter 2, we used GIS to show that over 13% of the 220 km^2 Pajaro Valley groundwater basin may be highly suitable for managed aquifer

recharge (MAR). Numerical model results suggest that over the next several decades, MAR projects distributed throughout the basin could be more effective at reducing seawater intrusion than a similar number of projects located mainly along the coast. In Chapter 3, we showed statistically significant increases in the intensity of extreme precipitation in the San Francisco Bay Area over the last 120 years. These changes exceed relative changes in mean annual precipitation during the same time, and are variable on a spatial scale of ~50 km scale. This last result suggests that city planning and risk management decisions should be based on local, rather than analyses complete at regional or continental scales.

The results from Chapters 1 and 2 have been provided to several organizations that are working to solve ongoing hydrologic problems. Model results and hypothetical flood scenario responses from Chapter 1 were provided to Yosemite National Park and the San Francisco Public Utilities Commission. The flood release in 2010, following conveyance of our results, had similar characteristics to flood scenario #3 presented in Chapter 1, including multiple high flow cycles which use surface inundation to achieve wetland saturation conditions more efficiently than lateral groundwater transport during medium river discharge periods. The MAR suitability map and modeling results were given to the Pajaro Valley Water Management Agency (PVWMA), the Resource Conservation District of Santa Cruz County (RCD), and presented several times at Pajaro Valley Community Water Dialogue meetings. The results will contribute towards development of the Pajaro Valley Basin Management Plan, a comprehensive effort to restore hydrologic

conditions which will likely include managed aquifer recharge, water conservation, and other approaches to bring the PVGB back into hydrologic balance. The RCD is using the MAR suitability map as part of a hydrologic assessment of the Watsonville Sloughs.

In all cases, restoration practices will introduce additional environmental changes on the hydrologic system. For example, the overall goal of the project in Chapter 1 was to restore wetlands that have been degraded by upstream river regulation. The overall goal of MAR, assessed in Chapter 2, was to increase groundwater recharge by diverting, detaining, and infiltrating excess surface water. These projects may seem contradictory from a management perspective: development of the second study's objective could create problems similar to that addressed in the first study. In practice, however, both projects clarify groundwater dynamics that will help improve conditions in response to major environmental changes. This dichotomy between theory and practice exemplifies the need for understanding relative impacts of restoration practices with respect to ecologic and human concerns, as well as hydrologic conditions.

Results from Chapter 3 have implications for fundamental research, including the influence of extreme rainfall changes on erosion, groundwater recharge, river discharge, and improvement of regional climate models. Implications for human activity include city planning and flood design, as well as water resource management. The study results are not yet published (a paper is in review as this thesis is being written), but the level of interest generated by presentations at

scientific meetings and discussions with water agency staff suggests that these findings will be put to use soon after publication.

As the climate continues to change and human population grows, studies that quantify the influence of environmental change on hydrologic systems will become even more necessary. Future wetland restoration research should be performed in other locations, and at multiple stages of the improvement process, including follow-up evaluation of restoration techniques. The next step required for the managed aquifer recharge study is implementation of pilot systems and full MAR projects. The Recharge Initiative and hydrogeology group at UCSC currently has one active pilot site and is performing field percolation tests at other potential sites in the Pajaro Valley (and elsewhere around Monterey Bay). Their results can be used to calibrate the MAR suitability map and improve the weighting system. The regional rainfall exceedance probability analysis should be performed in other settings where there are sufficiently long and detailed precipitation records, and updated as new records become available. Each of these projects will advance the study and application of hydrologic science by linking fundamental research objectives with developing efficient, effective, and broadly beneficial management practices.

APPENDICES

Chapter 2

A2.1 GIS ModelBuilder schematic

Input files for the MAR Suitability model:
1) Monterey County Surficial Geology
2) Santa Cruz County Surficial Geology
3) Calculated effective infiltration (function of soil infiltration capacity, slope and land use)
4) Calculated relative transmissivity (function of aquifer hydraulic conductivity, thickness and confining layer thickness)
5) Recent change in water table elevation
6) Storativity (function of specific yield and unsaturated thickness)
7) Losing stream reaches (measured)

The output is the final MAR Suitability coverage.

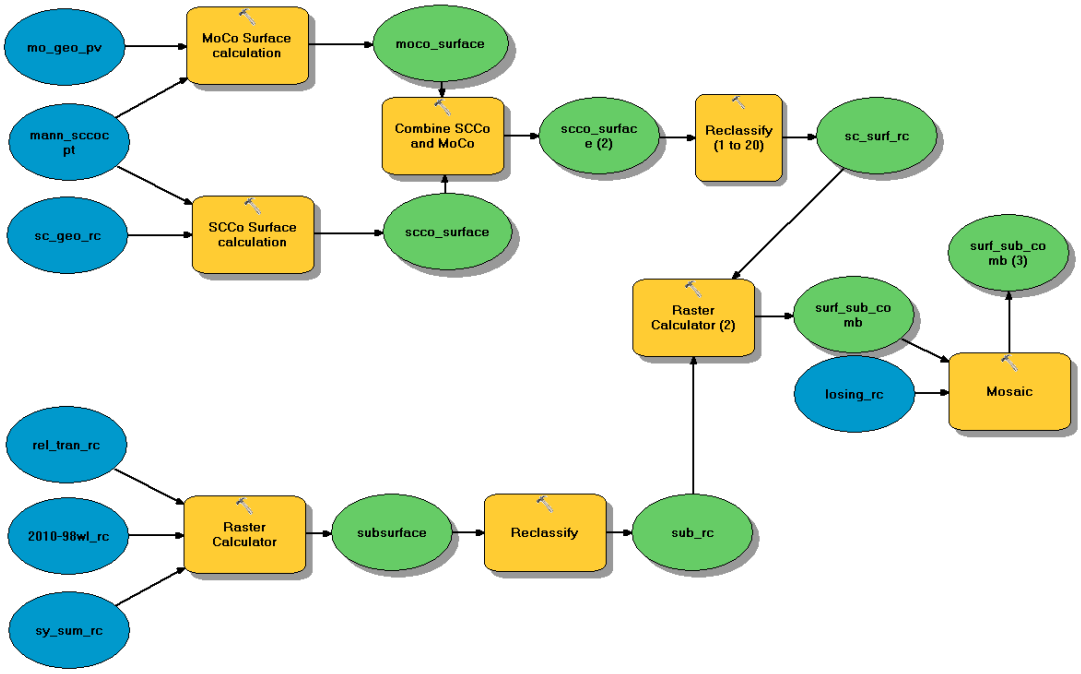

A2.2 Generate MAR input file (MATLAB)

```
% genwelin.m
% Generate-Well-Input

% The objective of this program is to generate the Domestic Well
input file for the PVHM. The program has 1527 wells that it runs at
the same flowrate for each 408 stress period. The MAR projects will
be represented as additional wells that operate only during months
defined as "active". During inactive months, the wells will still be
there, but they will not pump any water.

% The following files need to be created before running the code:
   1) dom_wells.txt - A list of the domestic well files without the
      input file header
   2) MAR_scen.txt – A list of the simulated MAR projects that
      contains the model layer they recharge to (the surface layer),
      and the model grid coordinates, and pumping/recharge rate
   3) MAR_inact.txt – A list of the simulated MAR projects identical
      to MAR_scen.txt, but with pumping rates of 0.

clear
nummar = input('Please enter the number of MAR projects:  ');
mactive = input('Please enter the number of active MAR months per
year:  ');

% Load the basecase domestic well input data

dmwel = load('dom_wells.txt');
[dr dc] = size(dmwel);

% Load the MAR input data

mars = load('MAR_scen.txt');
[mr mc] = size(mars);

% Load the MAR input data for inactive months

marinact = load('MAR_inact.txt');

numwel = dr + mr;

% We assume that stress period 1 is January and is an active month
in all cases.

% Write info for stress period 1, MAR and domestic wells
wmact = vertcat(mars, dmwel);
wminact = vertcat(marinact,dmwel);
numw = 1527;
numwm = numw + nummar;
save new_input.txt numwm -ascii
save -append new_input.txt wmact -ascii
```

```
minact = 12 - mactive;
rep = -1;
i = 1;
for i=1:34; % for each stress period (month)
    % Stress period 1 is already written
    % Repeat previous stress period input for active months
    for j=1:mactive-1;
        save -append new_input.txt rep -ascii
        j = j+1;
    end

    %Inactive MAR months
    if(minact>0),
        save -append new_input.txt numwm -ascii
        save -append new_input.txt wminact -ascii
        for n = 1:minact-1;
           save -append new_input.txt rep -ascii
           n = n +1;
        end
        if(i<=33),
            save -append new_input.txt numwm -ascii
            save -append new_input.txt wmact -ascii
        else end
    else end

    i = i+1;
end
```

A2.3 Plot change in head over model space

```
%headrdr.m

%The objective of this script is to take the PVHM head levels output
file, convert to model domain dimensions, and plot the results. The
head levels from the model basecase run are subtracted from the MAR
scenario run, then the resulting plot shows the difference in head
levels between MAR and basecase.

%There are 2 input files:
   1) MAR_heads.txt – This file contains the MAR scenario model
      output for the specific stress period and model layer that you
      are interested in.
   2) Basecase_heads.txt – This file contains the Basecase model
      output for the same stress period and model layer as file (1)

%This script produces three plots:
   1) Basecase head levels
   2) MAR scenario head levels
   3) MAR scenario minus Basecase head levels

%Input head values in model output format (15 columns)
%Convert to 150 x 150 grid dimensions

clear
mod = zeros(150);

headinb = load('Basecase_heads.txt');
rowc = 0;  %row counter
n = 1;
for m = 1:150;  %150 final output rows
    j = 1;
    for j = 1:10;%10 rows per new row in the model grid
        i = 1;
        for i = 1:15;   %15 columns of data per row in input file
            modb(n,m) = headinb(rowc+j,i);
      n = n+1;
      i = i+1;
      end
      j = j + 1;
    end
    n = 1;
    m = m+1;
    rowc = rowc + 10;
end

headin = load('MAR_heads.txt');
rowc = 0;  %row counter
n = 1;
for m = 1:150;  %150 final output rows
    j = 1;
    for j = 1:10;%10 rows per new row in the model grid
```

```
        i = 1;
        for i = 1:15;   %15 columns of data per row in input file
      mod(n,m) = headin(rowc+j,i);
      n = n+1;
      i = i+1;
      end
      j = j + 1;
    end
    n = 1;
    m = m+1;
    rowc = rowc + 10;
end

figure(1);
maxrb = max(modb);    %finds the maximum value in each row of the
grid
maxab = max(maxrb);   %finds the maximum value in the total grid
surf(modb);
axis([1 150 1 150 0 maxab]);

figure(2);
maxr = max(mod);    %finds the maximum value in each row of the grid
maxa = max(maxr);   %finds the maximum value in the total grid
surf(mod);
axis([1 150 1 150 0 maxa]);

figure(3);
headdif = mod - modb;
maxr = max(headdif);    %finds the maximum value in each row of the
grid
maxa = max(maxr);   %finds the maximum value in the total grid
surf(headdif);
axis([1 150 1 150 0 maxa]);
```

A2.4 Plot change in head at a single location over model run

```
% headdt.m

%The objective of this script is to extract the change in head level
at three points at 6 reported stress periods. Head levels are
considered from Layers 1, 3, and 6 (alluvial, upper Aromas, and
Purisima, respectively). One point is on the coast, one is in the
mid-basin and one is in the back-basin. Point location can be
modified by changing the variables (x1,y1),(x2,y2) and (x3,y3).

%The input file is:
   1) MAR_heads-all.xlsx - The complete head levels output file
      saved as .xlsx

%This outputs 3 files, one for each location point. Each is a 6x6
array:
Col 1: Stress period (L1)
Col 2: Head in Layer 1
Col 3: Stress period (L3)
Col 4: Head in Layer 3
Col 5: Stress period (L6)
Col 6: Head in Layer 6

%Columns 1, 3, and 5 should be equivalent, but this

% Point 1: Coastal

clear
x1 = 13;
y1 = 665;
y1f = y1-1;
[num,txt,raw] = xlsread('r07_heads.xlsx');
cnt = 1;
for i=1:6;
    headl1(i,1) = raw(cnt,2);
    headl1(i,2) = raw(cnt+y1f,x1);
    cnt = cnt + 9006;
    i = i+1;
end

L3a = 3002;
cnt = L3a+1;
for i=1:6;
    headl3(i,1) = raw(cnt,2);
    headl3(i,2) = raw(cnt+y1f,x1);
    cnt = cnt + 9006;
    i = i+1;
end

L6a = 7505;
cnt = L6a+1;
for i=1:6;
```

```
    headl6(i,1) = raw(cnt,2);
    headl6(i,2) = raw(cnt+y1f,x1);
    cnt = cnt + 9006;
    i = i+1;
end

for i = 1:6;
    heads(i,1) = headl1(i,1);
    heads(i,2) = headl1(i,2);
    heads(i,3) = headl3(i,1);
    heads(i,4) = headl3(i,2);
    heads(i,5) = headl6(i,1);
    heads(i,6) = headl6(i,2);
i = i+1;
end

headmat = cell2mat(heads);

save heads_point1_L136.txt headmat -ascii

% Point 2: Mid-basin

x1 = 13;
y1 = 637;
y1f = y1-1;

cnt = 1;
for i=1:6;
    headl1(i,1) = raw(cnt,2);
    headl1(i,2) = raw(cnt+y1f,x1);
    cnt = cnt + 9006;
    i = i+1;
end

L3a = 3002;
cnt = L3a+1;
for i=1:6;
    headl3(i,1) = raw(cnt,2);
    headl3(i,2) = raw(cnt+y1f,x1);
    cnt = cnt + 9006;
    i = i+1;
end

L6a = 7505;
cnt = L6a+1;
for i=1:6;
    headl6(i,1) = raw(cnt,2);
    headl6(i,2) = raw(cnt+y1f,x1);
    cnt = cnt + 9006;
    i = i+1;
end

for i = 1:6;
    heads(i,1) = headl1(i,1);
```

```
    heads(i,2) = headl1(i,2);
    heads(i,3) = headl3(i,1);
    heads(i,4) = headl3(i,2);
    heads(i,5) = headl6(i,1);
    heads(i,6) = headl6(i,2);
i = i+1;
end

headmat = cell2mat(heads);
save heads_point2_L136.txt headmat -ascii

% Point 3: Back-basin

x1 = 13;
y1 = 468;
y1f = y1-1;
cnt = 1;
for i=1:6;
    headl1(i,1) = raw(cnt,2);
    headl1(i,2) = raw(cnt+y1f,x1);
    cnt = cnt + 9006;
    i = i+1;
end

L3a = 3002;
cnt = L3a+1;
for i=1:6;
    headl3(i,1) = raw(cnt,2);
    headl3(i,2) = raw(cnt+y1f,x1);
    cnt = cnt + 9006;
    i = i+1;
end

L6a = 7505;
cnt = L6a+1;
for i=1:6;
    headl6(i,1) = raw(cnt,2);
    headl6(i,2) = raw(cnt+y1f,x1);
    cnt = cnt + 9006;
    i = i+1;
end

for i = 1:6;
    heads(i,1) = headl1(i,1);
    heads(i,2) = headl1(i,2);
    heads(i,3) = headl3(i,1);
    heads(i,4) = headl3(i,2);
    heads(i,5) = headl6(i,1);
    heads(i,6) = headl6(i,2);
i = i+1;
end

headmat = cell2mat(heads);
save heads_point3_L136.txt headmat -ascii
```

A2.5 Change in coastal fluxes

```
%zonebud.m

% This program takes the zone output data from the model and parses
it into total flow in and out of the ocean zone each year.

% The output of the program is a Matlab plot showing the basecase
and MAR scenario net flux in (intrusion minus flow offshore), and an
array with flux in and out, separately, and flux, given for each
year of the model run.

clear
%Load basecase data
basezbd = load('zbud_base.txt');

%Load scenario data
zones = load('r07_zones.txt');

[row,col] = size(zones);

pert = row/25;
% fprintf('The number of stress periods is' f, pert);
cnt = 1;
i = 1;
j = 1;
for i = 1:pert;
    j = j+1;
    tin = 0;
    tout = 0;
    for j = 1:25;
        tin = tin + zones(cnt,5);   %SWIn
        tout = tout + zones(cnt,6);  %SWOut
        j = j+1;
        cnt = cnt + 1;
    end
    zbud(i,1) = zones(cnt-1,2);  %record the stress period
    zbud(i,2) = tin*30.4167;   % m3/month
    zbud(i,3) = tout*30.4167;
    zbud(i,4) = tin - tout;  %Net intrusion in coastal zones (m3/mo)
    i = i+1;
end

% Calculate annual total flow in and out of coastal areas

i = 1;
j = 1;
cnt = 1;
cnty = 1;
for i = 1:34;
    j = 1;
    tiny = 0;
    touty = 0;
```

```
    for j = 1:12;
        tiny = tiny + zbud(cnty,2);
        touty = touty + zbud(cnty,3);
        j = j+1;
        cnty = cnty + 1;
    end
    zbudy(i,1) = i;  %record the year
    zbudy(i,2) = tiny; % m3/y
    zbudy(i,3) = touty;
    zbudy(i,4) = tiny - touty;
    zbudy(i,5) = zbudy(i,4)/1233.48;
   % cnty = cnty + 1;

    i = i+1;

end

% Save basecase data (in a previous run)
%save monthbd_base.txt zbud -ascii
%save yrbd_base.txt zbudy -ascii

% Extract basecase data for comparison
xb = basezbd(:,1);
yb = basezbd(:,5); % ac-ft/yr

% Scenario data for comparison
x = zbudy(:,1);
y = zbudy(:,5);

save zbud_mar.txt zbudy -ascii

% Change in SWI flux
yc = yb + y;

scatter(xb,y);  % MAR Scenario in blue
hold
scatter(xb,yb,'r');  %Basecase in red
%scatter(x,y,'k');  % Difference in black
hold off

hleg = legend('MAR','Basecase');
set(hleg,'Location','NorthWest')
xlabel('Year');
ylabel('SWI (Ac-ft/yr)');
```

Chapter 3

A3.1 Updated SFBA exceedance depth regression characteristics

Characteristic values of the regression equation relating exceedence depth to mean annual precipitation[1]

Duration (h)	*RI* (yr)	*m* *(-)*	*b* *(cm)*	Duration (d)	*RI* (yr)	*m* (median) (-)	σ_m *(-)*
1	2	0.009	0.31	1	2	0.10	0.004
1	5	0.010	0.46	1	5	0.14	0.006
1	10	0.010	0.57	1	10	0.17	0.006
1	25	0.011	0.71	1	25	0.20	0.007
1	50	0.011	0.82	1	50	0.22	0.007
1	100	0.011	0.93	1	100	0.25	0.007
2	2	0.017	0.37	2	2	0.14	0.005
2	5	0.019	0.56	2	5	0.20	0.007
2	10	0.019	0.69	2	10	0.24	0.007
2	25	0.020	0.88	2	25	0.29	0.008
2	50	0.019	1.02	2	50	0.32	0.008
2	100	0.019	1.16	2	100	0.36	0.008
3	2	0.024	0.41	3	2	0.17	0.005
3	5	0.028	0.61	3	5	0.24	0.007
3	10	0.029	0.76	3	10	0.28	0.008
3	25	0.030	0.96	3	25	0.33	0.008
3	50	0.030	1.12	3	50	0.37	0.008
3	100	0.029	1.28	3	100	0.41	0.009
6	2	0.042	0.41	4	2	0.19	0.006
6	5	0.052	0.59	4	5	0.26	0.007
6	10	0.057	0.74	4	10	0.31	0.008
6	25	0.061	0.93	4	25	0.37	0.008
6	50	0.064	1.07	4	50	0.41	0.009
6	100	0.067	1.23	4	100	0.45	0.009
12	2	0.067	0.31	5	2	0.20	0.007
12	5	0.088	0.48	5	5	0.29	0.008
12	10	0.099	0.61	5	10	0.34	0.008
12	25	0.112	0.80	5	25	0.41	0.009
12	50	0.121	0.95	5	50	0.45	0.009
12	100	0.129	1.11	5	100	0.50	0.010
				6	2	0.22	0.007
				6	5	0.31	0.009
				6	10	0.37	0.009
				6	25	0.44	0.010
				6	50	0.48	0.010
				6	100	0.53	0.011
				8	2	0.25	0.008
				8	5	0.35	0.009
				8	10	0.42	0.010
				8	25	0.49	0.011
				8	50	0.54	0.011
				8	100	0.60	0.012
				10	2	0.28	0.008
				10	5	0.38	0.010
				10	10	0.45	0.011
				10	25	0.52	0.012
				10	50	0.58	0.013

	10	100	0.63	0.013
	15	2	0.33	0.010
	15	5	0.44	0.012
	15	10	0.51	0.013
	15	25	0.59	0.014
	15	50	0.64	0.015
	15	100	0.69	0.015
	20	2	0.37	0.011
	20	5	0.50	0.013
	20	10	0.57	0.014
	20	25	0.66	0.015
	20	50	0.72	0.016
	20	100	0.77	0.017
	30	2	0.44	0.011
	30	5	0.60	0.015
	30	10	0.69	0.017
	30	25	0.79	0.019
	30	50	0.86	0.020
	30	100	0.92	0.021
	60	2	0.65	0.017
	60	5	0.86	0.023
	60	10	0.99	0.028
	60	25	1.13	0.032
	60	50	1.23	0.036
	60	100	1.32	0.039

[1] Characteristic values of the regression equation for the late time period (1956 to 2010) when exceedance depth (y) is plotted against MAP (x). Daily duration results include the average slope value and standard deviation of values from the full distribution (e.g. **Fig. 3-3B**).

A3.2 Exceedance depth calculation

```
%ddfanntot.m

% The objective of this program is to calculate storm exceedance
depths for several stations over a specified period of time.

% The input for this program are excel files containing the annual
maximum storms of several durations, listed for multiple years. An
example of the file format is given in the Supplemental Files,
section S3.1.

% The program allows the user to select a non-continuous time period
(e.g. so an anomalous period could be omitted) by asking for the min
and max values for two ranges of interest. The exceedance depths
will be calculated using the data from BOTH ranges together.

% To obtain exceedance depths for different time periods, the
program must be run separately for each time period.

% The output of this program is an array:
% Station# Period# RP1Dur1Dep RP2Dur1Dep RP3Dur1Dep... 72 depth
values

clear
% Load all the files from the active directory.
files = dir('*.xls');
[ro,co] = size(files);
nl = ro;
ncnt = 0;
RPtot = [0 0 0 0 0 0 0 0];

% Ask user for time periods over which to perform the exceedance
depth analysis

ymin = input('Enter the earliest year in first range of interest:
');
ymax = input('Enter the latest year in first range of interest:  ');
ymin2 = input('Enter the 2nd group earliest year in first range of
interest:  ');
ymax2 = input('Enter the 2nd group latest year in first range of
interest:  ');
decade = input('What is the Period number for this data set:    ');

 % Obtain lat/long/elevation from file titled, 'lle.csv'

  fid = fopen('LLE_Index_Space.csv');
  llelist = textscan(fid,'%s %f %f %f %*[^\n]','delimiter',',');

  % Convert cells from textscan to lists

 statname = [llelist{:,1}];
  lat = [llelist{:,2}];
```

```
  lng = [llelist{:,3}];
  elev = [llelist{:,4}];

  fclose(fid);

  [rlle,clle] = size(statname);

% Read data from each file in the directory. The years and maximum
amounts of precipitation for each duration will be recorded, and
then exceedance depths are calculated.

for q=1:nl;                          %For each file in the directory
    clear num
    clear txt
    clear raw
    [num,txt,raw] = xlsread(files(q).name);

    % Find the row number of the first year
    i = 1;
    for i = 1:50;
        TF = strcmp(raw(i,1),'Year');
if TF == 1;
        rown = i;
        break
        else
            i = i+1;
        end
    end

    rown = rown + 1;

    [rrow,rcol] = size(raw);

    dlen = rrow - rown;              %length of the data section
  clear data
    n = 1;
    for n = 1:dlen;  %Create an array 'data' with the data from raw
        data(n,1) = raw(rown,1);          %Year column
        data(n,2) = raw(rown,2);          %1 day column
        data(n,3) = raw(rown,3);          %2 day column
        data(n,4) = raw(rown,4);          %3 day column
        data(n,5) = raw(rown,5);          %4 day column
        data(n,6) = raw(rown,6);          %5 day column
        data(n,7) = raw(rown,7);          %6 day column
        data(n,8) = raw(rown,8);          %8 day column
        data(n,9) = raw(rown,9);          %10 day column
        data(n,10) = raw(rown,10);        %15 day column
        data(n,11) = raw(rown,11);        %20 day column
        data(n,12) = raw(rown,12);        %30 day column
        data(n,13) = raw(rown,13);        %60 day column
        data(n,14) = raw(rown,14);        %Annual total column
        rown = rown+1;
        n = n+1;
    end
```

```
    data = cell2mat(data);
    [urow,ucol]=size(data);

z = 1;
for z = 1:20;                          %Delete rows that are missing
data
    for m = 1:urow;
         if
and(and(data(m,1)>=0,data(m,2)>=0),and(data(m,13)>=0,data(m,14)>=0))
;
       else data(m,:)=[];
       end
        [urow,ucol]=size(data);
        m = m+1;
        if(m>urow), break, end
    end
    m = 1;
  if(m>urow), break, end
  z = z +1;
end

[row,col] = size(data);

jj = 1;
cct = 0;
checkpt = 0;
for jj=1:row;
    if and(data(jj,1)<=ymax,data(jj,1)>=ymin);
        cct = cct + 1;
        checkpt = 1;
    else
        jj = jj;
    end

    if checkpt== 0;

        if and(data(jj,1)<=ymax2,data(jj,1)>=ymin2);
           cct = cct + 1;
           jj = jj + 1;
        else jj = jj +1 ;
        end

    else  jj = jj + 1;
    end
    checkpt = 0;
end

% If there are at >=15 years of data in the defined time period,
then calculate the exceedance depths for this station, if not,
advance to the next station file.

if(cct>=15);
```

```
% Calculate the annual average based on the time range specified.

n = 1;
b = 0;                                  %counter
prectot = 0;                            %total precip
checkpt = 0;
clear firstg;
for n= 1:row;
    if and(data(n,1)<=ymax,data(n,1)>=ymin);
        prectot = prectot + data(n,14);
        b = b+1;
        n = n + 1;
    else n = n + 1;
    end
end

n = 1;
prectot2 = 0;
b2 = 0;
for n = 1:row;
       if and(data(n,1)<=ymax2,data(n,1)>=ymin2);
           prectot2 = prectot2 + data(n,14);
           b2 = b2+1;
           n = n + 1;
       else n = n + 1;
       end
end

annav = (prectot + prectot2)/(b+b2);

 % Calculate the exceedance depths for the active data file.
% Return period calculated using 'Chow's Handbook of Applied
Hydrology' %method.
% Output is an array with the following columns:
    % RP-YR   RP-Dur1  RP-Dur2   RP-Dur3  ... Annual Avg

    dtcol = 3;
      nf = 0;

    % Create return period output array
    RParray = [2; 5; 10; 25; 50; 100];
    for j=2:13;          %For each duration (1d - 60d)
            sump = 0;
            sump2 = 0;
            sump3 = 0;
            i = 1;
            rngct = 0;

        for i=1:row;   %Calculate the sums for future calcs
          if or((data(i,1) >= ymin & data(i,1) <= ymax),(data(i,1)
>= ymin2 & data(i,1) <= ymax2));
            sump = data(i,j) + sump;
            sump2 = data(i,j)^2 + sump2;
            sump3 = data(i,j)^3 + sump3;
```

```
            rngct = rngct + 1;
            i = i + 1;
          else i = i + 1;
          end

      end

        nf = rngct;                          %Number of records
        avgp = sump/nf;                      %average record value
        s = ((sump2 - sump^2/nf)/(nf-1))^0.5;   %standard deviation
        g = (nf^2*sump3-3*nf*sump*sump2+2*(sump^3))/(nf*(nf-1)*(nf-
2)*s^3);
                                             %g= coefficient of skew
        cv = s/avgp;                         %coefficient of variation

 % Calculate the 6 event depths for the active duration if (avgp >0)
        for k=1:6;
            % calculate the frequency factor (f(RI,distribution
type))
            rpy = RParray(k,1);
            w = (log(rpy^2))^0.5;
            ztop = 2.515517 + 0.802853 * w + 0.010328 * w^2;
            zbottom = 1 + 1.432788 * w + 0.189269 * w^2 + 0.001308 *
w^3;
            z = w - (ztop/zbottom);
            kvar = g/6;
            kj = z +(z^2-1)*kvar+(z^3 - 6*z)*kvar^2 /3-(z^2 -
1)*kvar^3+z*kvar^4 +kvar^5/3;
                                             % kj = frequency factor

            % Calculate the event depth
            rp = avgp*(1+cv*kj);
            RParray(k,j) = rp;

 % Write the event depth to the RP Array
            % station# dur1rp1dep dur1rp2dep dur1rp3dep...

            if (avgp == 0)
                k = k+1;
            else
            depthtab(q,1) = q;                   %station number
            depthtab(q,2) = decade;              %study period
            depthtab(q,dtcol) = rp;              %exceedance depth
            depthtab(q,75) = annav;              %station annual
average
            depthtab(q,79) = cct;                %years of record
            dtcol = dtcol + 1;
            k = k+1;          % Advance to the next RP calculation
            end
        end
        j = j + 1;                  % Advance to the next duration
    end
```

```
% Write Lat/Long and Elevation to the next three columns for each
station.
% This will require using the current file name (files(q).name) and
a
% true-false function to find its row number in the list 'statname'.

strs = files(q).name;
[a,b,c] = fileparts(strs);

ncnt = ncnt + 1;  %Write an array with the station number and name.
nmcode{ncnt,1} = q;
nmcode{ncnt,2} = b;

%[tok,rem]=strtok(b,'D');     % This extracts the extra characters
from the filename
%[nam,ext]=strtok(rem,'D');
n = 1;
for n = 1:rlle;
    TF = strcmp(b,statname(n));
    if(TF >0);
        % When the current station name finds its match in the list
of
        % stations, the lat/long and elevation are recorded in
columns
        % 76,77, and 78 of the final table, depthtab.
        depthtab(q,76) = lat(n);
        depthtab(q,77) = lng(n);
        depthtab(q,78) = elev(n);
        break
    else
        n = n+1;
    end
end
    else
    q = q+1;                  % Advance to the next file.
end
q = q+1;
end

% Count number of non-zero rows:

[ortot,foo] = size(depthtab);  % ortot will be the number of
stations included
nonz = 0;
m =1;
for m = 1:ortot;
    if(depthtab(m,1)>0)
        nonz = nonz + 1;
        m = m + 1;
    else
        m = m+1;
    end
end
% Delete all rows that didn't have data (station not applicable for
```

```
% selected range of years).

for z = 1:10;
p = 1;
for p = 1:nonz;
    if (depthtab(p,1)>0)
        p = p + 1;
    else
        depthtab(p,:)=[];
    end
end

z = z +1;
end

save depthtab.dat depthtab -ascii;
save nmcode.dat nmcode;
```

A3.3 Compare data from two time periods at individual stations

```
% comstat.m

% The purpose of this program is to compare the calculated
exceedance depths for the same station over two time ranges. I have
the exceedance depths for given duration and return period pairs for
1890-1955 and 1956-2010. Because not every station will have enough
data in both time ranges to be significant, that will be the first
check.

% The second step will be to calculate the change, percent change,
and normalized change and write this to an array with the station
number, duration and RP.

% Read in data:
clear
per1 = load('depthtab_1d.dat');  % Exceedance depths for 1st period
per2 = load('depthtab_2d.dat');  % Exceedance depths for 2nd period
durrp = load('Dur-RP_list.txt'); % List of duration and RPs in order
[r1,c1] = size(per1);
[r2,c2] = size(per2);
rwnum = 1;
b = 0;
xsd = 0;

% Check if station_i exists in both sets of data

for i=1:r1;
    num = per1(i,1);
        sumr = 0;
        sump = 0;
        sumn = 0;

    for j=1:r2;
        if per2(j,1)==num;
            row2 = j;
        b = b+1;

    % Now per1(i) is the same station as per2(row2)

    % Calculate change and percent change:

    datcol = c1 - 5; % subtract cols 'Stat, decade, lat, long, elev'
    pair = 1;
    rmap = per2(row2,75) - per1(i,75);    % MAP difference
    pmap = rmap / per1(i,75) * 100;       % percent change MAP
    map2 = per2(row2,75);
    map1 = per1(i,75);
    cct = 0;
    clear xsd;
    clear sumndel;
    for n = 1:datcol;
```

```
        pos = n + 2;
        rdel = per2(row2,pos) - per1(i,pos);
        pdel = rdel / per1(i,pos) * 100;
        ndel = pdel / pmap;
       if durrp(1,pair)>1;
          cct = cct +1;

        % write rdel, pdel and pmap to array
        delarr(rwnum,1) = per1(i,1);      % Write station number
        delarr(rwnum,2) = rdel;           % Write difference
        delarr(rwnum,3) = pdel;           % Write percent difference
        delarr(rwnum,4) = ndel;     % Write normalized % difference
        delarr(rwnum,5) = durrp(1,pair);  % Write Return Period
        delarr(rwnum,6) = durrp(2,pair);  % Write Duration
        delarr(rwnum,7) = map2;           % Write MAP from period 2
        delarr(rwnum,8) = pmap;
        delarr(rwnum,9) = per1(i,76);     % Write Latitude
        delarr(rwnum,10) = per1(i,77);    % Write Longitude
        delarr(rwnum,11) = per1(i,78);    % Write Elevation
        pair = pair +1;
        rwnum = rwnum + 1;

        sumr = sumr + rdel;
        sump = sump + pdel;
        sumn = sumn + ndel;
        xsd(cct,1) = ndel;
       else
           pair = pair + 1;
       end


    end           % close of delarr calculations

    reprt(b,1) = sumr / 72;               % Write mean rdel
    reprt(b,2) = sump / 72;               % Write mean pdel
    reprt(b,3) = sumn / 72;               % Write mean ndel
    reprt(b,4) = std(xsd);                % Write standard deviation
    reprt(b,5) = per1(i,76);              % Write station longitude
    reprt(b,6) = per1(i,77);              % Write station latitude
    reprt(b,7) = per1(i,78);              % Write station elevation
    reprt(b,8) = rmap/map1*100;           % Write percent change in
MAP

        else j = j+1;   % advance to next row in set 2.
    end

  end

 end

save delarr_120517.txt delarr -ascii
save ndel_report_wMAPdel.txt reprt -ascii
```

SUPPLEMENTAL FILES

Supplemental Files contain data tables that are too large to reasonably display in this thesis. The files are described here, and are available in digital format at: www.tessrusso.com/thesis/suppfiles

S3.1 Sample precipitation data file

S3.1_PrecipFormat_daily.xls

S3.2 Precipitation stations: Daily interval data

S3.2_PStat_daily.xls

Col 1: Station number (corresponds to station number in exceedance depth tables)
Col 2: Station name
Col 3: Latitude
Col 4: Longitude
Col 5: Elevation

The first five rows of precipitation stations with daily interval data:

Station number	Station name	Latitude	Longitude	Elevation (m)
1	Acampo 5 NE	38.217	-121.2	27
2	Acampo Callow	38.217	-121.133	38
3	Adobe Creek	38.925	-122.878	466
4	Aetna Springs	38.653	-122.483	244
5	Alameda East Portal	37.55	-121.867	236
…	…	…	…	….

S3.3 Exceedance depths for storms of hourly durations

S3.3_ED_hourly.xls

Exceedance depths calculated for hourly storm durations at recurrence intervals (*RI*) of 2 to 100 yrs.

Col 1: Station number
Col 2: Time period (1=early or 2=late)
Col 3: 1 hour, 2 yr *RI*

Col 4: 1 hour, 5 yr *RI*
Col 5: 1 hour, 10 yr *RI*
Col 6: 1 hour, 25 yr *RI*
Col 7: 1 hour, 50 yr *RI*
Col 8: 1 hour, 100 yr *RI*
Col 9 to 14: 2 hour storms, 2 to 100 yr *RI*s
Col 15 to 20: 3 hour storms, 2 to 100 yr *RI*s
Col 21 to 26: 6 hour storms, 2 to 100 yr *RI*s
Col 27 to 32: 12 hour storms, 2 to 100 yr *RI*s
Col 33: Mean annual precipitation
Col 34: Station Latitude
Col 35: Station Longitude
Col 36: Station elevation

The first eight columns and four rows of the hourly exceedance depth table, all depths are in cm:

Station	Period	1h2ri	1h5ri	1h10ri	1h25ri	1h50ri	1h100ri	…
14	1	1.5	1.9	2.1	2.4	2.7	2.9	…
42	1	1.1	1.3	1.4	1.5	1.6	1.7	…
61	1	1.0	1.2	1.4	1.7	1.8	2.0	…
107	1	1.4	1.7	1.9	2.0	2.2	2.3	…
…	…	…	…	…	…	…	…	…

S3.4 Exceedance depths for storms of daily durations

S3.4_ED_daily.xls

Exceedance depths calculated for daily storm durations at recurrence intervals (*RI*) of 2 to 100 yrs.

Col 1: Station number
Col 2: Time period (1=early or 2=late)
Col 3: 1 day, 2 yr *RI*
Col 4: 1 day, 5 yr *RI*
Col 5: 1 day, 10 yr *RI*
Col 6: 1 day, 25 yr *RI*
Col 7: 1 day, 50 yr *RI*
Col 8: 1 day, 100 yr *RI*
Col 9 to 14: 2 day storms, 2 to 100 yr *RI*s
Col 15 to 20: 3 day storms, 2 to 100 yr *RI*s
Col 21 to 26: 4 day storms, 2 to 100 yr *RI*s
Col 27 to 32: 5 day storms, 2 to 100 yr *RI*s

Col 33 to 38: 6 day storms, 2 to 100 yr *RI*s
Col 39 to 44: 8 day storms, 2 to 100 yr *RI*s
Col 45 to 50: 10 day storms, 2 to 100 yr *RI*s
Col 51 to 56: 15 day storms, 2 to 100 yr *RI*s
Col 57 to 62: 20 day storms, 2 to 100 yr *RI*s
Col 63 to 68: 30 day storms, 2 to 100 yr *RI*s
Col 69 to 74: 60 day storms, 2 to 100 yr *RI*s
Col 75: Mean annual precipitation
Col 76: Station Latitude
Col 77: Station Longitude
Col 78: Station elevation

The first eight columns and four rows of the daily exceedance depth table, all depths are in cm:

Station	Period	1D2rp	1D5rp	1D10rp	1D25rp	1D50rp	1D100rp	…
4	1	8.9	11.3	12.6	14.1	15.1	16.1	…
9	1	4.0	5.2	5.9	6.8	7.4	8.0	…
10	1	9.3	12.6	14.6	17.0	18.8	20.5	…
11	1	9.6	12.5	14.2	16.2	17.6	18.9	…
…	…	…	…	…	…	…	…	…